UNIVERSITY OF CALIFORNIA, SAN DIEGO

Control of Carbon Nanotube Growth Directions and Morphology by Direct Current Plasma Enhanced Chemical Vapor Deposition

A dissertation submitted in partial satisfaction of the

requirements for the degree Doctor of Philosophy

in

Materials Science and Engineering

by

Joseph Francis AuBuchon

Committee in Charge:

Professor Sungho Jin, Chair
Professor Prabhaker Bandaru
Professor Yu-Hwa Lo
Professor Vitali Nesterenko
Professor Deli Wang

2006

The dissertation of Joseph Francis AuBuchon is approved, and it is acceptable in quality and form for publication on microfilm:

_____

_____

_____

_____

_____

Chair

University of California, San Diego

2006

Dedicated to

my family

The glass is neither half empty nor half full,
It was simply made twice as big as it needed to be.

TABLE OF CONTENTS

LIST OF FIGURES

LIST OF TABLES

ACKNOWLEDGEMENTS

I wish to acknowledge and deeply thank my advisor, Professor Sungho Jin, for his strong encouragement, support, and direction during the course of this research. I would also like to thank Dr. Leon Chen for his guidance and assistance in the lab throughout the course of this project.

I wish to express my gratefulness to my committee members for their time and helpful suggestions: Professor Prabhaker Bandaru, Professor Vitali Nesterenko, Professor Yu-Hwa Lo, and Professor Deli Wang.

I would also like to recognize and thank the following individuals for their assistance in various aspects of this work: Chiara Daraio, Andy Gapin, Edin Chen, Jeongwon Park, Dr. Brian Oh, Jamie Neuberger, Matt Horner, and Ken Domond.

As this dissertation marks the concluding accomplishment in my last 20 years as a full time student, I would also like to show appreciation to the following individuals who have taught, helped, and encouraged me along the way: Professor Ronald Gronsky, Professor Fiona Doyle, and Dr. Anthony Thompson, Mr. Richard Parson, Mr. Al Holland, Ms. Joan Owen, and Mr. David Iverson.

I graciously acknowledge the financial support from the National Science Foundation (NSF-NIRT grant numbers DMR-0210559 and DMI-0303790), the University of California Discovery Fund (grant number ele02-10133/Jin,) and Lawrence Livermore National Lab (grant number MI-04-006.)

Finally, I wish to thank my parents and other family members for their prayers and loving encouragement during this time. I also wish to thank my many friends and other colleagues who are too numerous to mention all by name.

VITA

1981	Born in Virginia, USA
2002	B.S., Materials Science and Engineering, University of California, Berkeley
2003	M.S., Materials Science and Engineering, University of California, San Diego
2006	Ph.D., Materials Science and Engineering, University of California, San Diego

SELECTED AWARDS

Materials Research Society's (MRS) Graduate Student Gold Award
"In recognition of outstanding performance in the conduct of research"

Powel Graduate Fellowship recipient

Best Poster Award, MRS spring 2005 meeting

Best Poster Award, Jacobs School of Engineering Research Expo 2006

JOURNAL PUBLICATIONS

1. Joseph F. AuBuchon, Li-Han Chen, Andrew I. Gapin, Dong-Wook Kim, Chiara Daraio, Sungho Jin, "Multiple Sharp Bendings of Carbon Nanotubes during Growth to Produce Zigzag Morphology", Nano Letters 4 (9), 1781-1783 (2004).

2. C. Daraio, V. F. Nesterenko, J. F. AuBuchon, S. Jin, "Dynamic Nanofragmentation of Carbon Nanotubes", Nano Letters 4 (10), 1915-1918 (2004).

3. L. –H. Chen, J. F. AuBuchon, A. Gapin, C. Daraio, P. Bandaru, S. Jin, D. –W. Kim, I. K. Yoo, "Control of carbon nanotube morphology by change of applied bias field during growth", Applied Physics Letters 85 (22), 5373-5375 (2004).

4. D. –W. Kim, L. -H. Chen, J. F. AuBuchon, I.-C. Chen, S. –H. Jeong, I. K. Yoo, S. Jin, "Prevention of Si-contaminated nanocone formation during plasma enhanced chemical vapor deposition growth of carbon nanotubes", Carbon 43, 835 (2005).

5. Joseph F. AuBuchon, Li-Han Chen, Sungho Jin, "Re-Growth of Aligned Carbon Nanotubes via Control of Carbon Capping", The Journal of Physical Chemistry B 109, 6044-6048 (2005).

6. Joseph F. AuBuchon, Joel Hollingsworth, "A New Element for a New Weapon", Journal of the Minerals, Metals & Materials Society, 57 (5), 15-16 (2005).

7. Joseph F. AuBuchon, Li-Han Chen, Andrew I. Gapin, Sungho Jin, "Opening of Aligned Carbon Nanotube Ends via Room-Temperature Sputter Etching Process", Journal of Applied Physics 97, 124310 (2005).

8. Joseph F. AuBuchon, Li-Han Chen, Sungho Jin, "Control of Carbon Nanotube Growth Directions via Electric Fields within a DC Plasma Sheath", Electronic Materials Letters 1 (1) 1-6 (2006).

9. Joseph F. AuBuchon, Chiara Daraio, Li-Han Chen, Andrew I. Gapin, Sungho Jin, "Iron Silicide Root Formation in Carbon Nanotubes Grown by Microwave PECVD", The Journal of Physical Chemistry B 109, 24215-24219 (2006)

10. Joseph F. AuBuchon, Li-Han Chen, Chiara Daraio, Sungho Jin, "Multibranching Carbon Nanotubes via Self-Seeded Catalysts", Nano Letters 6, 324-328 (2006).

11. L. –H. Chen, J. F. AuBuchon, I. –C. Chen, C. Daraio, X. –R. Ye, A. I. Gapin, S. Jin, C. M. Wang, "Growth of Aligned Carbon Nanotubes on Carbon Microfibers by DC Plasma-Enhanced Chemical Vapor Deposition", Applied Physics Letters 88, 033103 (2006).

12. A. I. Gapin, X. R. Ye, J. F. AuBuchon, L. H. Chen, Y. J. Tang, S. Jin, "CoPt patterned media in anodized aluminum oxide templates", *Journal of Applied Physics* **99**, 08G902 (2006).

13. Y. J. Tang, J. F. AuBuchon, L. H. Chen, S. Jin, J. W. Kim, Y. H. Kim, C. S. Yoon, "Fabrication and Magnetic Properties of Nano-Patterned FePt Media", *Journal of Applied Physics* **99**, 08G909 (2006).

14. Joseph F. AuBuchon, Li-Han Chen, Andrew I. Gapin, Sungho Jin, "Electric Field Guided Growth of Carbon Nanotubes during DC PECVD" *Chemical Vapor Deposition* **12**, 1 (2006).

15. L.-H. Chen, I. –C. Chen, J. F. AuBuchon, A. I. Gapin, D. –W. Kim, S. Jin, "Miniature Vacuum Tube MEMS Devices with Carbon Nanotube Electron Emitters" submitted to Small (2006).

16. Xiang-Rong Ye, Joseph F. AuBuchon, Li-Han Chen, I-Chen Chen, Jan B. Talbot, Sungho Jin, "Vertically Aligned Carbon Nanotube Array on Carbon Paper Substrate as Electrochemical Biosensor", submitted (2006).

17. Xiang-Rong Ye, Li-Han Chen, Chongmin Wang, Joseph F. AuBuchon, Edin Chen, Andrew Gapin, Jan B. Talbot, and Sungho Jin, "Ultrafast Electrochemical Tip Opening of Vertically Aligned Carbon Nanotubes." submitted (2006).

18. C. Daraio, V. F. Nesterenko, J. F. AuBuchon, S. Jin, "Dynamic insulator-conductor transition in a strongly nonlinear media" (in preparation).

19. Joseph F. AuBuchon, Andrew I. Gapin, Li-Han Chen, Sungho Jin, "Spiraling Arrays of Carbon Nanotubes", (in preparation).

ABSTRACT OF THE DISSERTATION

Control of Carbon Nanotube Growth Directions and Morphology by

Direct Current Plasma Enhanced Chemical Vapor Deposition

by

Joseph Francis AuBuchon

Doctor of Philosophy in Materials Science and Engineering

University of California, San Diego, 2006

Professor Sungho Jin, Chair

Vertical alignment of individual carbon nanotubes (CNTs) and CNT arrays during their growth has been demonstrated by many groups; however, there has been much less progress towards more complicated morphologies. In this work, I show the ability to use direct current plasma enhanced chemical vapor deposition to control the growth direction of CNTs. By careful engineering of the cathode geometry, the electric field directions within the cathode plasma sheath are controlled and the CNTs grow along these customized field lines. The ability to dramatically change the growth direction of CNTs and create sharp bends and zigzag structures is also demonstrated. A model for the electric fields within the plasma sheath and in the region of CNT growth is proposed. Using this model to assist in the experimental design of the electrode geometries, both the CNT growth directions and sharp bend angles can be predicted to within 2°.

Additional morphology control over CNTs is also demonstrated including the ability to control the carbon capping to allow easy re-growth of CNTs, a method of opening the ends of aligned CNTs without using any wet chemical processing or oxidation step, the creating of multiple aligned branchings formed from a single CNT creating Y- or T- junctions of desired angles, and the creation of three dimensional structures such as coiled CNTs.

The novel CNT morphologies created in this work could serve useful in a variety of applications and initial results are presented for their use as a catalyst particle support structure for potential fuel cell applications, field emission sources for flat panel display or projection e-beam lithography, improved probe tips for scanning probe microscopy, and templates for guided growth of nerve cells.

CHAPTER 1: INTRODUCTION

Miniaturization of devices has allowed great advances in semiconductor technology over the past few decades. While demands push for a continuation of these advances, the cost and feasibility of miniaturization on the nanoscale are increasingly becoming more problematic. Because of their exceptional properties, carbon nanotubes (CNTs) have drawn considerable attention for researchers seeking to find different ways to continue the push for miniaturization. The proposed applications for CNTs are numerous, ranging from using a single CNT as an improved probe tip in scanning probe microscopy at the nm scale, all the way to being used in constructing a giant cable to form the basis for a space elevator to facilitate the transport of materials into space.

While some of the observed properties of CNTs have been exceptional, the ability to synthesize CNTs with the desired structure, properties, size, and morphology is still rather limited. The growth of vertically aligned CNTs or CNT arrays has been shown by several groups, and these have been used to demonstrate many of the proposed applications for CNTs. The ability to grow CNTs along other directions is very lacking. A couple of groups have shown that CNTs can be grown between two electrodes with a potential differences applied between them, and a few straight CNTs were grown between them demonstrating that CNT growth can be affected by electric fields, but there has not been any demonstration of the ability to make a more complicated structure, such as a sharp bend in a CNT during its growth.

In this work, I show how by direct current plasma enhanced chemical vapor deposition (dc PECVD) the growth directions of CNTs can be controlled with great

precision and these growth directions can be dramatically changed to leave sharp bends in the CNTs with predictably engineered angles. Using related processes, I also show other new ways to control the morphology of CNTs and demonstrate the creation of several novel CNT structures.

Chapter 2 gives a brief background on CNTs including history, properties, synthesis, and applications. Although some of this background is more general, the majority of it focuses specifically on the type of CNTs that are typically grown in a dc PECVD process.

Chapter 3 discusses the experimental setup and includes details of the custom built dc PECVD system that was used in this work.

Chapter 4 contains all of the results and discussion and is divided into 8 sections. Section 4.1 shows vertically aligned CNTs grown by dc PECVD similar to those that have been reported elsewhere. Section 4.2 shows how the morphology of vertically aligned CNTs can be adjusted from tube shaped to cone shaped by change of applied bias field. Section 4.3 demonstrates how the growth directions of CNTs can be controlled by the altering the directions of the electric fields with the dc plasma sheath. Section 4.4 demonstrates that sharp bends and even zigzag structures can be created by changing the directions of the electric fields in the middle of CNT growth. Section 4.5 demonstrates how by using post growth plasma etching, regrowth of CNTs can be facilitated or the ends of CNTs can be opened. Section 4.6 demonstrates the creation of multiple aligned branchings from an initial CNT. Section 4.7 presents the initial results in the creation of CNT coils and section 4.8 discusses some of the initial applications that the CNTs made in this work have been used for.

Chapter 5 gives a summary of the main results in the work, discusses some of the ongoing research, and what needs to be done in the future.

CHAPTER 2: BACKGROUND

2.1 History:

A few years before the discovery of carbon nanotubes (CNTs), a new form of carbon was observed by team including Sir Harold W. Kroto, Robert F. Curl, and Richard E. Smalley.[1] Their 1985 discovery of Buckminster fullerene, C_{60}, led to the three of them receiving the 1996 Nobel Prize in chemistry. Related to these new tiny balls of carbon, CNTs are composed of graphene sheets that are rolled up into tubes. The discovery of CNTs is usually credited to Sumio Iijima.[2] In 1991 at the NEC Fundamental Research Laboratories in Japan, Iijima observed something very amazing on the cathode of a carbon arc while he was attempting to synthesize C_{60} and other fullerenes. Iijima's high-resolution electron micrographs revealed multiwalled nanotubes (MWNTs) and their hemispherical end caps, clearly showing that these carbon species are extended members of the then recently discovered fullerene family. While it was necessary for good transmission electron microscopy (TEM) images to prove the existence of this unique and unexpected form of carbon, CNTs actually have roots extending much further back in time.

For over a century it has been known that carbon filaments can be formed by the catalytic decomposition of carbon containing gases on hot metal surfaces. A report of carbon filaments that were grown from carbon containing gases using an iron crucible can be found in a United States patent published in 1889.[3] This very early report most likely consisted of carbon nanofibers (CNFs) which were entangled into larger filaments; but, the observation of individual CNFs could not be accomplished without

availability of high-resolution (HR) TEM. In 1952, Radushkevich and Lukyanovich presented TEM images of "soot particles" that showed the presence of CNFs.[4] This was followed by several additional reports between the 1950s and 1970s which showed that similar types of carbon filaments could be synthesized by using a broad range of hydrocarbon and metal containing gasses, with most of the reports involving the presence of cobalt, iron, or nickel. Many of these early studies were motivated by the formation of unwanted carbon deposits, such as in industrial steam cracker tubes used to produce various olefins,[5] or similar carbon deposits found on fuel cladding in the nuclear industry where hydrocarbon gases or CO were used for heat transfer.[6]

Following the discovery of CNTs, many others proceeded to study this more. In 1993, two separate groups simultaneously discovered single walled CNTs (SWNTs). The two papers, one from Iijima's group at NEC,[7] and the other from a group at IBM's Almaden Research Center in San Jose,[8] were published consecutively as the first and second letters in the June 17, 1993 issue of Nature. The arc discharge synthesis technique was refined[9] and subsequently led to alternative processing techniques such as laser evaporation[10] and the pyrolysis of hydrocarbon gases.[11] These methods had some control over the resulting CNT morphology and allowed for a lot of research to be done, but they offered very little feasibility for large scale production with control of structure and low cost. Due to these limitations, for the synthesis of CNTs, gas-phase reactions such as chemical vapor deposition (CVD) have received the greatest attention recently.

2.2 Nomenclature of Carbon Nanotubes:

There is actually a great variety in the structures that make up different types of CNTs, and to complicate things, there is an equally great variety of the terms used to describe these structures. All of these structures have certain things in common. The most obvious thing is that they are all made of carbon. They also have high aspect ratios with diameters on the "nano" scale which ranges from as large as a few hundred nanometers down to as small as 1 nm and lengths ranging from less than a micron to a few centimeters.

Graphene sheets are two-dimensional (2D) structures made up of carbon atoms which are covalently bonded and arranged into hexagonal networks. Graphite, the equilibrium phase of carbon at standard temperature and pressure, is a three-dimensional (3D) structure made up of layers of 2D graphene sheets. Details on the structure of CNTs are discussed in the following section, but for right now I will define CNTs as nano-scale tubes made up of rolled 2D graphene sheets. These tubes can consist of a single rolled graphene sheet known as a single walled CNT (SWNT) or as multiple graphene sheets rolled up concentrically which is called a multi-walled CNT (MWNT.) In an ideal CNT, these graphene sheets are rolled parallel to the tube axis and each sheet will extend the entire length of the CNT. Tubes like this will have completely hollow cores which also extend the entire length of the tube (capping will be discussed later.) While CNTs are usually presented having this geometrically elegant structure, in reality the majority of CNTs synthesized are not like this.

There are a number of recurrent variations to this ideal CNT structure that result in different types of CNTs. One common defect found in MWNTs is the presence of

graphene layers which bridge the interior tube of the CNT. This structure is often called a bamboo structure since these graphene layers will divide the hollow core of the CNTs into many sections, similar to the way that the hollow core of bamboo is divided. Figure 1 shows both photographs of real bamboo and transmission electron microscopy (TEM) images of CNTs which have the bamboo structure.

Another common defect is to have the graphene planes form into a stacked cone configuration instead of cylinders in which each graphene plane extends the entire length of the CNT. Schematic illustrations comparing the stacked cone geometry to the concentric cylinder geometry are shown in Figure 2. While both of these structures can have hollow cores and walls made up of graphene sheets of carbon, their structures are quite different. In a cross sectional image, like those shown in Figure 2 (c) and (d), we can see that the graphene planes are parallel to each other, but in the stacked cone geometry these graphene plans are not parallel to the tube axis. Structures like this are often referred to as a herringbone structure since the graphene planes in their cross sections resemble the bones of a fish skeleton. The angle of displacement between the graphene planes and the tube axis is labeled as α; this angle is zero for CNTs made up of cylinders, and has some positive value for stacked cone configurations. While the diagrams in Figure 2 (b) and (d) depict large values for α, herringbone structured CNTs are commonly seen with very low α values. Such CNTs with α values close to zero sometimes appear to be composed of true graphene cylinders and TEM images are often shown of them which appear to support this, however these images typically show ~100-200 nm sections of the CNTs. Sometimes it is necessary to follow individual

graphene planes for hundreds of nanometers before you can trace one of these planes from the interior core to the exterior of a CNT and observe the herringbone structure.[12]

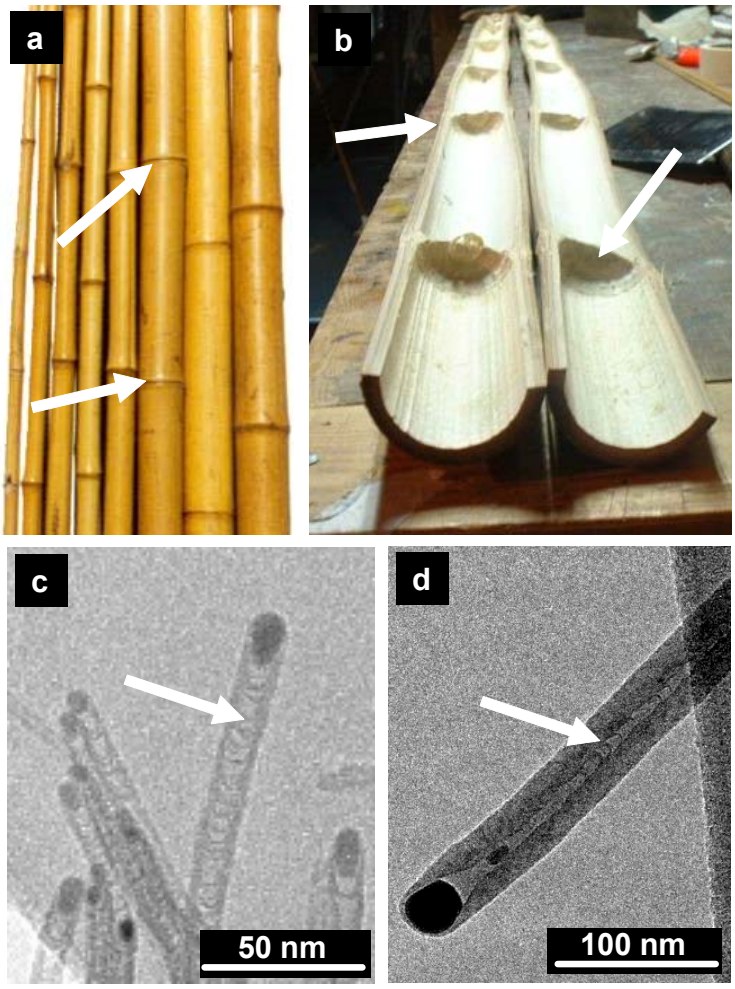

Figure 1: Photographs and TEM images comparing the structure of bamboo and CNTs. The bamboo plant has a hollow tubular core which is divided into separate cells at periodic breaks identified by arrows in (a) where a picture of taken of a group of bamboo shoots and in (b), where a single bamboo shoot has been split down its middle so that the interior is visible. The TEM images in (c) and (d) of CNTs show divisions of the hollow CNT cores into separate cells similar to the bamboo pictured above.

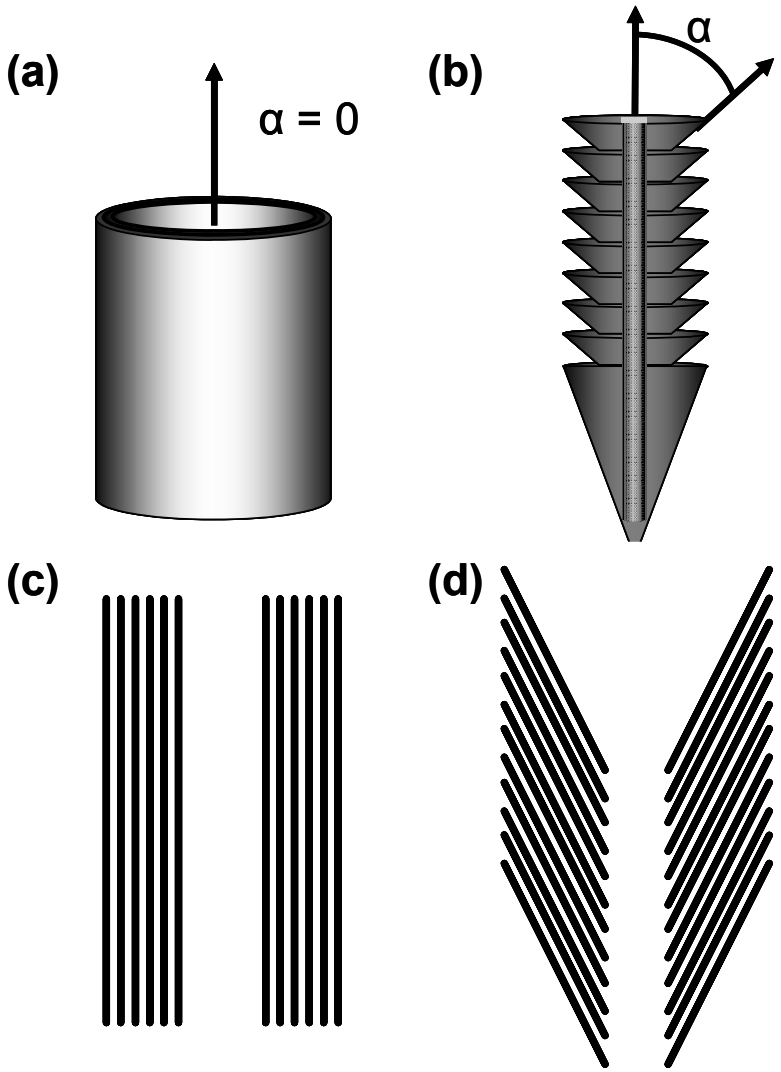

Figure 2: Schematic 3D illustrations of CNTs made up of graphene cylinders which extend the entire length of the tube (a) and herringbone type CNTs made up of stacked graphene cones (b). Corresponding 2D cross sectional illustrations of the graphene plane geometries are shown in (c) and (d).

Herringbone structured CNTs frequently also have the bamboo structure, so these two names are often confused with each other. Both bamboo and herringbone structured CNTs are sometimes called carbon nanofibers (CNFs) since they are not made of perfect graphene tubes like the name "carbon nanotube" might imply. Prior to

the discovery of CNTs, various forms of filamentous carbon were known and they were given names such as “carbon filaments” or “carbon whiskers”. After the discovery and naming of CNTs, the term “nano” began to be added to various filamentous carbon structures which were of the appropriately small size.

While many people use the different names given to carbon nanostructures interchangeably, others attempt to follow some sort of classification. Some reserve the name “carbon nanotube” only for carbon structures that are made out of true graphene cylinders which extend their lengths and call all other carbon nanostructures CNFs. Often one person will publish something using one term (such as CNTs) and someone else will cite it as being something else (such as CNFs). Currently there is no strict classification for these structures. In reality, there are very few people working with true CNTs, so a broadening of what can be classification under this name is called for.

In this dissertation, CNTs were grown by a dc PECVD process which will be described in detail in following sections. Although some authors might claim otherwise, I believe that all of the CNTs which have been reported from a process like this show a herringbone structure. These are referred to as CNTs by some and CNFs by others. I will use the term CNT to describe them since they are still nanostructured carbon made up of graphene planes with tubular and generally hollow cores (broken up by bamboo defects.)

2.3 Properties of carbon nanotubes:

From the preceding section, it is easy to see how the large variety in the types of CNTs will lead to different properties for each type of CNT. Since in this dissertation I focus on CNTs grown by dc PECVD, I will have my background on CNT properties also focus on these types of CNTs.

2.3.1 Structure:

To understand the structure of CNTs, we should first understand carbon. With atomic number 6 on the periodic table of elements, carbon has 4 valence electrons occupying $2s^2$ and $2p^2$ atomic orbitals. Although the 2p orbital is higher in energy than the 2s orbital, the difference is sufficiently small that the electrical wave functions of carbon's valance electrons can hybridize in sp, sp^2, and sp^3 states. The majority of carbon is found in the form of graphite or diamond. The sp^2 bonding leads to planar structures such as the graphene sheets that make up graphite and the sp^3 bonding leads to the tetrahedral geometry found in diamond. At standard temperature and pressure, graphite is the stable phase of carbon. Under the proper pressure and temperature (at room temperature about 30 kbar), conditions can be made such that diamond is the equilibrium phase of carbon, but there are no regions on the carbon phase diagram where CNTs are the expected equilibrium structure.[13]

The majority of the carbon nanostructures are based on sp^2 bonded carbon including CNTs and fullerenes (although the fullerenes have many defects where some of the hexagonal carbon rings have only 5 atoms and form into pentagons resulting in curvature of the sheet.)

The planer geometry formed by sp^2 bonded carbon atoms consists of hexagonal rings arranged in a honeycomb pattern. I refer to a single sheet of carbon bonded in this fashion as a graphene sheet. A schematic drawing showing a graphene sheet is shown in Figure 3.

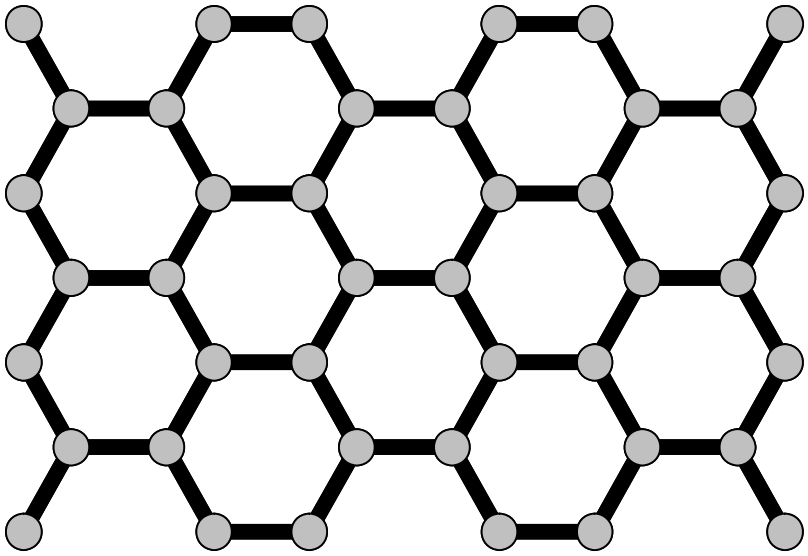

Figure 3: Schematic illustration of a graphene sheet made up of carbon atoms sp^2 bonded into a 2D sheet in a hexagonal honeycomb pattern.

Ideal CNTs can be pictured as sheets of graphene rolled up into cylinders. This process allows for the unfavorable creation of strain in the bending of the graphene sheet to be offset by the energetically favorable elimination of the dangling bonds at the edges of the graphene sheet. Although not the thermodynamically stable bulk phase, for fragments of graphene planes of the right size, the formation of a CNT is sometimes the most stable option available.

The rolling of a graphene sheet into a tube can be done along virtually any direction. In Figure 3 above, the right and left sides of the diagram are said to have a zigzag geometry while the top and bottom sides are said to have an armchair geometry. If the graphene sheet is rolled such that the two armchair edges meet and the zigzag edges are left at the ends of the tube, then it is called a zigzag CNT. If the graphene sheet is rolled up such that the two zigzag edges meet and the armchair edges are left at the ends of the tube, then it is called an armchair CNT. We could also roll the graphene sheet along several directions between these two high symmetry directions, and these result in what are called chiral CNTs. The mathematical identification of ideal CNTs can be done using their diameter and chiral angle θ. The chiral vector C_h is defined as:

$$C_h = na_1 + ma_2 \qquad (1)$$

The chiral vector is shown and explained graphically in Figure 4. Different types of carbon nanotubes have different values of n and m. Zigzag nanotubes correspond to (n, 0) or (0, m) and have a chiral angle of 0°, armchair nanotubes have (n, n) and a chiral angle of 30°, while chiral nanotubes have general (n, m) values and a chiral angle between 0° and 30°.

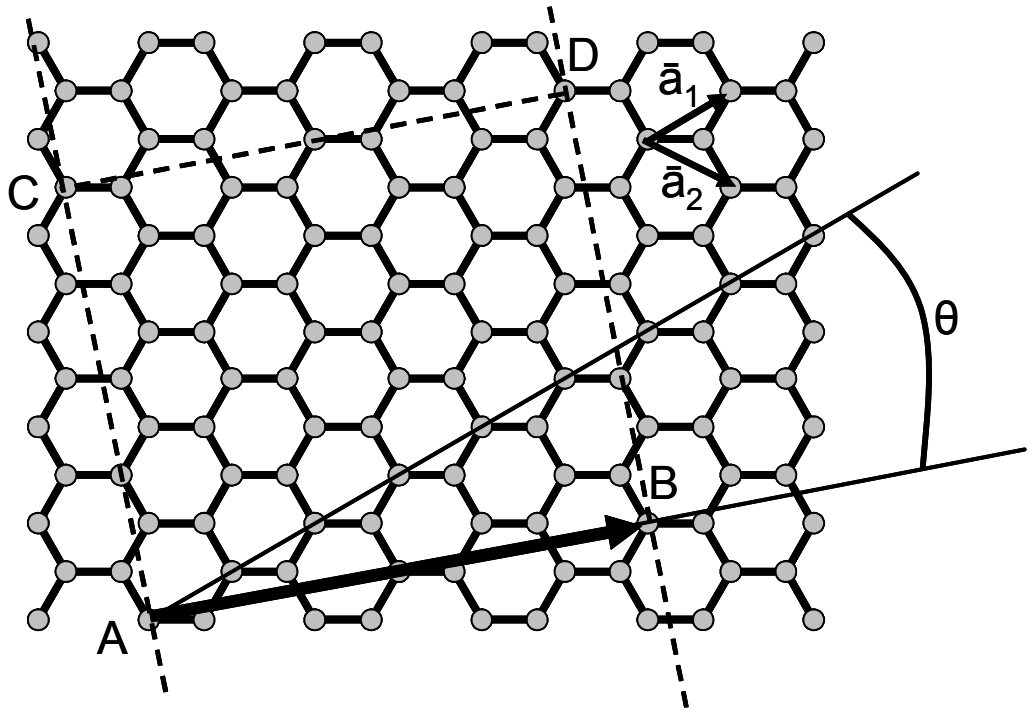

Figure 4: (a) The chiral vector is defined on the hexagonal lattice as $C_h = na_1 + ma_2$, where a_1 and a_2 are unit vectors, and n and m are integers. The chiral angle, θ, is measured relative to the direction defined by a_1. This diagram has been constructed for (n, m) = (4, 2), and the unit cell of this nanotube is bounded by ABCD. To form the nanotube, imagine that this cell is rolled up so that A meets B and C meets D, and the two ends are capped with half of a fullerene molecule.

These CNTs can consist of a single rolled graphene sheet known as a single walled CNT (SWNT) or as multiple graphene sheets rolled up concentrically which is called a multi-walled CNT (MWNT.) The rolling direction or chirality of a CNT is usually only important for SWNTs since in MWNTs each tube layer will have its own chirality and in neighboring layers these favor staggering rather than aligning of these rolling directions.

2.3.2 Mechanical properties:

The mechanical properties of CNTs have been studied experimentally and theoretically. One of the well known characteristics of CNTs, which is also true for most materials, is that a small diameter fiber is actually much stronger than the bulk material.[14] Table I summarizes some of numbers found in literature for various forms of carbon.[15, 16, 17, 18, 19, 20, 21, 22, 23, 24, 25, 26, 27] It can be seen that there is a large variance in the numbers that are reported, but a common general range can be drawn from this.

Table 1: Mechanical properties of carbon-based materials.

Material	**Tensil strength (GPa)**	**Young's modulus (GPa)**
Graphite	0.0138-0.069 (Ref. 14) 0.01-0.08 (Ref. 15)	1060 in plane (Ref. 16) 1020 parallel to basal, 36.4 perp. (Ref. 17)
Diamond	0.8-1.4 (Ref. 14)	1054 (Ref. 18) 700-1200 (Ref. 14)
SWNTs	50-200 (Ref. 14)	1000 (Ref. 14) 900-1700 (Ref. 19)
MWNTs	6.2-2.2 (Ref. 16) 11-63 (Ref. 20)	1800 (Ref. 21) 690-1870 (Ref. 19) 270-1280 (Ref. 22) 270-950 (Ref. 20)
Carbon Fibers	20 (Ref. 24) 2-5 (Ref. 25) 0.3-8 (Ref. 23) 1.5-4.8 (Ref. 14) 0.6-3.7 (Ref. 26)	700 (Ref. 14) 80-700 (Ref. 23) 228-724 (Ref. 14) 680 (Ref. 27)

Diamond is well known for having the highest stiffness of any known material due to its very strong sp^3 bonds which have a very high volumetric density. In the same way, the high planer density of strong but short sp^2 bonds in a graphene sheet result in a Young's modulus that is comparable to that of diamond.

Prefect SWNTs are the strongest known materials and have specific tensile strengths reported up to 100 times that of steel.[28] They have tensile strengths up to 200 GPa, Young's modulus around 1 TPa, and fracture strains up to 20%. Despite these amazing numbers, SWNTs are to expensive to produce and purify in bulk so are not yet utilized for their mechanical properties outside of laboratory research. Conversely, MWNTs are easier to produce in high volumes and are being more seriously investigated for applications which might utilize their mechanical properties. The mechanical properties of MWNTs are not quite as impressive as those for SWNTs due to the difficulties of making them defect free and the ability for graphene layers to slide past each other; however, their strength and modulus are still typically higher than that of steel.[14]

Carbon fibers, such as those presently used in polymer-matrix composites, are composed of both polycrystalline and amorphous carbon and have diameters ranging from hundreds of nanometers to several microns. Their mechanical properties are much less appealing than those of CNTs with tensile strengths about an order of magnitude lower and roughly half the Young's modulus. Despite this, since they are relatively easy and cheap to produce, they are used today in many applications and are the most commonly used reinforcement in many composits.

2.3.3 Electrical properties:

There is tremendous interest in CNTs for their electrical properties and there have been many theoretical and experimental results reported. Much of this reported work deals with SWNTs. The electrical properties of the various types of CNTs are quite different, so here I will focus on the conduction properties of CNTs like those grown by dc PECVD.

The resistance of CNTs which were suspended over two electrodes has been reported by measuring the current-voltage (I-V) curves.[29] These CNTs showed linear I-V curves at slight positive and negative applied voltages which corresponded to a resistance estimated at 1 kΩ/μm along the length of the CNT and resistivities, estimated using the CNT geometries, between 10^{-6} and 10^{-5} Ω m. Comparable values have also been reported for CNTs grown by arc discharge[30] and for ropes of SWNTs.[31]

It was demonstrated that the electrical breakdown occurred at current densities of 10^{7}-10^{8} A/cm^{2}, which is one to two orders of magnitude higher than that at which metal wires undergo electromigration.

To remove the effect of contact resistance in the measurement, four-point probe measurements were recently used to measure the I-V characteristics.[32] Zhang et al. used Ti/Au contacts which were patterned by electron beam lithography on top of individual CNTs. Their results also showed linear I-V behavior with a resistivity of approximately 4.2 X 10^{-5} Ω m. These results were also consistent with a basic model of electron transport through inter-graphitic planes as is necessary in the herringbone structured CNTs grown by dc PECVD.

2.3.4 Field emission:

Field emission involves the tunneling of electrons from a solid through the surface-potential barrier, which is typically equal to the work function φ of that material. An applied electric field can lower this barrier potential, but for most cases a very large field is required. The electric field that is of importance is the local electric field at the emitting surface, and this very much depends on the geometry of that emitting surface. For a thin rod, the geometric field-enhancement factor β is roughly proportional to height-diameter aspect ratio.[33] Since CNTs can have very high aspect ratios, it is possible to have very high electric fields at their ends when only modest electric fields are applied.

Field emission from carbon cathodes has advantages over other materials. It has been shown that carbon fibers can operate with performance similar to conventional tungsten field emitters at 20 times the pressure.[34] Also, due to the strong nature of the sp^2 bonding, graphitic carbon has the lowest sputtering yield of any material and is therefore more resistant to sputtering from ionized residual gas molecules than typically used refractory metal cathodes.[35]

2.3.5 Chemical and electrochemical properties:

In general, CNTs synthesized by dc PECVD are chemically stable. They are resistant to many of the standard etch processes including nitric acid, hydrofluoric acid, resist spin coating, exposure and development of resist, and fluorine-based dry etch processes. They also survive quite well in a variety of coating process including metal,

nitride, and oxide depositions. Etching of CNTs is usually achieved by electrochemical oxidation or by using oxygen containing plasmas.[36]

There are a number of ways to functionalize CNTs. Non-covalent methods have been used since the aromatic nature of the CNTs walls leads to strong absorption of aromatic compounds.[37] A review of covalent functionalization methods for CNTs is written by Bahr and Tour.[38] In highly defect free CNTs, the number of sites available for functionalization is limited. These CNTs are usually subjected to either mechanical or oxidative treatments such as sonication in sulfuric and nitric acid or piranha etch (sulfuric acid and hydrogen peroxide), electrochemical oxidation, or exposure to oxygen containing gasses or plasmas. Under these treatments, defect sites are usually formed at the ends of the CNTs.[39] In contrast to this, the CNTs grown by dc PECVD processes have a large number of defect sites along their walls at the ends of the inclined graphene planes which make up the walls of the CNTs. The CNTs grown by dc PECVD, with no surface treatment, provide many sites that can be easily functionalized. If a surface treatment like those listed above is employed, then the affected areas of the CNTs will cover their entire exterior and is not limited to the ends like in parallel walled CNTs.

One of the most used functionalization methods for CNTs is carbodiimide chemistry. Materials that contain amines, such as DNA and proteins, can be covalently attached using, for example, 1-ethyl-3-(3-dimethylaminopropyl) carbodiimide (EDC), to create carboxylic acid sites.[40] Using this method, functional enzymes have been attached to the tips of carbon nanostructures and used for the electrochemical sensing of glucose.[41]

Various carbon materials have been widely used as electrodes in chemical production and measurement equipment.[42] The electrochemical properties of vertically aligned CNTs have been reported by several groups. These results discussed densely packed MWNTs grown by thermal CVD,[43] less aligned and dense CNTs growth by thermal CVD,[44] low density arrays of vertically aligned CNTs growth by dc PECVD,[45] and dense vertically aligned CNTs grown by dc PECVD.[46]

2.4 Synthesis of carbon nanotubes:

2.4.1 Methods of synthesis of carbon nanotubes:

With the great range in the structure and properties of CNTs it is not surprising that there is also a variety of methods that these CNTs are made in. Early studies of CNTs involved synthesis by arc discharge,[47] and laser vaporization. While arc discharge and laser vaporization did allow for very high purity CNTs to be produced in reasonable yields, they did not allow any control over the location or spatial morphology of the CNTs. Also, although the CNTs produced were often high purity, they needed to go through complicated separation procedures to isolate them from the residual catalyst material and amorphous carbon particles that they were surrounded by.

Currently, catalytic growth of CNTs by CVD is the most efficient way to have a controlled synthesis of CNTs.

2.4.2 Catalytic growth of carbon nanotubes:

The catalytic growth of carbon nanostructures has been studied for some time now, as was summarized in section 2.1. Generally, in the growth of CNTs, the catalyst takes the form of a metal nanoparticle. Some type of carbon containing species is brought into contact with the catalyst particle (through a process such as CVD, which will be discussed below), the species is decomposed, and carbon diffuses across the catalyst particle.[48] The metal nanoparticle continues to incorporate carbon into it until it becomes supersaturated. Once this occurs, the carbon will begin to precipitate at the surfaces of the metal catalyst particle.[49] The equilibrium phase of carbon at the temperature and pressure that growth is carried out is typically graphite. A CNT is never the thermodynamically expected phase of carbon, but under the right conditions, it is kinetically favorable for the graphitic carbon that is precipitated at the surface of the catalyst particle to be formed into cylinders or funnels and grow into CNTs. By precipitating a section of a graphene plane at the surface of a catalyst particle, and then repeatedly precipitating a new graphene plane at that same interface, a CNT grows by continuously creating the new CNT at the interface of the catalyst particle. A schematic illustration of this is shown in Figure 5.

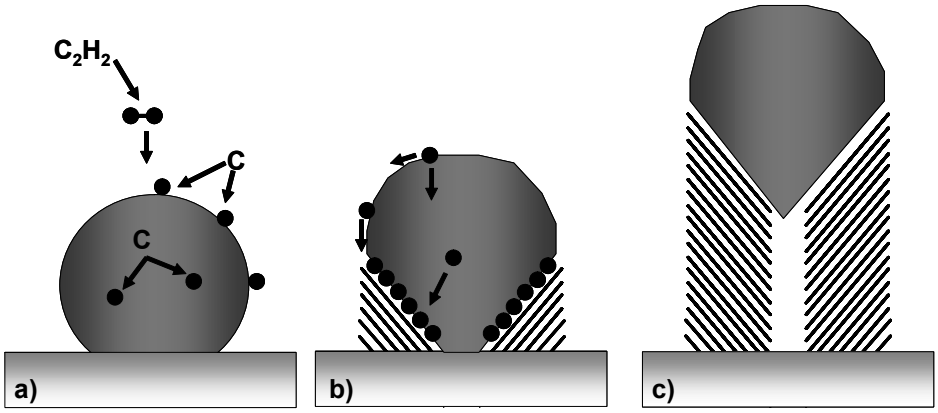

Figure 5: Schematic illustration of the catalytic growth of carbon nanotubes grown by dc PECVD.

In Figure 5, the schematic illustration shows a catalyst particle which is initially on the surface of a flat substrate; this is a typical starting configuration for CNTs grown by dc PECVD. A carbon source, in this case C_2H_2, is decomposed at the surface of the metal catalyst particle (such as Ni.) Elemental carbon diffuse either through the bulk of the catalyst particle or along the surface of the catalyst particle. After the catalyst particle becomes supersaturated with carbon, it begins to reject some of it out and precipitate it at a surface to form sections of graphene planes. The process continues dynamically as new carbon source is continuously supplied and broken down, carbon diffuse across or through the catalyst particle, and new graphene planes are created at an interface of the catalyst particle causing the CNT to grow. The catalyst particle shape and inclined planes shown here are typical of those observed when Ni is used as the catalyst particle in a dc PECVD process. Recently, direct observation by in situ electron microscopy have shown CNTs growing from metal catalyst particles during the decomposition of acetylene.[50]

There are two distinct growth modes that have been observed for the catalytic growth of CNTs. In one case, the catalyst particle can remain on the substrate while the CNT is grown up above it. At the end of growth, a CNT which has its catalyst particle at the substrate is said to have grown in a base-growth mode. In contrast, if the catalyst particle lifts off of the substrate and the growing CNT is beneath it, like pictured in Figure 5, then at the end of growth the catalyst particle will still be at the tip of the CNT and this is referred to as tip-growth. The choice between base and tip growth modes has been largely related to interaction between the catalyst metal and substrate upon heating and initiation of CNT growth processing. Although the choice of materials plays the largest role, there have been reports of controlling which mode will be used by altering other processing conditions such as the plasma power or gas compositions.[51, 52]

2.4.3 Chemical vapor deposition:

CVD involves the incorporation of a vapor species at the surface of a growing film. This incorporation can take various forms including adsorption, desorption, decomposition, or other reactions. As most reactions of these sorts run faster at higher temperatures, CVD growth of CNTs is usually carried out in a furnace or with a heater near the substrate that the growth is taking place on. The CVD growth of CNTs is almost exclusively a catalytic growth process involving metal catalyst particles. Here I discuss two types of CVD for the growth of CNTs, thermal CVD, and plasma enhanced CVD.

2.4.3.1 Thermal chemical vapor deposition:

The majority of thermal CVD systems consist of a quartz tube inside of a furnace with a gas flowed through it. Although processing temperatures between 400 °C and 1200 °C are used, most of the thermal CVD growth of CNT is carried out above 800 °C. A schematic illustration of a typical tube furnace type thermal CVD system is shown in Figure 6.

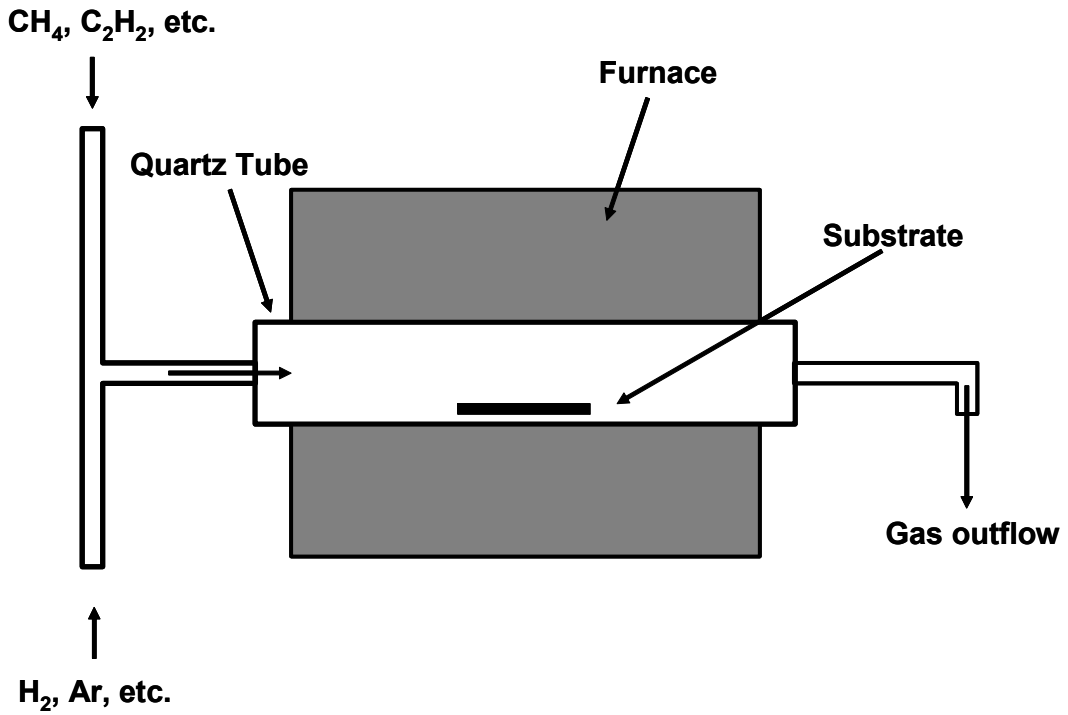

Figure 6: Schematic illustration of a typical tube furnace type thermal chemical vapor deposition system.

The CNTs are usually grown on a substrate and this substrate is positioned in the quartz tube in the desired temperature region of the furnace. The catalyst particles can either start on the substrate in what is usually referred to as the supported catalyst

method,[53] or the catalyst particles are carried in or form from a source gas which passes over the substrate in what is referred to as the floating catalyst method.[54] Various carbon sources can be used such as methane (CH_4) and acetylene (C_2H_2).

Thermal CVD has been shown very effective in producing both MWNTs[55] and SWNTs.[56] Generally, to make SWNTs the catalyst particle size needs to be sufficiently small, the carbon gas supply should be low, and the processing temperature should be high (at least above 900 °C).[57] By optimizing the catalyst particles and other processing conditions, dense arrays of vertically aligned CNTs have been reported having lengths of 3.5mm[58].

In the CVD growth of CNTs, the supply of carbon depends on the rate of arrival of the carbon containing gas species, their adsorption rates to the surface of the catalyst particle, and their decomposition rates. It has been suggested for some time that the rate determining step in the growth of CNTs by this method is the diffusion of carbon through the metal catalyst particle. This theory is supported by the fact that the activation energies for CNT growth are very similar to that for the diffusion of carbon through the metal used as the catalyst. The driving force for the diffusion of carbon from one side of the catalyst particle to the other was initially attributed to a temperature gradient[59] which was believed to result because of exothermic decomposition reactions taking place at one surface of the catalyst particle. It was later proposed that rather than temperature gradients, it was a concentration gradient that drove the diffusion of carbon. The reason for such a concentration gradient could be because of different carbon solubility at the gas-metal and metal carbon interfaces,[60] a

solubility difference between the metal-carbon and the metal carbide-carbon interfaces,[61] or one of several other proposed theories.[62, 63]

Recently, detailed time resolved atomic resolution in situ TEM observations of the growth of CNTs from a Ni catalyst particle have been performed.[64] They observed the nucleation and growth of graphene planes assisted by the dynamic reshaping of the Ni nanoparticles. In their new proposed mechanism, the graphene planes form at terraces between the steps in the curved but constantly changing Ni nanoparticles. The process involves the diffusion of C and Ni atoms along the surface and does not require any carbon to diffuse through the bulk of the catalyst particle.

Although many people have been working on explaining the catalytic growth of CNTs in a CVD process for some time, the proposed theories are still varied and it is still unclear which mechanisms are really dominant.

2.4.3.2 Plasma enhanced chemical vapor deposition:

A variation of CVD that is often used to grow CNTs is plasma enhanced chemical vapor deposition (PECVD). This process combines the basic processes from thermal CVD with one major addition; the presence of a plasma around or in the vicinity of the substrate.[65] In thermal CVD, it is thermal energy that activates the gas and leads to decomposition; however, in PECVD, the impact from ions and especially electrons activates the molecules in the gas. Most CNT growth by PECVD is carried out at a heated temperature, but the presence of the plasma reduces the activation energy for the growth of CNTs and allows for the deposition to take place at lower temperatures than those required for thermal CVD.

There are a number of different types of PECVD systems that have been used in the synthesis of CNTs including direct current (dc),[66] hot-filament dc,[67] radio frequency (rf),[68] microwave,[69] inductively coupled plasma (ICP),[70] electron cyclotron resonance (ECR),[71] hollow cathode dc,[72] and corona discharge plasma.[73] Although many of these are closely related, they do each have distinct differences and have their own advantages and limitations. In this work, all of the CNTs have been grown in a dc PECVD system, so I will limit my discussion to this specific PECVD process.

A schematic illustration of a dc PECVD chamber is shown in Figure 7. The sample is placed on the cathode which is either heated by a nearby heater, or the heater itself is used as the cathode. One limitation of this process is that the choice of substrates is generally limited to those that are conductive.[74] An anode is place above the cathode and sample. With a controlled supply of gas flowing through the chamber, a negative bias is applied to the cathode and with the right combination of pressure, temperature, and applied bias, a dc glow discharge will form. Since the sample is generally conductive and becomes an extension of the cathode, the cathode sheath forms over the substrate and within this sheath the CNTs grow up from the substrate. This configuration conveniently has a strong electric field perpendicular to the majority of the substrate surface, and it is common to use this to grow vertically aligned CNTs. I will discuss this in greater detail in Chapter 4.

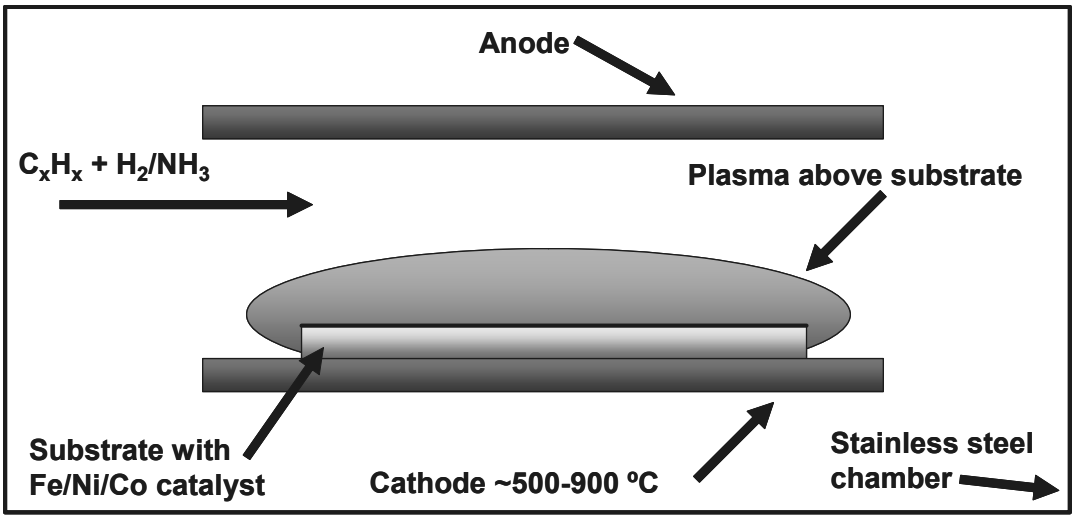

Figure 7: Schematic illustration of a dc plasma enhanced chemical vapor deposition system.

2.5 Applications of carbon nanotubes:

Since their discovery, CNTs have been studied for many different applications because of their exceptional properties which we summarized above. They have already been shown useful for a variety of applications such as field emission devices,[75, 76, 77] nanoscale electromechanical actuators,[78, 79] field-effect transistors (FETs),[80] CNT-based random access memory (RAM),[81] and atomic force microscope (AFM) probes.[82] There has also been work demonstrating the potential of CNTs has nanointerconnects[83] including no obvious degradation after 350 h in their current carrying capacities at very high current densities of 10^{10} A/cm^2,[84] the manufacture of deterministic CNT wiring networks,[85] and using an electron beam to form mechanical connections between two CNTs.[86] While the range of potential applications is quite varied, the majority of these are still far from being used outside of research laboratories. Two areas where CNTs, especially those grown by dc PECVD, have a

good chance at being used more widely are as field emission sources or as scanning probe microscopy tips.

2.5.1 Electron field emission sources:

There have been several recent reports of simple electron field emission devices using nanostructured carbon as the electron sources.[87, 88, 89] While some devices have been made based on CNTs which were grown in a thermal CVD system, so far only the dc PECVD process has been able to provide the spacing and alignment necessary to make a good field emission device.

One way to create a CNT based field emission device is to grow CNTs in the center of prefabricated holes with the gating electrodes already in place.[90] This has been done, but these devices suffered from the fact that the prefabricated gate structure was inevitably damaged by the plasma processing due to charging and arcing of the electrically isolated gate electrode. Guillorn et al. was able to fabricate gated structures around already grown vertically aligned CNTs.[91] Their process produced multiple devices on a substrate which operated with less than 2% of the emitted current being colleted by the gate electrode. Eventually, a microfabricated electron field emitter with a CNT source was fabricated that included not only a gate electrode, but also an integrated electrostatic focusing electrode.[92] This focusing electrode allowed them to adjust the electron beam size and allowed for an array of these emitters to be used for projection electron-beam lithography.[93] A device like this might also be used as the electron source to generate light by exciting a traditional phosphor display (replace the scanning electron beam in the CRT with multiple electron emitters for each pixel.)

2.5.2 Scanning probe microscopy tips:

Scanning probe microscopy has become one of the most often used tools for metrology and profilometry of various surfaces. The atomic force microscope (AFM) is used is used in the semiconductor industry, for biological samples, and in many other areas to observe surface features.[94] The most important part of an AFM is its probe tip, and these tips are usually made out of Si which has been etched into pyramidal shapes. While it is possible to etch a pyramidal Si tip down to a tip sharpness under 10 nm, there are several disadvantages of using Si tips.

The resolution of an image obtained with an AFM is, among other things, limited by the sharpness of the probe tip. While 10nm tips are possible with Si, this is a difficult standard to achieve uniformly. Also, these single crystal Si tips are extremely brittle and their sharp tips dull or break very quickly. This causes a limited lifetime for the Si tips and a degrading image quality the longer a particular tip has been used. Also, the pyramidal shape of the Si tips is limited to low aspect ratio configurations due to the preferred etching directions of Si and of the difficulties in micromachining Si without breaking the tips.

For several reasons, CNT probe tips show great promise for use in AFM. The tip diameters of CNTs can be made smaller than 10nm, down to as small as 1nm, and therefore can offer very high resolution.[95] The mechanical properties of CNTs are far superior to those of Si. Tips made from CNTs are much more resistant to breaking and do not loose their tip sharpness like pyramidal tips do. For advanced applications, specific chemical functionalization can be done to CNT tips.[96] While some early CNT

AFM tips were made by attaching already grown CNTs to conventional Si tips, this process is difficult and unreliable to reproduce. Directly growing CNTs on the AFM cantilever seems to be a superior way to make useable tips and this has been demonstrated to be feasible on for large scale production on a wafer scale.[97]

CHAPTER 3: EXPERIMENTAL TECHNIQUES

3.1 Carbon nanotubes growth by dc PECVD:

The growth of aligned arrays of CNTs was carried out using a dc PECVD process using Ni catalyst particles with a tip-growth mechanism. A mixed gas of ammonia (NH_3) and acetylene (C_2H_2) was used for the CVD growth. The forest like arrays had densities ranging from ~10^9 to ~10^{10} CNTs/cm^2. They were fabricated by first sputter depositing a 50 Å thick Ni film over the surface of an n-type Si (100) substrate. The substrates were then transferred (in air) to the CVD chamber. Upon heating to ~700 °C in a low pressure hydrogen atmosphere, the Ni film breaks up into islands with average diameters of 30 to 40 nm. After the formation of the catalyst islands, the atmosphere was changed to NH_3 gas flowing at a rate of 150 sccm. A DC bias of 550 V was applied between an anode above the sample and a cathode just below the sample. Under the applied voltage, plasma formed and C_2H_2 gas was added to the chamber flowing at 30 sccm with the total NH_3 and C_2H_2 pressure held at 3 torr.

The substrates were heated with an electrical resistance heater which was beneath the sample stage. The heater was powered by a dc power supply and could take a maximum current of 10 amps (A), a maximum voltage of 45V, and reach a maximum temperature of 950 °C. The heater was always operated within these limits. In a typical experiment, the heater was given 5 A for 3 minutes, then 7 A for 3 minutes, and finally 9 A for the reminder of the experiment. A normal heating time was 30 minutes including the ramping stages. The temperature of the stage was monitored with a K-

type thermocouple which was embedded between the stage and the heater. A typical temperature profile is shown in Figure 8.

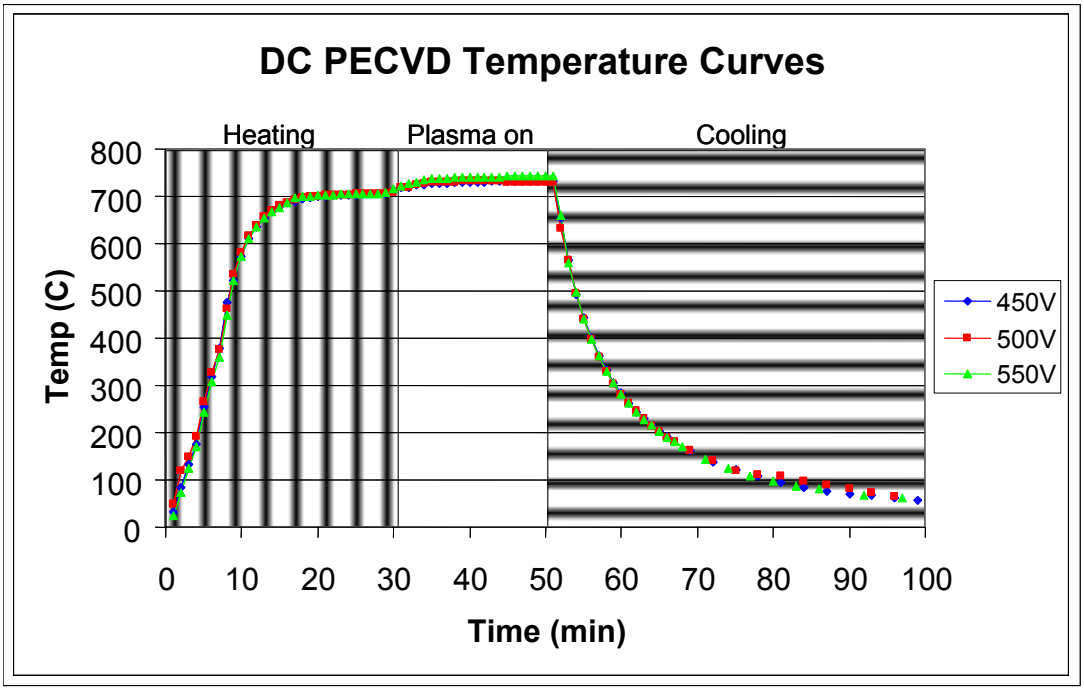

Figure 8: Plots of the dc PECVD stage temperature during the heating, growth, and cooling stages in three typical CNT growth experiments carried out with different applied biases to the cathode.

The plots in Figure 8 show the temperature curves for three experiments carried out under different applied biases to the cathode. In all three experiments, the total heating time was 30 minutes, the CNT growth time was 20 minutes, and the samples were cooled at least 50 minutes. After heating, the temperature is slightly above 700 °C. Once CNT growth is started, the temperature rises again slightly due to heating from the plasma. Higher applied biases will lead to higher plasma powers which will in turn lead to a greater increase in temperature due to the presence of the plasma.

The heater temperature had a close to linear relationship with the current that was supplied to it. A plot of this is shown in Figure 9.

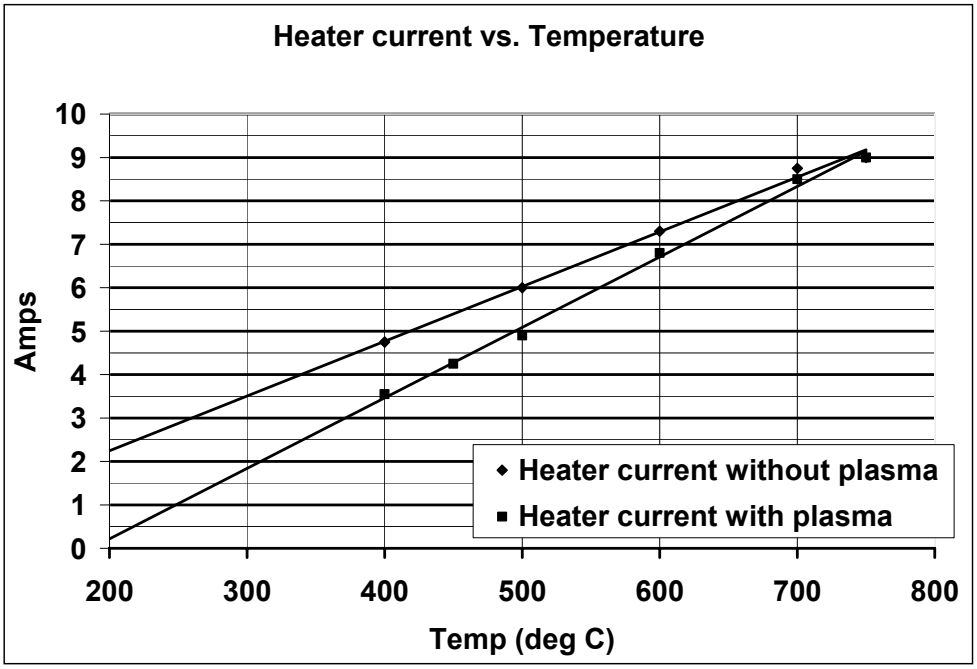

Figure 9: Heater current verses substrate temperature with and without the presence of plasma in the dc PECVD system.

From Figure 9 we can see that the temperature has a linear relationship with the current supplied to the heater both with and without the presence of plasma. The temperature increase due to the plasma is larger at lower temperatures, as can be seen by the divergence of the two lines.

A schematic illustration of the entire dc PECVD system is shown in Figure 10.

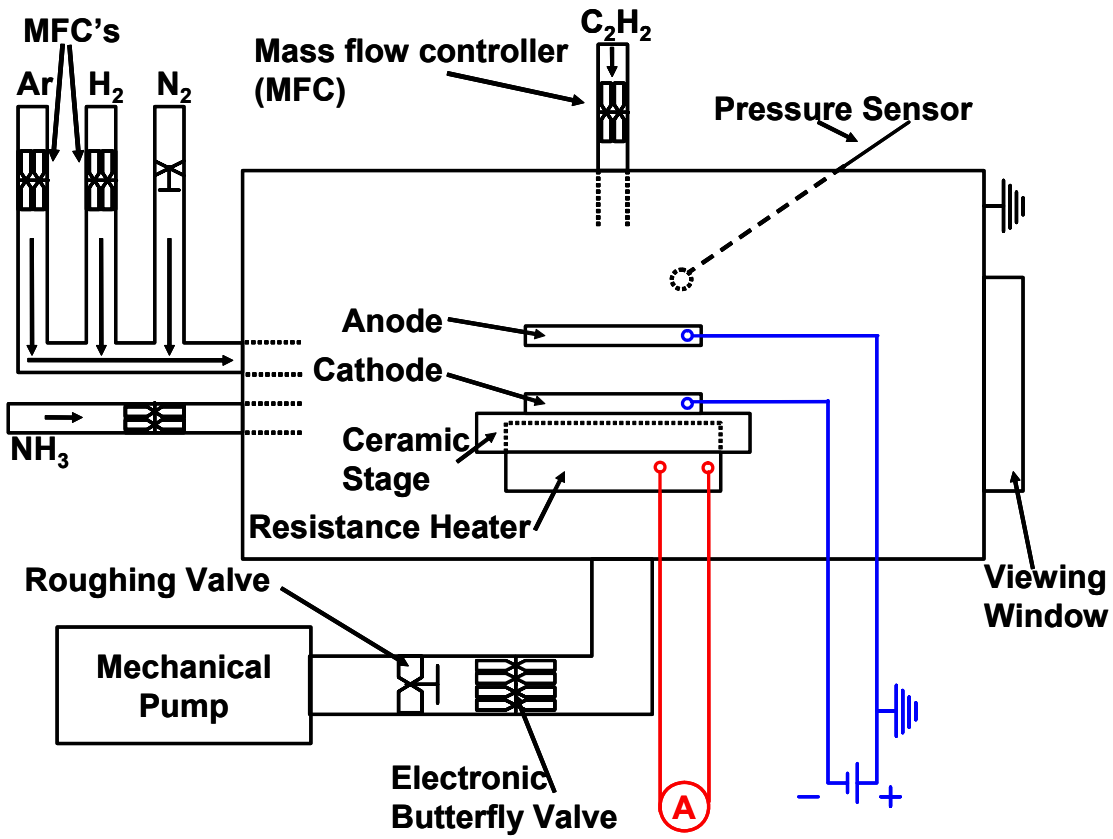

Figure 10: Schematic illustration of the dc PECVD system used to grow the CNTs shown in this work.

The chamber is stainless steel and has a total internal volume of approximately 11 liters. Gas was introduced to the chamber through stainless steel tubing and feedthroughs. While C_2H_2 was flowed from the top of the chamber directly at the substrate stage, all other gases were flowed from the side of the chamber parallel to the substrate stage. With the exception of nitrogen (N_2), all gas flows were controlled by MKS mass flow controllers which were periodically calibrated. The NH_3 mass flow controller contained all metal seals and all of the other mass flow controllers were elastomer sealed. Since N_2 was principally used as a chamber venting gas, its flow was

controlled by a pressure regulator on the compressed gas cylinder and a pin valve just outside of the chamber.

Pressure control was achieved using an electric motor mechanical pump, a pressure sensor and controller, and a butterfly valve. The mechanical pump had only an on and an off setting and was isolated from the chamber by a manual roughing valve. When a controlled low pressure was desired, the roughing valve was left completely open and the pressure controller would adjust how much to open the butterfly valve based on its reading from the pressure sensor. The gas flow rate through the system was dictated by the total input flow through the mass flow controllers. By adjusting the position of the butterfly valve, a desired constant chamber pressure could be achieved (open the butterfly valve more to get a lower pressure, and less to get a higher pressure.)

The cathode also served as the substrate stage. The cathode was electrically isolated from the anode and the rest of the chamber. The anode and the chamber walls were both connected to the same ground. A negative bias was applied to the cathode by an external power supply. Insulated high voltage electrical feedthroughs were used along with 1 mm copper wires insulated in ceramic designed for high temperatures.

3.2 Substrate preparation:

The substrates used were predominantly n-type Si wafers with (100) orientations. Care was taken to keep the Si wafers in clean (dust free) containers and storage areas, however no effort was made to clean the wafers or to remove the native oxide (SiO_2) present on the wafers' surfaces. For random forests of CNTs, a catalyst thin film was deposited across the entire surface of a Si wafer. The films were

deposited with various magnetron sputtering or electron beam evaporation systems. Although Ni was the most often used catalyst metal, Co and Fe were used for certain experiments. The thickness of the thin film ranged from 10-200 Å, with the most often used thickness being 50 Å. For patterned growth of CNTs, electron beam lithography was used to create circular patterns in a resist (polymethyl methacrylate, PMMA). After removing the PMMA in the patterned locations, metal thin films were deposited as before across the entire substrate, but only actually coming into contact with the exposed areas of the substrate. The remaining resist was then lifted off leaving metal catalyst circles in the desired pattern. Various pattern sizes and spacings were chosen with the most common island diameter being 200 nm and a typical spacing being 2 μm.

3.3 Pre-etching and post-etching:

For some samples, after heating but before initiation of CNT growth, a plasma pre-etching step was inserted. Typically this was carried out at the same temperature that the subsequent CNT growth was to be carried out at. An atmosphere of H_2 or NH_3 at a pressure similar to the intended growth pressure (typically about 3 torr) was placed in the chamber and a plasma was ignited by applying a negative bias to the cathode in the same way as during growth. For samples grown at lower temperatures, typically a 1 minute NH_3 pre-etch preceded the addition of C_2H_2 to that same plasma which initiated the growth of the CNTs.

For the removal of carbon capping on the catalyst particle after growth, sputter etching was performed at room temperature in the same dc PECVD system as the CNTs were grown in after the growth was completed and the chamber was cooled to room

temperature. Samples were placed under H_2 flowing at 35 sccm and held at 0.5 Torr within the chamber. A bias of 500 V was applied and plasma formed with a current of 2 mA. A sputter etching time of 5 to 10 min. was used to remove the carbon deposition on the catalyst particles of the CNTs.

For the removal of the catalyst particles after CNT growth, sputter etching was performed at room temperature in the same dc PECVD system after the CNT growth was completed and the chamber was cooled to room temperature. In order to track the microstructural evolution during the nanotube opening, the etching of samples was interrupted in stages, with the sample removed and examined before replacing in the chamber for further processing. Samples were first placed under H_2 flowing at 35 sccm and held at 0.5 Torr within the CVD chamber. A bias of 500 V was applied and plasma formed with a current of 2 mA. Subsequent plasma processing stages involved increasing the H_2 flow rate to 70 sccm, increasing chamber pressure to 1 Torr, and increasing the processing time. Cumulative sputter etching time for samples was typically 45 – 60 minutes with the majority of the minutes spent under very mild plasma conditions to cause a very controlled and gradual evolution of morphology so that all of the CNT opening stages could be observed. The etching was started with the sample and chamber at room temperature (23 °C) and the temperature increase for the Si sample substrate during hydrogen plasma processing was very small, typically being less than 5 °C. It should be noted that the local temperature at the tip of a CNT will likely be very different than the sample temperature under ion bombardment. In addition to hydrogen ions, sputter etching was also performed using heavy ions such as

argon. The flow rates employed were in the range of 20 to 65 sccm, with a pressure of 0.5 to 1 Torr. Plasma was formed under applied biases ranging from 300 to 500 V.

3.4 Electrode geometry modification:

The majority of electrode modification in this work was done to the cathode in order to control the directions of the electric fields which control the growth directions of the CNTs. The anode was made of 3 copper (Cu) wires of 1 mm diameter which were parallel to each other over the substrate stage and bended to meet each other at their ends. The only issue of concern with the anode was to support it while keeping it electrically insulated from the cathode. The main cathode was made of a flat molybdenum (Mo) disk shaped plate (Alfa Aesar, 99.95%) with 1 mm thickness and 4 cm diameter. This main cathode stage was modified by either replacing that cathode stage with one of a different geometry or by placing in electrical contact additional cathode modification pieces. These modified cathode pieces were made from either Mo or tungsten (both Alfa Aesar, 99.95%) plates, foils, or rods of various thicknesses or diameters. The pieces were cut using a Buehler Precision Diamond Wafering Saw. Shaping was done on a rotary abrasive grinder and polishing was carried using standard metallographic sanding and diamond slurry polishing solutions.

3.5 Sample analysis:

For microstructural analysis, scanning electron microscopy (SEM) was performed in a Philips field emission SEM. Cross sectional high resolution transmission electron microscopy (HRTEM) was performed on a JEOL 3010

transmission electron microscope (TEM) operated at 300 kV. Nanodiffraction analysis was performed in convergent beam electron diffraction (CBED) mode.

CHAPTER 4: RESULTS AND DISCUSSION

4.1 Growth of vertically aligned carbon nanotubes:

Vertically aligned CNTs have been demonstrated by dc PECVD by other groups.[57, 74, 107] The majority of the CNTs grown in this work were in the form of "forests" where the diameter and location of each CNTs was not controlled but on average the CNTs found at any area of the forest were similar to those found elsewhere. Such a forest of CNTs was usually grown from catalyst particles that formed from an initially continuous Ni thin film. After heating to CVD processing temperatures (typically around 700 °C) the Ni was still well below its melting temperature, but as the thin film begins to crack under the stresses it experiences due to heating, the Ni atoms rearrange and agglomerate into spherical particles in order to minimize surface energies.

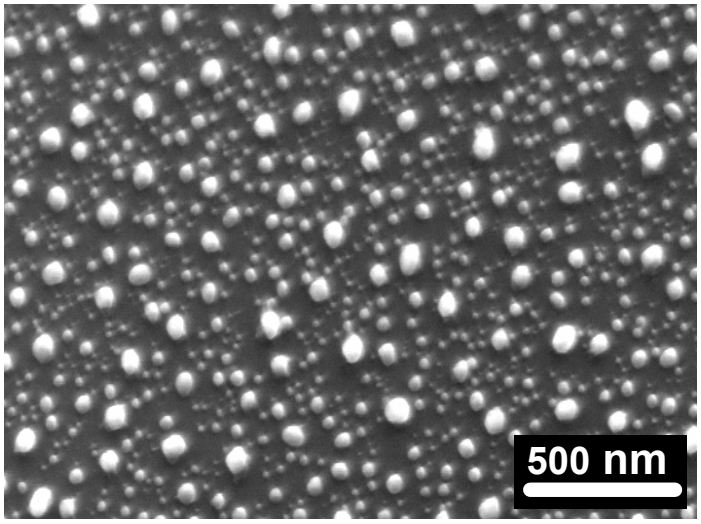

Figure 11: SEM image taken perpendicular to a Si substrate showing Ni nanoparticles formed after heating a 5 nm Ni thin film to 700°C and holding for 15 minutes.

An SEM image of a typical distribution of Ni nanoparticles that were formed after heating a 5 nm sputtered Ni thin film is shown in Figure 11. It can be seen that some of the particles are two or three times larger than the smaller ones and that the arrangement of the particles is random; however, the number of particles in a given area is very consistent across the Si substrate as is the distributions of diameters.

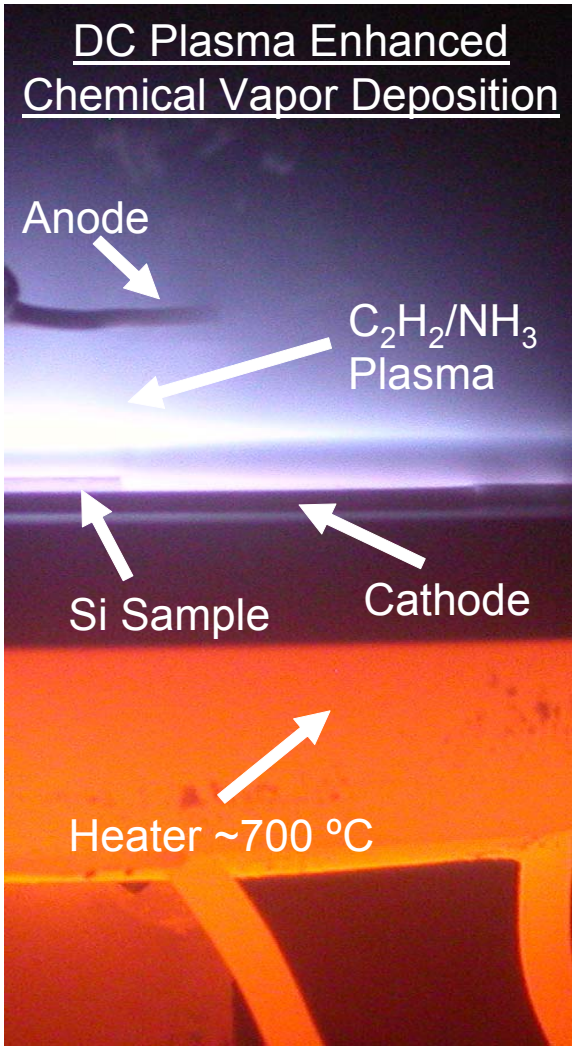

Figure 12: Photograph showing the experimental process for growth of CNTs by dc PECVD.

A photograph which was obtained during the growth of CNTs in our dc PECVD system is presented in Figure 12. The CNTs were grown on the surface of a Si wafer which was placed in the center of the cathode stage. The sample is heated by the resistance heater beneath it and the carbon source comes from the acetylene/ammonia plasma that is present above the sample.

A typical image showing a vertically aligned forest of CNTs grown by dc PECVD is shown in Figure 13. The distributions in the diameters is much more narrow than was observed from the Ni nanoparticles since at the start of plasma processing, the majority of the smallest Ni particles become incorporated into the larger particles. The sample is tilted at 45° so it is difficult to see the real height distributions, but it is clear that not all CNTs are the same height.

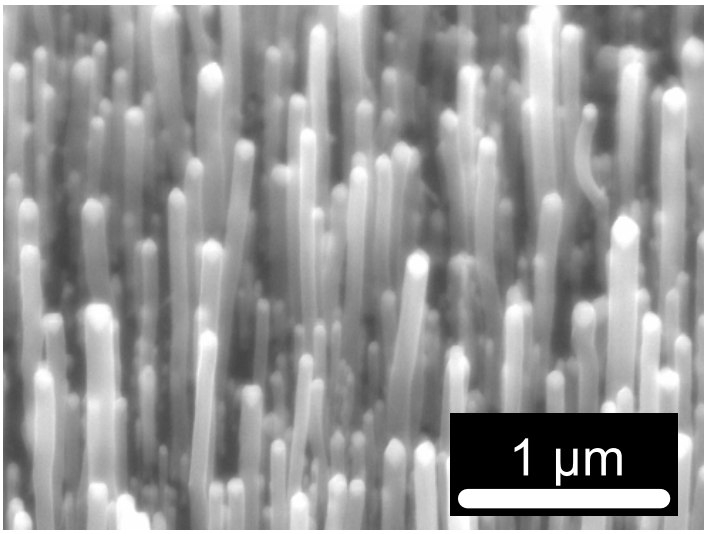

Figure 13: SEM image of a forest of CNTs growth from Ni catalyst particles. Sample is tilted away at 45°.

Some of the CNTs grown in this work were patterned using photolithography or electron beam lithography. By patterning circles of the proper size, it was possible to deposit only enough catalyst material to form one catalyst particle for each patterned circle, allowing us the ability to control the location of each individual CNT. Shown in Figure 14 are examples of individually patterned cone shaped CNTs. The cone versus tube morphology will be discussed in the following section.

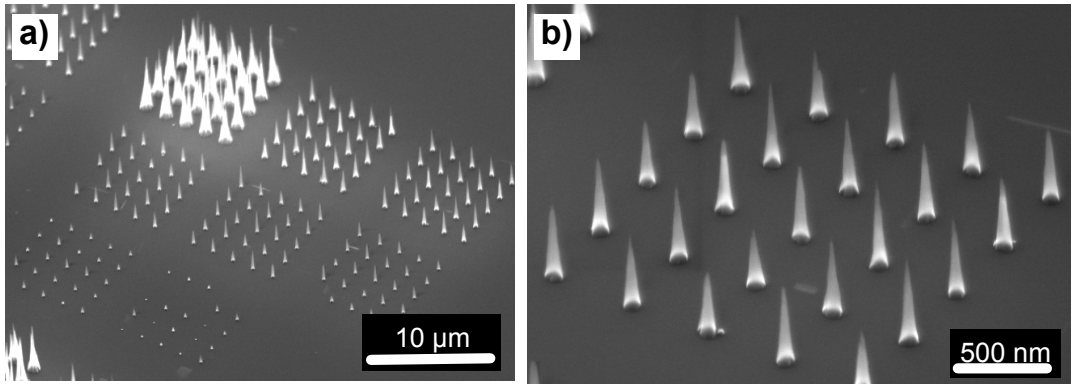

Figure 14: SEM images of individually patterned cone shaped CNTs. The patterning was achieved by electron beam lithography of circular patters in which enough catalyst material was deposited so as to create only one catalyst particle on each pattered circle and result in one CNT. Various sizes are shown in a) and an enlargement of the CNTs grown on 300 nm patterns is shown in b).

4.2 Cone versus tube morphology:

While there have been a very large number of publications on CNT growth itself, there have been few reports on enabling discoveries as to how to manipulate them to move up to the next level of scientific or technical advances. Engineering the shape of CNTs is an important issue for successful applications of CNTs. A cone-shape structure can provide mechanical stability yet provide very sharp tips, which may be

useful for enhanced electron field emission. In this section, I report how a manipulation of applied dc bias can be utilized to control the CNT morphology, from tube to cone shape, as well as to synthesize composite CNT configurations during CVD growth.

Shown in Figures 15 (a)-(d) are the SEM images of CNT samples grown on Ni (~5 nm thick) coated Si substrate at a dc bias voltage of 450 V, 500 V, 550 V and 600 V, respectively, for 20 min. As the plasma power was kept in a small range of 35-50 W for different applied bias voltage and the heater current was kept the same, samples in this study were grown at similar temperatures. All other processing parameters including the heating time and ammonia/acetylene gas composition were kept constant. The striking difference in CNT morphology induced by the voltage change is apparent from the figure. At the lower bias fields, such as 450 V and 500 V, slender, straight and equi-diameter CNTs with ~30-60 nm diameters were grown vertically aligned as shown in Figures 15 (a) and 1(b). The Ni catalyst particles with about the same diameters as those for the CNTs are present at the tips of all nanotubes indicating the occurrence of tip-growth mechanism. In contrast to the 450 V sample, the 500 V sample (Figure 15(b)) begins to show the tendency toward transition to a cone-like structure, with the CNT diameter still wire-like but becoming slightly tapered and getting larger at the lower part of the CNTs. It is also noticeable that the catalyst particle diameter is beginning to get smaller as compared to the 450 V sample.

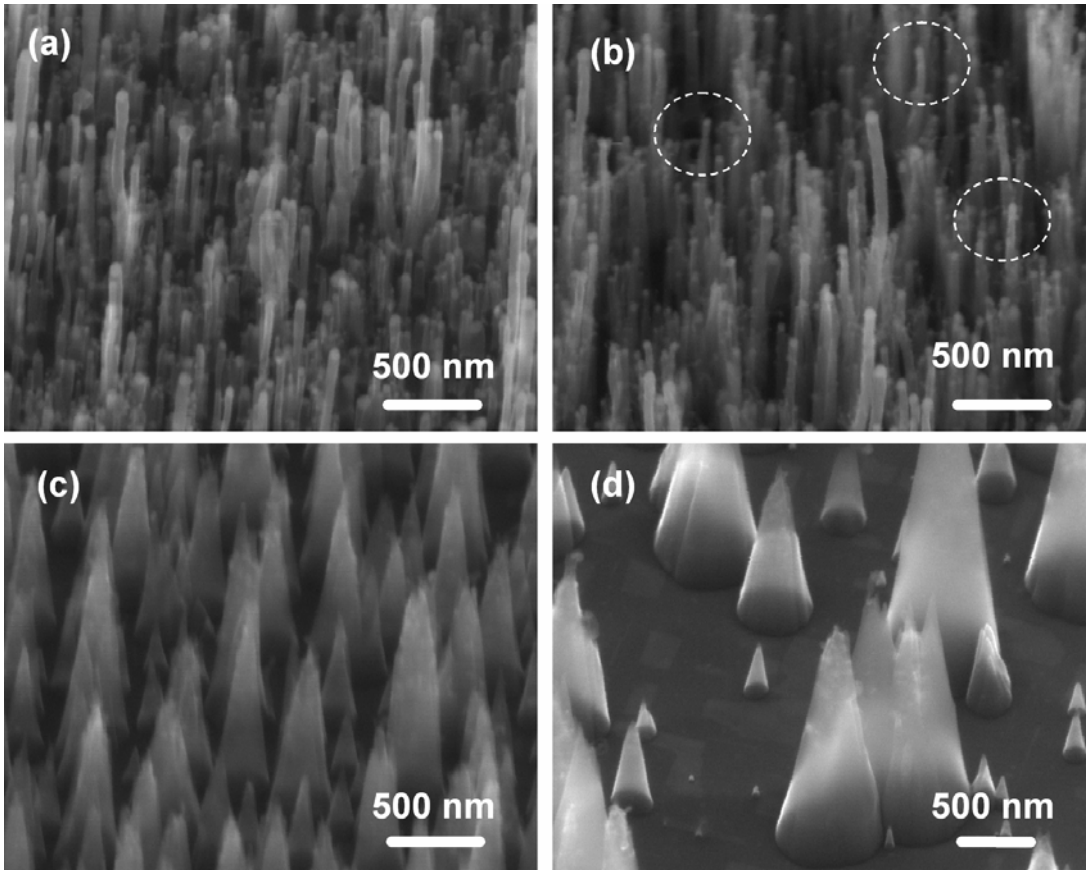

Figure 15: SEM images of CNT samples grown on Ni (5 nm) coated Si substrate at a dc bias of (a) 450 V , (b) 500 V, (c) 550 V and (d) 600 V, respectively, for 20 min.

For a higher applied voltage of 550 V, Figure 15(c), predominantly nanocone-like CNTs with very sharp tips are obtained. The base diameter at the bottom of the nanocones is much larger than the nanotube diameter in Figure 15(c), with the cone base diameter varying from 100-300 nm. It is important to note that almost all nanocones show no Ni catalyst particle on the tip, which indicates that the carbon nanotubes essentially stopped growing once the nanocone structure is completed. Perhaps related to this is the observation that the nanocone tips are very sharp, with the radius of curvature estimated to be as small as ~5 nm dia. The nanocone tip appears to

be much sharper than the typical equi-diameter nanotubes in which tip radius of curvature is dictated and limited by the presence of a spherical catalyst particle which has a finite radius of curvature. At an even higher bias of 600 V, Figure 15(d), the nanocones become much shorter and the aspect ratio gets smaller. These cones have larger base diameters as large as 500 nm, and their density is much lower compared to the ones grown at 550 V. The simultaneous appearance of smaller nanocones may imply that the larger nanocones grow at the expense of smaller nanocones.

TEM images of the samples grown at 450 V and 550 V respectively for 20 min, are shown in Figures 16(a) and 2(b). Figure 16(a) shows the tube-like structure with a Ni catalyst cap on top of carbon nanotubes. Figure 16(b) is the TEM micrograph of a broken-off nanocone from the 550 V sample. The cone is crystalline with some inclusions. In some of the nanocones there appears to be a darker, shell-like region. EDX spot analysis indicates that the cone matrix contains carbon as well as Si. The tiny inclusions, which may be present either inside or on the surface of nanocones, were identified to be mostly composed of Ni. Further microstructural analysis is required to fully understand the detailed structure of the nanocones.

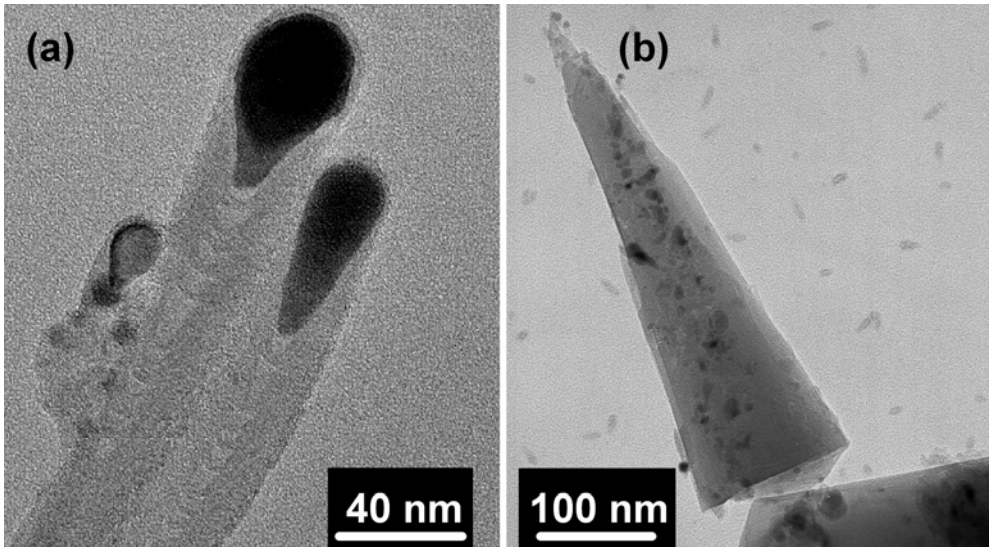

Figure 16: TEM images of carbon nanotubes, grown at (a) 450 V and (b) 550 V respectively for 20 min.

To better understand the formation process of the nanocone structure, we monitored the change of microstructure as a function of time during the CVD at a constant bias of 550 V. Figures 17(a)-17(c) display SEM microstructures of the samples CVD grown for 2 min, 6 min, and 14 min, respectively. As is evident from the figures, the CVD starts out with the formation of equi-diameter nanotube structure on Ni catalyst particles, as shown in the 2 min sample of Figure 17(a). On longer CVD for 6 minutes, these nanotubes are quickly transformed to the nanocone structure as shown in Figure 17(b). The Ni catalyst particles begin to get smaller as compared to the 2 minute sample. On a longer time CVD of 14 minutes, Figure 17(c), only nanocones are left, with their base diameter increasing with CVD time. On additional CVD (e.g., 20 – 30 min.), it is seen that the nanocone base diameter increases and the aspect ratio decreases.

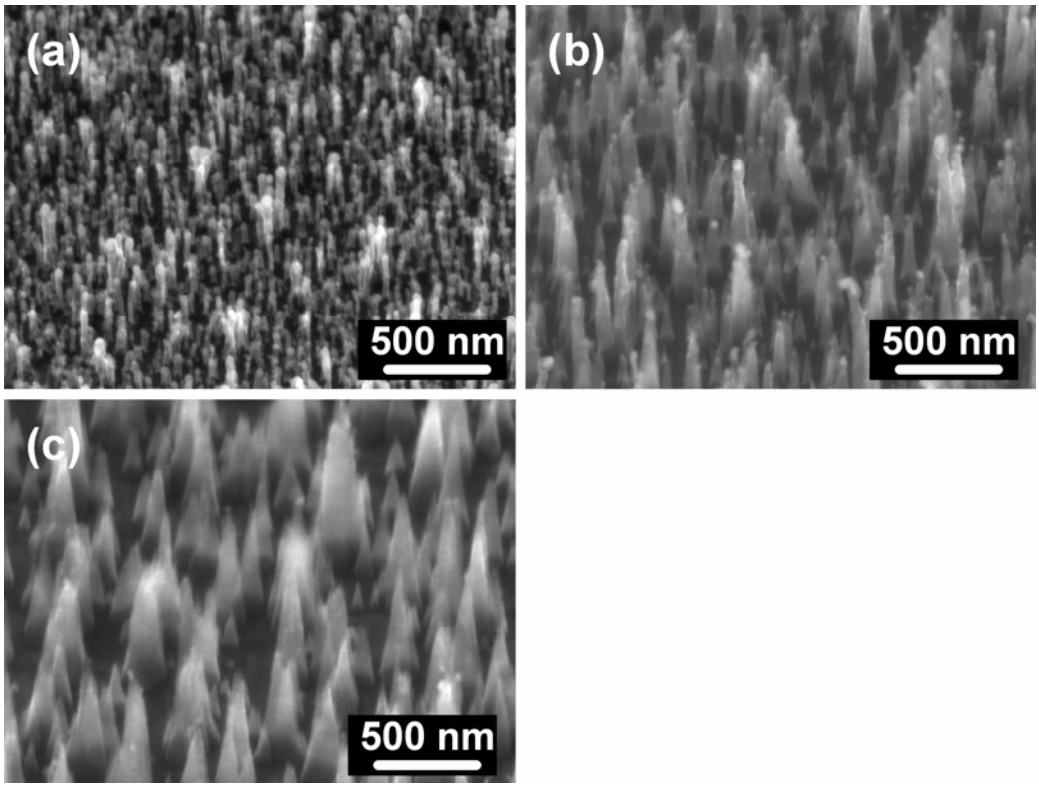

Figure 17: Nanocone morphology vs CVD growth time at 550 V for (a) 2 min, (b) 6 min, and (c)14 min, respectively.

The mechanism for the strong electric-field dependence of nanotube morphology observed in this work is described as follows. The formation and geometry of the nanotube vs. nanocone structure appear to be dictated by the plasma etching of catalyst particles at the growth tip. During the dc PECVD, plasma etching of the Ni catalyst particles continuously occurs if the applied voltage (and hence the energy of plasma sputtering) is sufficient. SEM examinations of various samples clearly indicate that the size of catalyst particle on top of the CNTs decrease as a function of time in the presence of plasma. The reduced catalyst size limits the kinetics of carbon uptake and nanotube growth along the upward direction, while the lateral growth continues with the

continued addition of carbon from the CVD gas. Eventually the vertical growth stops completely when the last small catalyst particle is sputtered away. The lateral growth and broadening of the nanocones is believed to be enhanced by the incorporation of Si (presumably from the substrate) into the cones; this is supported by our EDX analysis in TEM.

At a low bias voltage of 450 V, the energy of the ions in the plasma is lower and the plasma etching effect (sputtering effect) is not strong enough to significantly reduce the size of the Ni catalyst particles. The lateral growth of nanocones is negligible and not obvious. Due to the continued existence of the Ni catalyst particles on the tip (Figure 15(a)), longer nanotubes are obtained as the vertical growth lasts much longer. When the bias is raised to 500 V or higher, the plasma etching effect begins to reduce the particle size (e.g., see the nanotubes marked by circles) and hence the upward nanotube growth slows down and base lateral growth begins to get enhanced. The morphology of nanotubes begins to take the form of a nanocone shape. When the bias voltage is further raised to 550 V, the magnitude of the catalyst sputter etching is increased to the extent that the Ni particles are completely sputtered away, and only the base lateral growth occurs, Figure 15(c). At an even higher bias voltage of 600 V, the nanocones just continue to have the lateral growth, Figure 15(d). It appears that coarsening of the nanocone occur at the expense of other nanocones.

The observed phenomenon of strong field-dependence of nanotube morphology can be utilized to design and fabricate some unique shapes of nanotubes, for example, a nanotube configuration useful for conductance AFM tip. As is well known, the resolution of AFM imaging is determined by the sharpness, size and shape of the probe

tip. Typical commercially available AFM probe tips are made of silicon or silicon nitride (Si_3N_4) which is bulk micromachined into a pyramid configuration. Such probes exhibit a limited lateral resolution, and their rigid pyramid shape does not allow easy access to narrow or deep structural features.

The long and slender geometry of carbon nanotubes (high aspect ratio) offers obvious advantages for probing narrow and deep features. The elastically compliant behavior of high aspect ratio nanotubes is also advantageous. While the attachment or growth of carbon nanotubes on AFM tips has been demonstrated, such nanotubes are not always straight and vertically positioned, and the adhesion strength, reproducibility/reliability in shape, size, and attachment angle of nanotube probes still remain as major issues.

Manipulating the applied electric field during CVD growth of nanocones, we have demonstrated a direct creation of dual-structured nanotube configuration. It consists of a broad and mechanically stable nanocone base (200 – 500 nm base diameter) and one very thin and straight nanotube probe vertically emanating from the nanocone apex as illustrated and supported by example SEM micrographs in Figure 18. Instead of growing the standard, vertically aligned nanotube structure of Figure 18(a) by low field CVD, we start with growing a nanocone first, e.g., using a higher bias voltage, such as 550 - 600 volts, or alternatively, by allowing a longer CVD time of 5 – 10 minutes as in the case of Figure 17. Such a CVD treatment prepares a base nanocone structure and at the same time reduces the catalyst particle size to as small as a few to several nanometers, Figure 18(b). The CVD processing at the high voltage is then stopped when the catalyst particle diameter is substantially reduced to a nanometer

regime but not completely sputtered away. By intentionally lowering the applied voltage at this stage (e.g., to 450 V), and continuing on with CVD, we successfully nucleated and grew a single, straight nanotube from the apex of the broad nanocone utilizing the still-remaining, very small catalyst particles. The diameter of the vertically aligned nanotube on top of each of the nanocones is estimated to be ~7 nm as shown in Fig. 4(c).

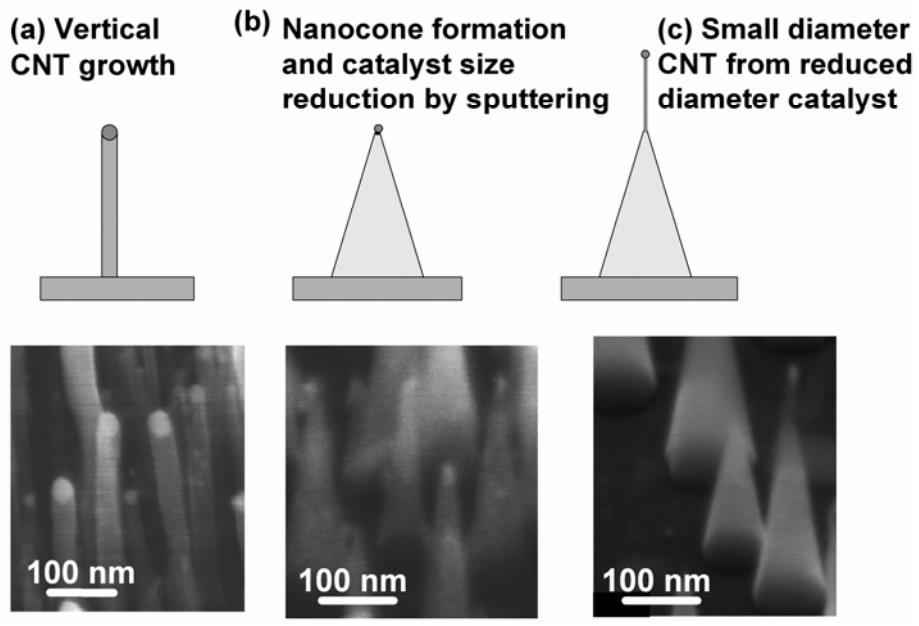

Figure 18: Controlled CNT tip geometry; (a) straight nanotube, (b) nanocone with small-diameter catalyst, (c) dual-structured nanotubes synthesized by high-field and low-field two stage CVD.

It is conceivable that further optimization of the catalyst size reduction as well as the specifics of the two-step CVD process could even further reduce the catalyst size and the diameter of the apex nanotube (e.g., ~1-3 nm diameter) on top of the nanocone. Such a dual-structured AFM probe configuration with a smaller-diameter and flexible

CNT on top of a mechanical stable cone base structure is highly desirable for enhanced reliability of high resolution CNT-AFM, especially with an assurance of only one nanotube on the tip, in a desirably straight and vertical geometry. Electron beam lithography patterning of the catalyst layer is underway to provide catalyst configurations suitable for CVD growth of only one or an array of nanocones, each with a vertically positioned, small-diameter probe nanotube directly grown from the nanocone apex. Some of these results will be presented in the application section at the end of this chapter.

4.3 Controlling electric field directions within a dc plasma sheath:

In order to synthesize CNTs for specific applications, the ability to control their growth directions is instrumental. Control over their growth directions can enable the creation of new CNT morphologies and gives us the possibility of growing CNTs directly into a desired position, eliminating some of the major challenges associated with assembly of CNTs. This section shows how the growth directions of CNTs can be controlled by controlling the electric field directions within the dc plasma sheath.

4.3.1 Alignment mechanisms of carbon nanotubes:

The alignment of CNTs by electric fields has been demonstrated by several groups. The application of both dc and ac fields in a thermal CVD process was shown to align SWNTs and grow them suspended above a substrate.[98] These results were attributed to the anisotropic polarizability of a SWNT resulting in a dipole which aligned itself with the electric field directions. The dipole moment of a SWNT **P** is given by

$$\mathbf{P} = \alpha\mathbf{E} \qquad (2)$$

where **E** is the applied electric field and α is the static polarizability tensor For a CNT orientated some angle θ away from the direction of the electric field, the dipole moment of the CNT is along the tube axis with

$$\mathbf{P} = \alpha_{\parallel}\,\mathbf{E}\cos\theta \qquad (3)$$

Where $\alpha_{\parallel}$ is the polarizability parallel to the tube axis. This means that the force acting on the dipole to align the CNT with **E** is:

$$\mathbf{F} = \alpha_{\parallel}\,\mathbf{E}^2 \sin\theta\cos\theta / L \qquad (4)$$

where L is the length of the CNT. This would mean that the alignment was due to the body of the CNT aligning with the electric field directions. Results similar to these have also been achieved for MWNTs.[99]

Bower et al. reported that in a microwave PECVD environment, without the direct application of an applied field, the plasma creates a self-bias on a substrate which results in an electric field perpendicular to the surface strong enough to align the CNTs. This microwave plasma induced self bias was used to grown CNTs which were perpendicular to flat substrates and radially perpendicular to an optical fiber,

demonstrating that the field directions in this case were always perpendicular to the local surface.

For the specific case of CNTs growth by dc PECVD under a tip growth mechanism, Merkulov et al. suggested that the alignment with electric field was due to compressive and tensile stresses created at the interface of the catalyst particle and the precipitating graphene planes.[100] In the plasma environment, the metal catalyst particle will develop a negative charge and since this charged particle is in an electric field, there will be a force exerted on it pulling it along the directions of the electric (towards the positive direction.) As a growing CNT bends to one side, there will be compressive stresses acting on the graphene planes that are forming on the side of the CNT which is now above the catalyst particle in the bent over CNT. On the opposite side of that same catalyst particle, there will be tensile stresses on the graphene planes precipitating on the side of the catalyst particle which is now beneath the bent over catalyst particle. In order to relieve these stresses, the CNT will straighten out and now matter what direction the CNT begins to bend, the stresses caused in that bending will result in the CNT growth direction being straightened out again.

Although there are several different theories on why CNTs grow aligned with electric fields and for a given set of conditions one mechanism generally appears to be more applicable than the others, the one thing that they all have in common is the final result, that CNTs can be aligned by electric fields. In the following section, we rely on this result to control the growth directions of CNTs.

4.3.2 Manipulating electric fields by change of cathode geometry:

Vertically aligned CNTs grown with a perpendicular electric field (90° with respect to the Si substrate) are shown in the SEM image in Figure 19A. The CNTs have a fairly narrow diameter distribution with the majority being between 30-40 nm, and have lengths of 1-2 μm. The sample is tilted 45° away from the viewer to allow better view of the growth morphology. Additional SEM images showing CNTs grown at angles of 80°, 71°, and 51° with respect to the substrate are shown in Figures 19B, 19C, and 1D, respectively. These four images were taken from four different samples, but the sample substrates were prepared identically and the images were taken from equivalent positions on each of the four samples. The only experimental difference between the four experiments was the cathode geometry. The sample in Figure 19A was grown on a flat molybdenum (Mo) cathode while the other three had a modified cathode geometry that had additional Mo pieces forming extensions of the cathode to a side of the sample in order to alter the electric field distribution.

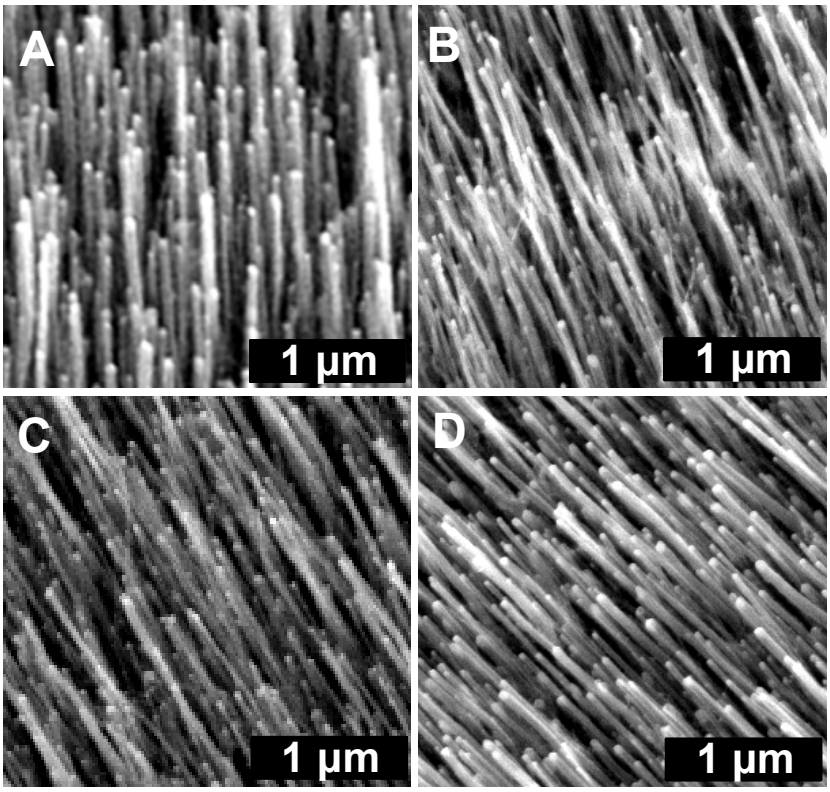

Figure 19: SEM images of aligned CNTs grown along a range of growth directions that have CNT-substrate angles of A) 90°, B) 80°, C) 71°, and D) 51°. The images are taken with the flat substrates on the SEM stage tilted away by 45° so the angles as viewed in the images are not the real angle that the CNTs make with the substrate. The actual listed CNT angles were obtained from cross sectional images taken parallel to the substrate, which are presented later.

Since the SEM images presented in Figure 19 were taken at an angle, it is difficult to see the true angle that the CNTs have with respect to the substrate, since most of their bases were obscured by other CNTs. In order to accurately represent the actual CNT angles, cross sectional SEM images taken along the plane of the substrate are shown in Figures 20A, 20B, and 20C, for the same samples that were presented in Figures 19B, 19C, and 19D, respectively. The three different angles that the CNTs make with the substrate is evident in the figures. We can also more easily see the

distribution of heights in the CNTs. The samples are the same as those shown in Figure 19B-D, and the CNTs were grown with tilt angles of 80°, 71°, and 51° with the substrate in A, B, and C, respectively. In Figures 20D, 20E, and 20F, photographic images of the three corresponding cathode geometries and resultant plasma sheath configurations used to obtain the CNT growth morphologies are presented with each image corresponding to the SEM image to its left. The CNTs were grown on identical substrates with identical growth conditions, and the images were obtained in the same manner and from equivalent positions on the samples 1 mm from the edge of the sample. The images were taken through the growth chamber view port during the CVD growth processing. The presence of a dc plasma sheath above the cathode and Si sample is clearly shown. The three modified cathode geometries each contain an extension to the cathode stage by a 2.5 mm thick Mo piece that had been carefully shaped. In Figures 20D-20F, each Si sample is placed on the left side of the cathode extension and in contact with that extension. In the first cathode geometry, Figure 20D, the side wall of the Mo cathode extension plate that is next to the Si sample on the right makes an angle of 55° with respect to the horizontal cathode stage, and that slope is inclined away from the Si sample. In the next cathode geometry, Figure 20E, the Mo plate makes a 90° angle with the stage. In the final cathode geometry, Figure 20F, the Mo plate again makes a 55° angle with the stage, but this time it is inclined towards (or over) the Si sample. It can be seen that as the angle that he cathode extension plate makes with the stage changes, so does the resulting angle that the synthesized CNTs make with the Si substrate.

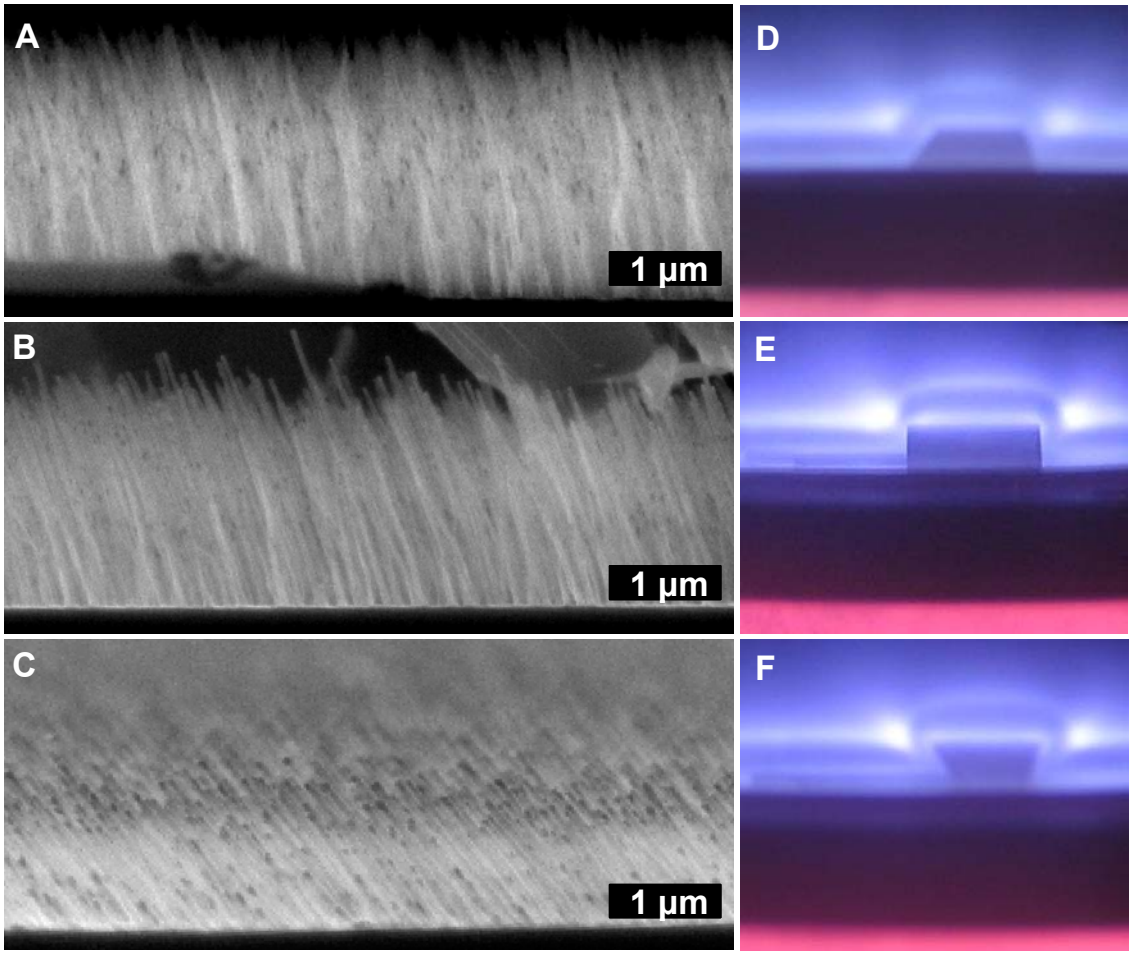

Figure 20: Cross sectional SEM images taken parallel to the Si substrates are shown in A-C and photographic images showing the different cathode geometries and resulting dc plasma sheaths are shown in D-F with each image corresponding to the SEM image to its left.

4.3.3 Calculation of electric field strength:

Our dc PECVD chamber uses a flat disk-shaped main Mo cathode stage 1 mm thick and 38 mm in diameter. Under normal plasma processing conditions, a dc plasma sheath forms above the surface of the cathode.[101] A schematic illustration of the voltage distribution for a dc glow discharge is show in Figure 21.

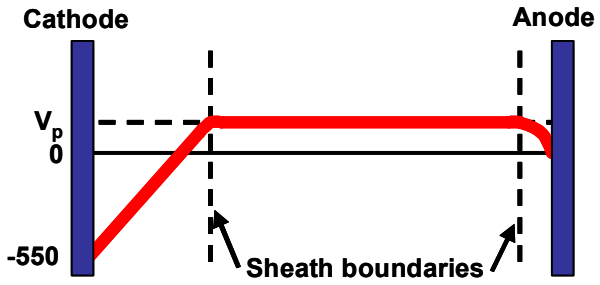

Figure 21: Schematic plot of the voltage distribution in a dc glow discharge. The voltage in the plasma (V_p) is at a slight positive voltage of typically less than 10 V with respect to the grounded electrode (the anode as pictured). Since the cathode has a negative bias of -550 V the voltage drop across the cathode sheath is 550 V + V_p, which is approximately equal to the applied negative bias for small values of V_p.

At each electrode a plasma sheath forms. The voltage within the bulk of the plasma is not at a potential between those of the two electrodes as one might expect, rather it takes on the slightly positive V_p which is typically less than 10 V and is actually the most positive body in the glow discharge. Since the cathode is negatively charged, there is an electron depleted region directly above the cathode. This electron depleted region decreases as the distance from the cathode increases, and this gradient of charges within the plasma sheath is referred to as the space charge density and results in an electric field within the dc plasma sheath. The fields within the electrode sheaths

have a direction such that they repel electrons trying to reach either electrode. Poisson's equation relates the variation of potential difference V (between V_p and an electrode) with a distance x across regions of net space charge:

$$\frac{d^2V}{dx^2} = -\frac{\rho}{\varepsilon_0} \qquad (5)$$

where ρ is the space charge density and ε0 is the permittivity of a vacuum. Since the electric field intensity E = -dV/dx and the space charge density ρ = ne, where n is the ion number density and e is the elementary charge, eq. (5) can also be expressed as

$$\frac{dE}{dx} = \frac{ne}{\varepsilon_0} \qquad (6)$$

Model calculations for the electric fields within a dc plasma sheath using an expression like equation (6) have been reported in literature.[102]

The electric field strength in the cathode sheath has a function that can, to a first approximation, be taken as linear. Under such a linear approximation, the field can be expressed as

$$E = \frac{2V_b}{l}\left(1 - \frac{x}{l}\right) \qquad (7)$$

where V_b is the absolute value of the negative bias applied to the cathode (with respect to V_p), l is the thickness of the plasma sheath, and x is the distance from the cathode.[103] A plot of this for the portion of the glow discharge near the cathode in our system is shown in Figure 22. We estimate V_b as the difference between the cathode bias and the grounded anode, which assumes V_p is negligible, and we calculate l as 2.14 mm based on plasma probe measurements reported elsewhere for a similar dc PECVD system[104]. The electric field beyond the sheath thickness has a constant value of zero due to the

constant potential Vp, however, within the plasma sheath, the field strength increases linearly to 5.14 X 10^5 V/m close to the cathode surface. Blazek et. al also calculated the force acting on the CNT tip due to a dc plasma sheath. Based on these calculations, the electric field strength near the cathode that we calculated above would lead to a force of ~5 X 10^{-13} N, which for a 30 nm Ni catalyst particle is more than two orders of magnitude higher than the weight of the catalyst particle and for a 10 nm Ni catalyst particle it is more than four orders of magnitude higher; these numbers are very similar to what Blazek et. al reported.

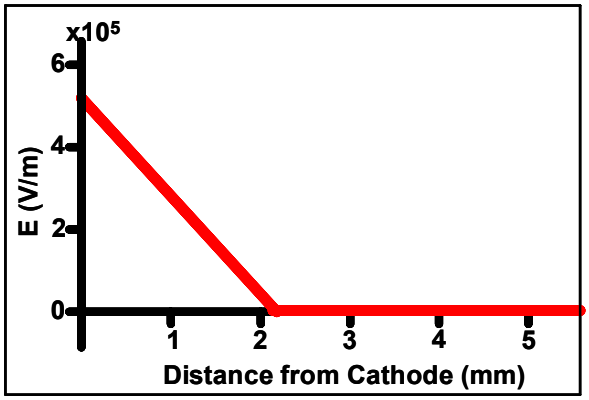

Figure 22: The electric field strength near the cathode sheath region for a bias of -550 V. The voltage between the cathode and anode electrode sheaths is assumed to be constant at a slightly positive V_p, so there is no electric field present in that region. The field inside of the cathode sheath is assumed to be a linear function related to the applied bias and the ratio of the distance from the cathode to the total sheath thickness as shown in equation 7.

The electric fields calculated in Figure 22 are one dimensional since we only consider the distance from a flat cathode of assumed large area. The cathode geometries that we used in this work to create various tilted CNT orientations are more

complicated. In the absence of an applied DC bias, CNT growth in a microwave plasma environment has been shown to produce CNTs aligned perpendicular to the substrate.[105] The presence of the plasma environment creates a potential self-bias where the field lines are always perpendicular to the surface. Even when a substrate's surface is tilted at an angle, the field lines will bend and within a narrow region (less than 10 μm above substrate surface where CNT growth occurs) the field lines will be straight and perpendicular to the surface. Bower et. al. estimated for a microwave plasma environment with no applied DC field that the self bias potential is on the order of 10V and the electric field has a magnitude on the order of 0.1 V/μm in the vicinity of the surface.

The application of a standard DC potential bias results in a different electric field around the sample. For our system, since the sample substrate is located on the cathode, the resulting direction of the electric field due to the applied bias is towards the sample. The field lines will again be perpendicular to the local surface and will bend as they move away from the surface to connect the two electrodes of the applied bias. As was the case before, within the region close to the sample surface where CNT growth occurs, the field lines will be straight and perpendicular to the surface resulting in vertically aligned CNTs like those shown in Figure 19A. The alignment mechanism for CNTs in a DC field like this has been reportedly due to stresses created at the interface of the catalyst particle and CNT by the electric field. This mechanism provides one possible reason why tubes that grow with the catalyst particle at the top of the tube (tip-growth) are aligned, although this does not apply to the case of nanotube alignment with the bottom-growth seen by Bower, et al. The CNTs are expected to grow along the

field line directions and are also expected to bend with those lines if they were to grow sufficiently long. These length scales strongly influenced by bending field directions are normally much longer than the lengths of nanotubes that we grow which are typically less than 10 μm.

4.3.4 Modeling of applied electric fields:

The true net electric field is a combination of several components including the applied bias and the plasma induced self-bias. It has already been shown that the electric fields within a dc plasma sheath are of sufficient strength to control the growth direction of CNTs, but the quantitative calculation of the field directions has yet to be reported. To estimate the directions of the electric fields, we start by making an assumption that their directions due to the applied bias and due to the formation of the dc plasma sheath will be similar. If this is the case, then modeling either case should give us a reasonable model. In Figure 24, we present plots generated using Maxwell 2D (Ansoft Corp., Pittsburgh, PA) of the calculated electric fields due only to the applied bias under the assumption of a vacuum between the electrodes. The potential at the surface of a conductor is assumed to have the same potential as its interior and all metals are assumed to be perfect conductors, therefore no electric field will exist inside of one. The tangential component of the electric field at a surface is assumed to be zero, which forces the electric field E to be perpendicular to the boundary of a conductor. The chamber wall is assumed to be at infinite distance representing an electrically grounded system. The 2D cross section which was modeled was divided into a grid and given the boundary conditions above the program solved the Laplace

equation at all of the vertices of the triangular grid. The spacing of the vertices was decreased for the areas that were nearer to the CNT growth region. Within the actual CNT growth region the spacing of these points was less than 1 μm. An example of an initial triangular grid is shown in Figure 23.

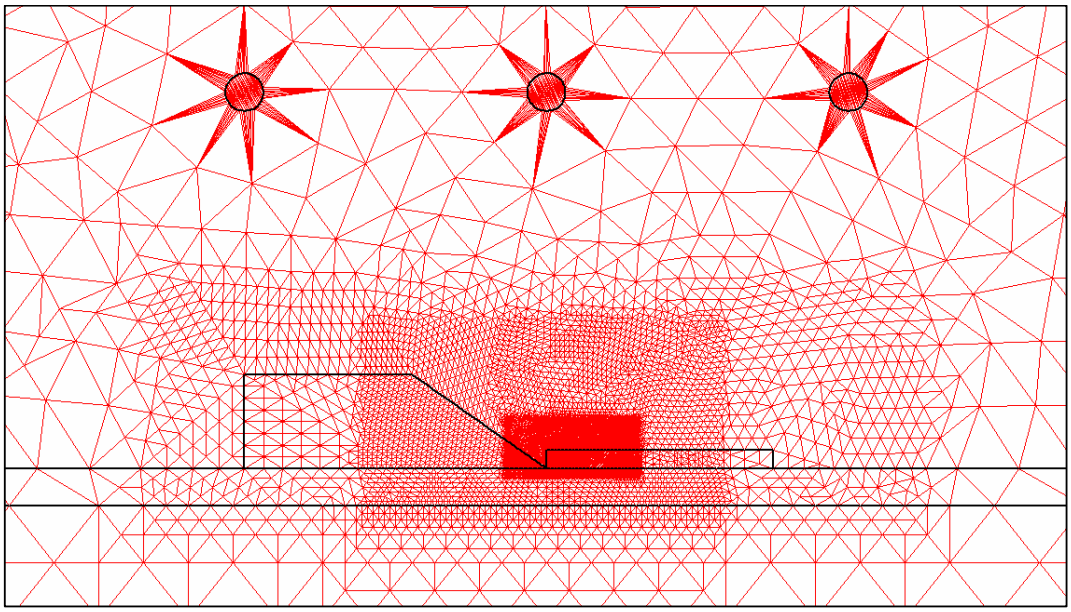

Figure 23: Example of an initial triangular grid for one 2D cross section within the CNT growth chamber. As the distance to the actually CNT growth region was decreased, the spacing of the vertices in the triangular grid was decreased.

The only difference among the Figures 24A-C is the geometry of the cathode extension plates, which are the same three geometries presented earlier. In Figures 24A-C, the Si sample is shown as an outlined rectangle to the left of the cathode plate, as was pictured in Figure 20. Figures 24D and 24E show progressively enlarged sections of 24B focusing on the area where the CNTs seen in Figures 1 and 2 would grow. In Figure 24E, a solid square marks a location 1 μm above the sample substrate.

The calculated field direction for this case is 71.4°, which is remarkably close to what is observed experimentally.

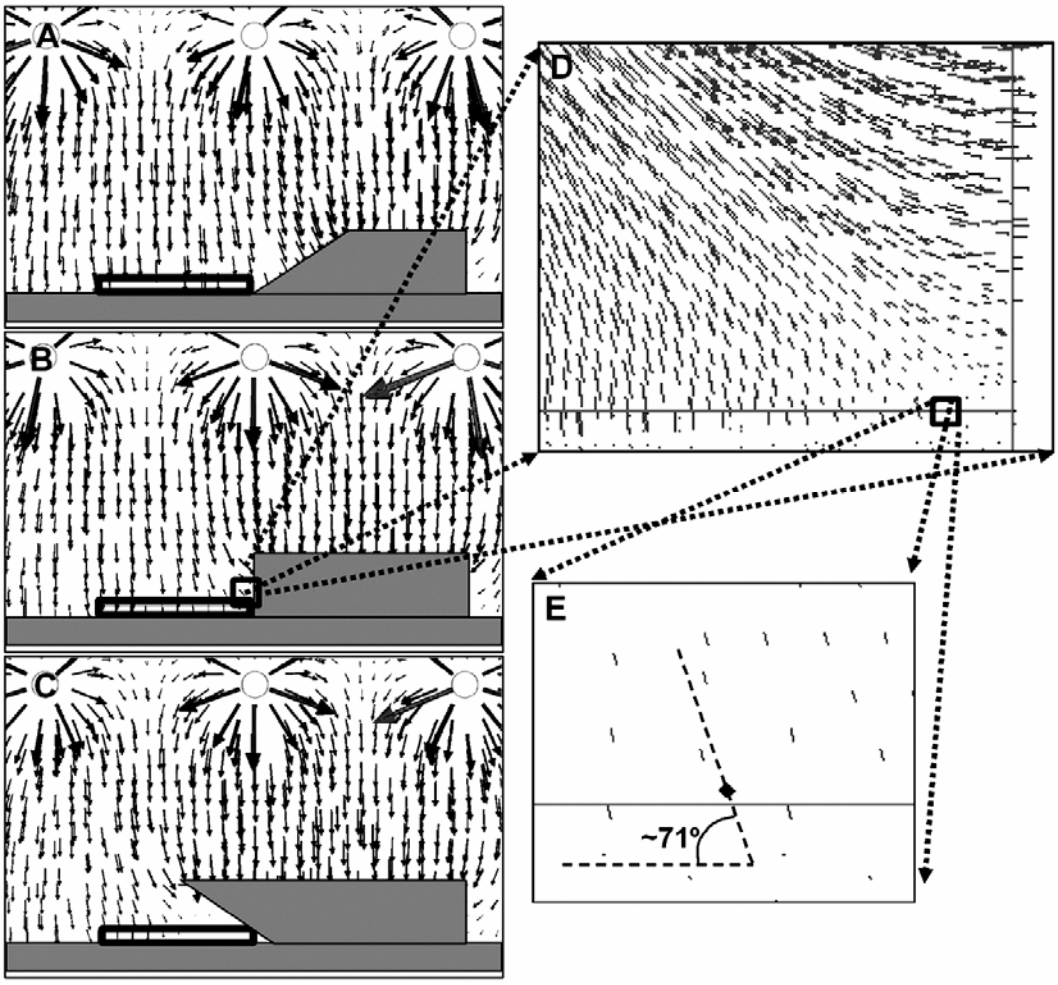

Figure 24: Plots of the calculated electric fields between the anode and cathode with the assumption of a vacuum between the electrodes. The cathode is shown with grey shading, the Si sample is show as an outlined rectangle to the left of the upper cathode plate, and the three copper anode wires are shown as circles near the tops of the images. Progressively enlarged areas of the CNT growth region in B are shown in D and E.

A summary of the calculated angles and actual observed experimental angles is shown in Table 2. The results are very similar, which supports the assumption that the directions of the net electric field will coincide with the directions of the field due only

to the applied bias. It is important to note that in the calculated fields in Figure 24, the Si substrate is not assumed to be a perfect conductor, so it is not an extension of the cathode itself. The fields were calculated both above and within the Si substrate. Had we used the same boundary conditions as we used for the metal electrodes, then the field directions within the CNT growth region would have been forced to be perpendicular. We believe that these electric fields within the Si sample could be part of the reason that our experimental results show a degree of bending greater than the present electrostatic prediction, but additional study is needed to confirm this. Further modeling is being done that takes into account the formation of a dc plasma sheath and these results will be reported in future, but initial findings appear to support the assumption that the dc plasma sheath only has a significant effect on the magnitude of the electric field in the growth region of the CNTs, not on the direction in which the field acts.

Table 2: Comparative CNT orientations based on the electrostatic model prediction vs. the experimental results for the three cathode geometries presented above.

Cathode	Electrostatic	Experimental
Inclined away	80.6º	80º
Vertical	71.4º	71º
Inclined towards	52.7º	51º

4.3.5 Electric fields at the substrate interface:

By using a modified conductor plate geometry as described previously, I have been able to grow CNTs which are well aligned and make various angles with their Si substrates. In Figure 25 we show SEM images of CNTs which are grown at a ~55° angle with the substrate. Although tilting the sample, as in Figure 25A, makes it easier to see many aspects of the CNT morphology, the actual angle that the CNTs make with the substrate is easier to determine from the cross sectional image taken along the plane of the substrate shown in Figure 25B. In both parts we are able to see that the CNTs are well aligned even right up to the surface of the Si substrate. It was presented previously that the alignment of CNTs grown in a PECVD process such as this appears to be due to the directions of the electric fields. Since the Si substrate is in electrical contact with the Mo cathode beneath it, one might expect that the electric field responsible for the alignment of the CNTs would be perpendicular to the substrate at the surface and that the synthesized CNTs will begin their growth perpendicular to the substrate; however, even at higher magnifications, we do not see evidence that the CNT growth begins like this.

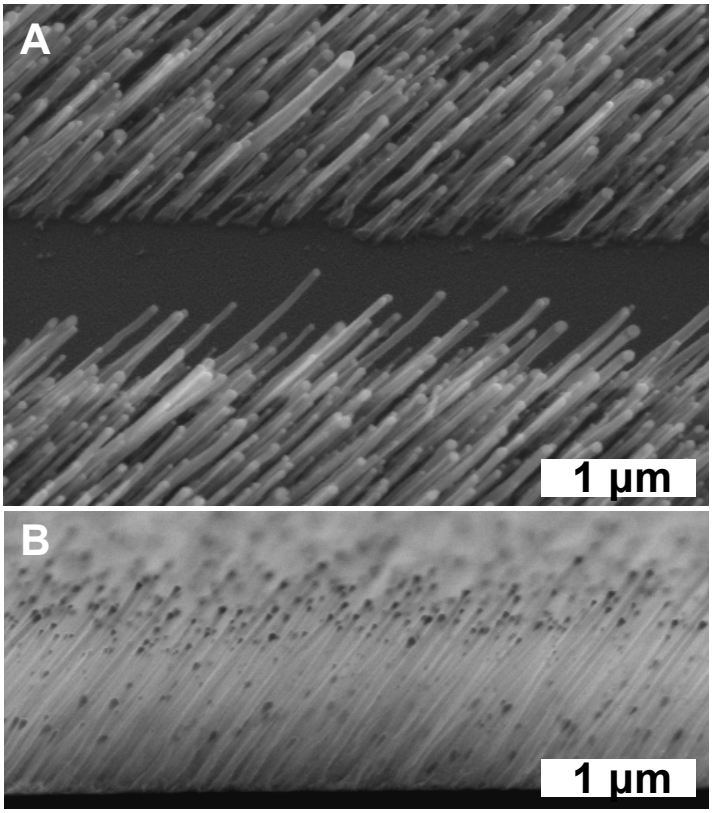

Figure 25: Scanning electron microscopy (SEM) images of CNTs grown aligned at an angle strongly displaced from perpendicular with the Si substrate. In A, the sample is tilted at 45°, while in B, the image is taken parallel to the plane of the substrate. In both images, the CNTs are observed to grow at non-perpendicular angles even right next to the substrate. When looking at the cross sectional image in B, we can see that the CNTs make a ~55° angle with the Si substrate, this is also true of the sample in A, but the tilting of the sample makes it less obvious.

In order to explain the results in Figure 25 where the CNTs do not have a vertically aligned section we must assume that the electric field directions are not perpendicular to the surface of the Si wafer. For continuity across the interface, the directions of the electric fields just above and just below (inside) the Si substrate must be equally displaced from perpendicular. To experimentally test if this is the case we

grew CNTs on two otherwise identical Si substrates which were placed in slightly different cathode configurations.

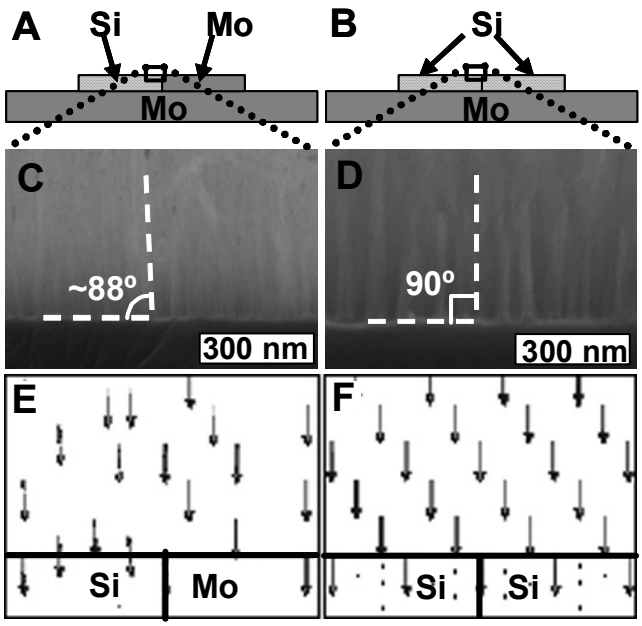

Figure 26: Schematic illustrations of two similar experiments used to show the difference in the direction of the electric field at the interface of the Si substrate where the CNTs are grown are shown in A and B. Experimental SEM images are shown in C and D and electric field models are shown in E and F corresponding to the SEM images and schematics above each.

The first, shown in Figure 26A, had a Mo conductor plate that was equal in thickness to the Si substrate next to it, and the second, shown in Figure 26B, instead had another piece of Si from the same wafer placed next to it. After identical PECVD growth processing, the samples were observed at equivalent locations on each of the Si substrates near the interface with the Mo or 2nd Si piece. The CNTs that were grown on the sample that was placed next to the Mo plate were aligned along a direction slightly tilted away from that Mo piece as can be seen in Figure 26C. By contrast, the

CNTs grown on the Si substrate that was placed next to another Si substrate grew perpendicular to their substrate, as we would expect, since this is the same as observing the CNTs growing in the center of a larger piece of Si.

The applied bias and the bias across the dc plasma sheath are the main components that will result in the net electric fields in our dc PECVD process. Since it has already been shown that the electric fields within a dc plasma sheath are of sufficient strength to control the growth direction of a CNT and that we can use a simplified model to predict the directions between two electrodes, I use a similar approach in this experiment. To estimate the directions of the electric fields, we start by making an assumption that their directions due to the applied bias and due to the formation of the dc plasma sheath will again be similar and that modeling either case should give us a reasonable model.

I have again done simple two dimensional modeling of the electric fields due only to the applied bias under the assumption of a vacuum between the electrodes using Maxwell 2D. In the previous results, the electrostatic models predict electric field directions that are actually slightly farther from perpendicular than the experimental results, but within 2° of the CNT growth directions for the cathode geometries reported previously. As before the potential at the surface of a conductor is assumed to have the same potential as its interior and all metals are assumed to be perfect conductors, therefore no electric field will exist inside of any metal electrodes. The tangential component of the electric field at a surface of a perfect conductor is assumed to be zero, which forces the electric field E to be perpendicular to the boundary of a conductor. The chamber wall is assumed to be at infinite distance representing an electrically

grounded system. The Si substrates were n-type with a conductivity of ~100 siemens/m. So unlike the Mo plates which are modeled as perfect conductors, the Si substrates are not extensions of the cathode itself. The fields were calculated both above and within the Si substrate. Had we used the same boundary conditions as we used for the metal electrodes, then the field directions within the CNT growth region would have been forced to be perpendicular.

Since for the sample geometries shown in Figure 26 the Si sample has the same thickness as whatever is placed next to it, we eliminate the protruding electrode geometry that was used previously. With no extension of the cathode taller than the Si sample, any alterations of the electric field directions at the top surface of the Si substrate would have to be due to a field which passed through that Si substrate. The results in Figures 26E and 26F show the calculated fields for the region near the interface between the Si substrate and either the Mo piece or the 2nd Si piece, respectively. Here we see for a point at the surface of the Si substrate and in the area of the sample near the edge where the CNTs were observed that the predicted electric field directions are within ½° of the experimental results. Further modeling is being done that takes into account the formation of a dc plasma sheath and these results will be reported in future, but initial findings appear to support the assumption that the dc plasma sheath only has a significant effect on the magnitude of the electric field in the growth region of the CNTs, not on the direction in which the field acts.

4.4 Continuing the growth of carbon nanotubes:

4.4.1 Creation of sharp bends:

Understanding how to control the growth direction of CNTs is important for many applications. Being able to continue the growth of CNTs to produce more complicated morphologies opens up doors to many more applications. Control over growth direction can enable the creation of bent CNTs with specific bend angles and zigzag type configurations, which could be useful for circuit nano-interconnections, spring related device applications, and so forth. For in-plane nano-interconnections between device components or contact pads, routing of circuit connections often require not just a straight but also sharp-turn conductor circuit lines. Carefully engineered CNTs with specific bend angles could also be useful for such applications, especially if SWNTs or small diameter MWNTs can also be made to respond to electric field manipulations in a similar fashion.

By adjusting the cathode geometry to result in electric field lines that were inclined with the substrate in the CNT growth region, I was able to achieve bending of the CNTs. Initial results did demonstrate that this method could work, but did not produce very exciting structures. In Figure 27 we see some of these initial CNT bending results.

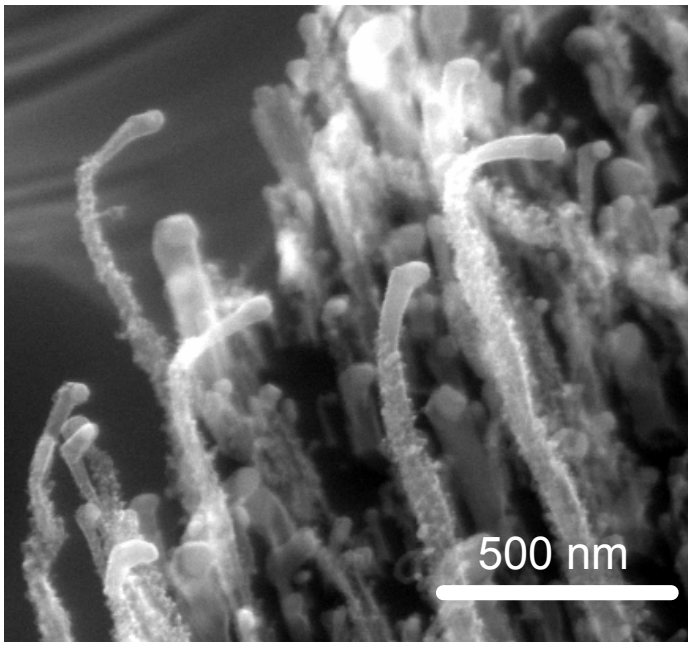

Figure 27: Initial results showing CNT bending. There is a clear tendency for the CNTs to bend towards the right of the image, but there is not much sharpness in the created bend angle.

After refining the electrode geometry as was shown in the previous sections, greatly improved results were observed. In Figure 28 we show SEM images of CNTs which have been grown along a patterned line and have been engineered to have 90° bends. Although some of the angles might look slightly acute, as was the case before, when the samples are viewed parallel to the substrate, they were all shown to be very close to 90° bend angles. In the lower magnification image of Figure 28A, we can see that the bend angles can be made uniform over CNTs of various heights, diameters, and over a reasonably large area. These bend angles were engineered by using an electrostatic model as above for cathode geometries with protruding Mo features and careful placement of the sample at the proper distance from the cathode features to obtain the desired angle of 90°.

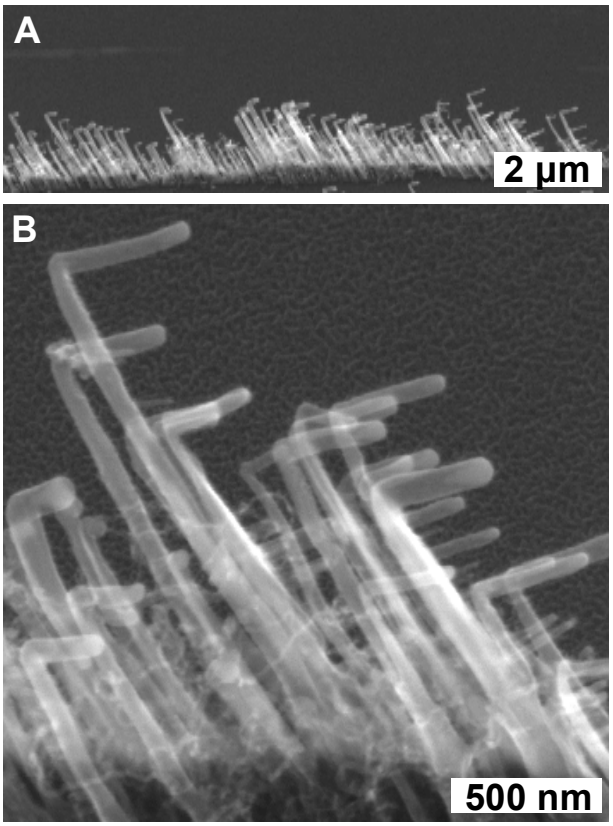

Figure 28: Sharply bent CNTs which were grown along a patterned line of Ni catalyst are shown in A. The CNTs were initially grown aligned along one direction as before, but an additional step was added to engineer a 90° bend into each of them. A higher magnification image taken from the same line is shown in B.

Also CNTs grown at various angles from a substrate or CNTs that are grown in bent configurations could be useful as a component for micro/nano mechanical devices or as improved AFM tips for probing side walls of channels or pores. In Figure 29 we show CNTs which have been grown in an individually patterned array (using electron-beam pattern Ni catalyst particles) with 40° bends at their tips and a short growth segment after their bends. These angles were engineered as before and were consistent over a 100 µm square area. For potential AFM applications, CNTs similar to these can

be patterned in the same method as used above, grown directly onto cantilevers, and used to obtain improved probe images. For inspecting narrow trenches or pores, tips with even shorter bent segments and smaller CNT diameters are desired as feature sizes for semiconductor processes get smaller in future advanced devices.

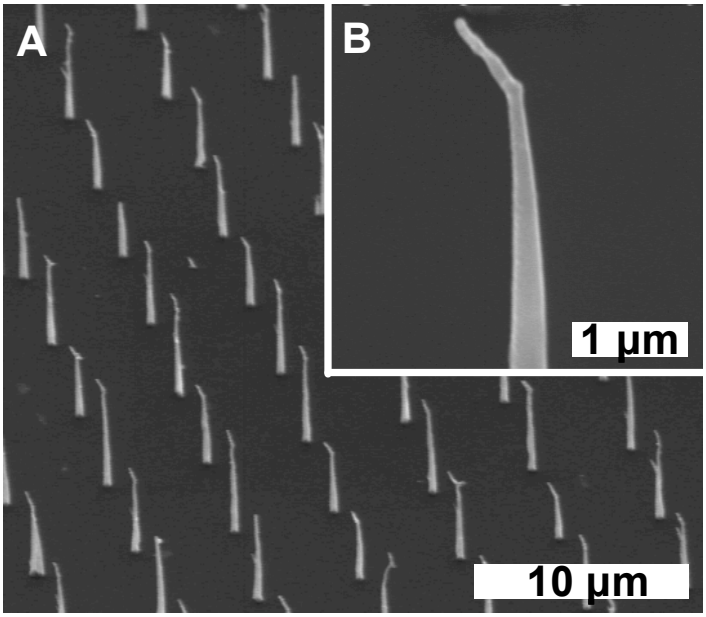

Figure 29: An SEM image of a patterned array of sharply bent CNTs is shown in A with a higher magnification image shown in B. The CNTs were grown from patterned islands of Ni catalyst particles over a square area of 100 µm on each side. CNTs with this morphology could potentially be useful as improved AFM probes for inspecting the side walls of channels or pores.

4.4.2 Multiple sharp bends to produce zigzag morphology:

Although alignment of individual CNTs and CNT arrays has been demonstrated, there has been very little work done towards more complicated morphologies. Merkulov et al. showed a fabrication of bent CNTs consisting of one section perpendicular to a substrate and a second section aligned ~45° off of the substrate

normal with radii of curvature on the order of 1μm.[106] The off-normal growth was achieved by positioning the sample near the edge of the sample holder where bending of the electric field lines occurs. In this section, I show the ability to grow CNTs with sharp bends that maintain a constant tube diameter before and after a bend and the ability to grow structures with multiple bends resulting in a zigzag morphology. Zigzag structured or signally bent CNTs could be used for many applications, e.g., related to mechanical nano-springs, or complicated circuit nano-interconnections.

Electric-field-concentrating metal plates (Molybdenum slabs) 1mm thick (the same as the cathode stage) were placed in electrical contact with the cathode in the vicinity of the Si substrate in two different geometries (Figure 30.) After the first growth stage was carried out resulting in CNTs grown at an inclined angle (aligned away from the sample edge) in the area 100-200 μm from that sample edge, the location of the Mo slabs was changed and the above process was repeated to result in the second growth stage where the nanotubes continued to grow but aligned in a direction towards the edge of the sample. The switching between the two growth stage setups was carried out by stopping the CVD growth process, cooling the sample under 60 torr H_2 flowing at 150 sccm, and manually repositioning the objects involved. These two growth stages were repeated to result in CNTs containing multiple segments joined by multiple sharp bends.

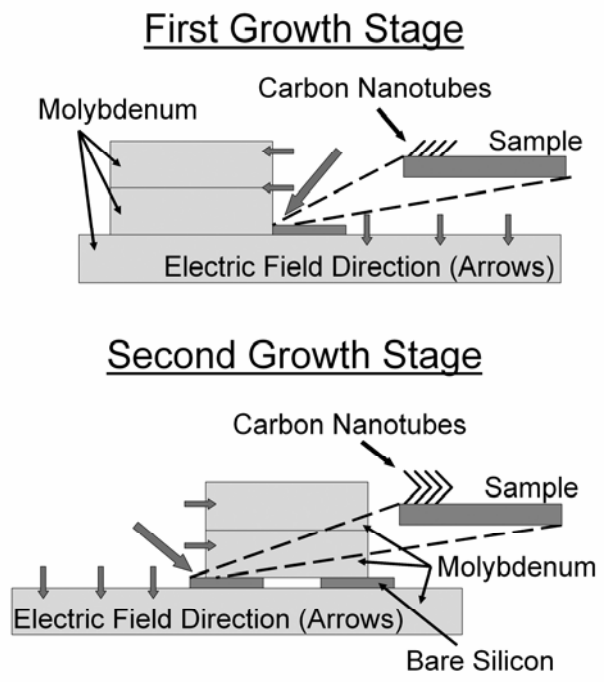

Figure 30: Schematic illustration of the two experimental geometries used to control the growth direction of the CNTs. By alternating between the two geometries, CNTs with zigzag morphologies were achieved as shown in locally expanded diagrams (marked by dashed-lines).

In order to cause bending in the CNTs, we need to manipulate the electric field such that the field lines in the growth region of the CNTs are bent. Growth along field lines at angles not perpendicular to the substrate surface has previously been achieved by positioning the sample near the sharp cornered edge of the sample stage where the field lines are bent towards that sharp corner direction even at distances within the growth region. In this section, I used a different geometry that allowed for the presence of electric-field-concentrating metal plates to cause very large and dramatic changes in the direction of the electric field lines in the CNT growth region. The metal plates were made of the same material as the cathode stage, and were in electrical contact with the stage. The resulting electric field lines were bent dramatically and even for distances

~10nm above the surface the resulting CNTs were grown aligned at angles greatly tilted from perpendicular direction (to the surface). By moving the metal plates, we were able to again dramatically alter the direction of the electric field lines, which is how such sharp bends were obtained.

An SEM image of three-step zigzag CNTs obtained by using the conductor plate arrangement of Figure 30 is presented in Figure 31. The image shows that arrays of carbon nanotubes with an average diameter of ~30 nm were grown aligned at an angle ~57° from normal, then bent ~90° and continued to grow as an aligned array until they were again bent ~90° and grown along the original growth direction. Each growth stage had a duration of 8 minutes and each straight segment in the bent nanotubes is on the order of ~500 nm in length. The two opposing ~90° bends are in-plane. The sample was grown two additional steps to produce five-step zigzag tubes with four alternating opposing in-plane bends shown in Figure 32. Such a multiple, sharp bend structure of carbon nanotubes has previously not been reported.

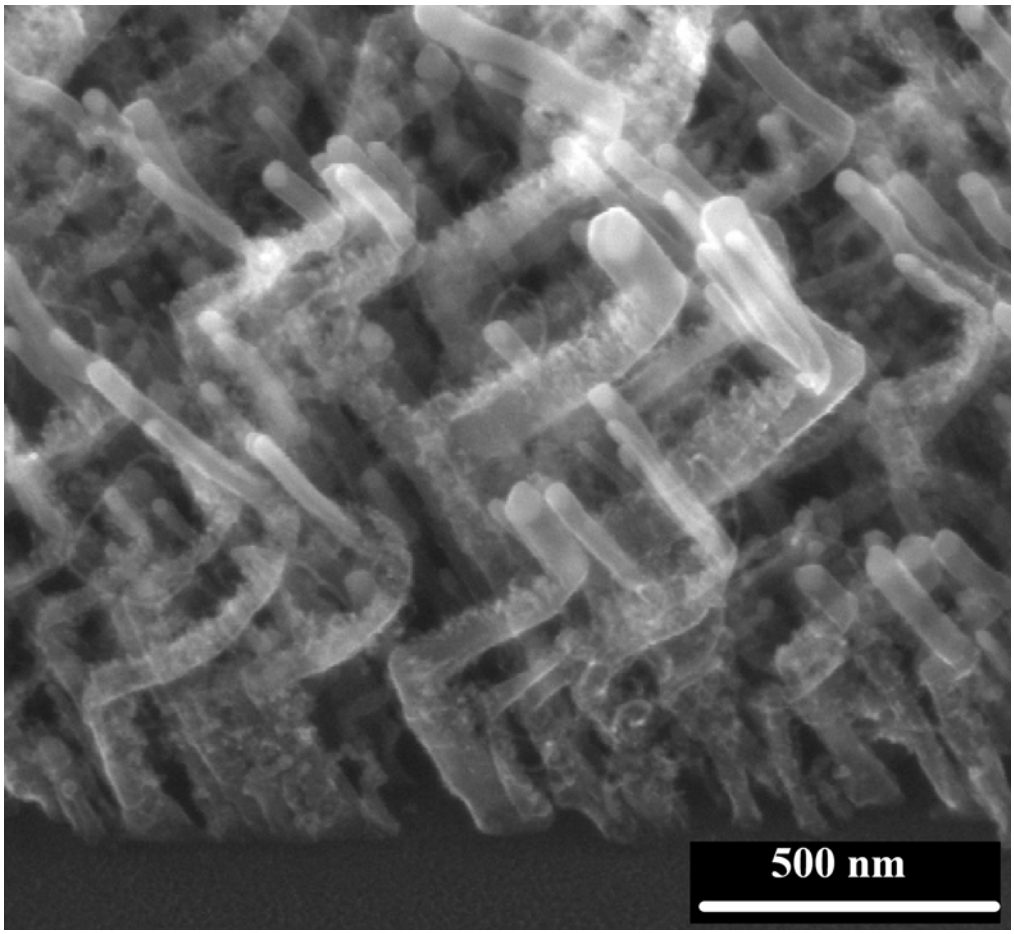

Figure 31: Array of CNTs grown with zigzag morphology using a three stage growth process. Sample tilted 45° for SEM analysis.

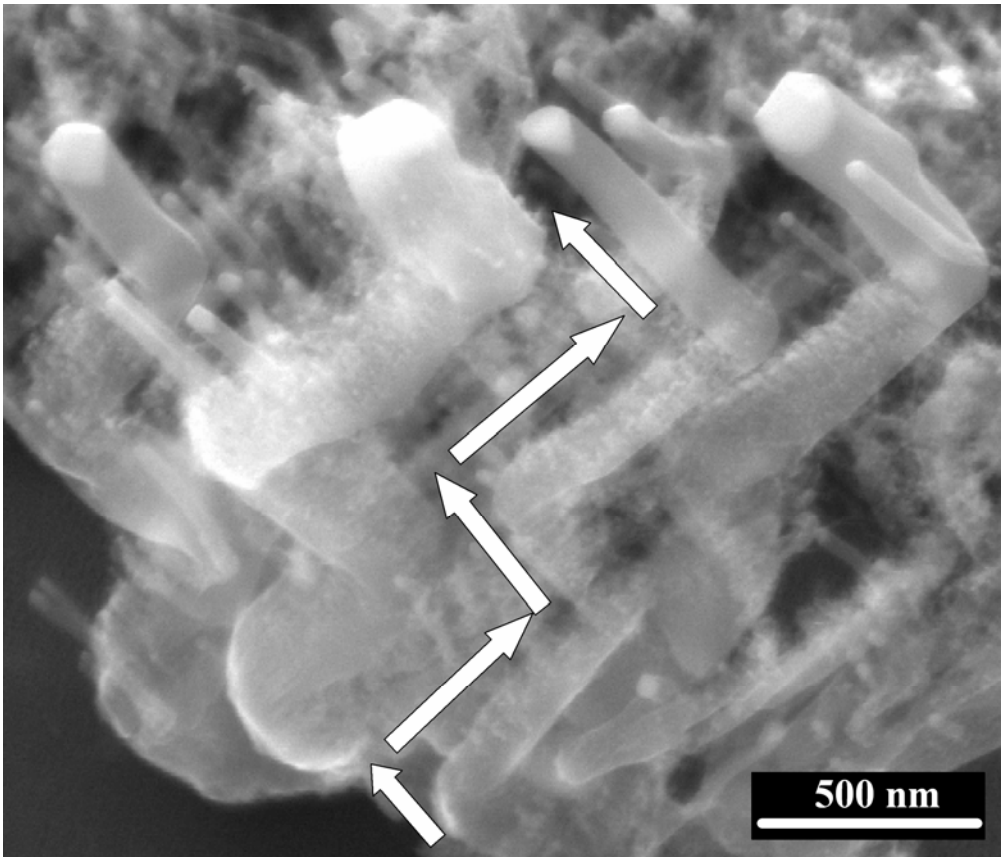

Figure 32: Multiple-bent CNTs grown with five growth stages.

The bends present between two growth stages have small radii of curvature of only ~25nm. These nanoscale bend angles obtained using a recessed corner of metal blocks in contact are much sharper than the micrometer scale bends previously demonstrated in literature using an open (convex) corner of a metal plate by Merkulov et al. While the nanotubes have a variation of diameter determined by the initial size of the catalyst particle formed upon heating, each individual tube shows essentially the same diameter for all growth stages. It is anticipated that such a sharp bend in a nanotube is likely to contain many defects, which will be an interesting subject of future study.

The surface of the CNTs appears clean on the last growth stage, while the earlier growth stages appear to have some fuzzy surfaces with additional, tiny CNTs and amorphous carbon present. This deposition is clearly most prevalent along the sides of the CNT segments that are orientated in the direction of the subsequent growth stages. A possibility of some sputtering of original Ni catalyst particles on CNT tips followed by re-deposition as smaller catalyst particles for re-nucleation and growth of nanotubes may be speculated. The extra small nanotubes (as small as ~5 nm in diameter) generally appear to be growing along the direction of the electric field and perpendicular to the length of the segments previously grown. It is not clear whether this observed phenomenon can be further optimized/utilized for creation of much smaller diameter nanotubes (e.g., 1-5 nm regime) from a coarse MWNTs (e.g., 20 – 100 nm regime). On a freshly growing segment in which the field direction coincides with the segment length, such a growth of tiny nanotubes is not observed. The exact cause for this additional material deposition is not clearly understood at the moment, and further study is needed to determine the nature of such additional deposition. Further optimization and modification of CVD processing conditions are being pursued to minimize such small features and grow cleaner nanotubes.

Our CNTs are all grown through a tip-growth process, and the catalyst particles are still clearly visible at the tips of the structures shown. The limited presence of carbon capping (for example, amorphous carbon coating that may poison the catalyst surface and prevent further CNT growth) implies that these shape-engineered carbon nanotubes can be grown further producing additional zig-zag bends or other morphologies. The bends shown here are all in-plane bends (in a three dimensional

sense moving away from the substrate, not on the substrate plane). This was done to simplify the set-up geometry and to make it easier for us to see the resulting structures. Using similar setups, we should be able to engineer out of plane bends and make more complicated three dimensional structures like nanocoils, segmental helixes, box-helixes, or horizontal-vertical 90 degree zig-zag shapes, for example. Motorized rotational movement and stepper-motor movement of field-concentrating-metal plates with respect to the substrate can be designed to continuously grow a variety of complex CNT shapes and this work is presently underway.

4.5 Post growth plasma etching:

4.5.1 Removal of catalyst particle carbon capping:

It was previously reported that the metal catalyst particle becomes capped with a film of carbon during CNT growth.[107] Chhowalla et. al. reported that the carbon capping was graphitic in nature when deposited under high temperature conditions, and resembled disordered carbon at lower deposition temperatures. It has also been reported that the carbon film on the catalyst particle forms at a faster rate with a higher carbonaceous gas content. It has been proposed that under the right conditions the carbon film may form in patches that are not continuous across the catalyst surface.[108] In this model, the growth rate of a CNT is faster when there is a greater area of catalyst particle not coated by carbon and the areas of carbon coating and clean catalyst surface would dynamically change as carbon film islands emerge and disappear. This would

lead to carbon supply limited growth for the CNTs as a greater exposed catalyst surface area would lead to a greater amount of decomposed carbon species.

In this section, I investigated the controlling parameters and processes for nanotube re-growth in relation to the synthesis of sharply bent carbon nanotubes. I use the terms "re-growth" and "continued growth" to describe a second growth stage that occurs after a first growth stage has been completely stopped. The ability to stop and re-grow nanotubes, especially along a different direction can be useful for a variety of nanotech applications. The use of sharply bent nanotubes also allows one to study the occurrence and extent of CNT re-growth. Continued growth or re-growth of CNTs after one stage of growth had been completely stopped has been reported for CNTs growth in both thermal[109] and PECVD systems[110]. These PECVD re-growth results were simply accomplished by loading the samples back into the growth chamber and exposing them to plasma with the standard parameters used for the initial growth stage. However, aligned forests of CNTs grown from catalyst particles that were initially a continuous thin film on a silicon substrate exhibit a considerable size distribution in both diameter and height (this can be avoided by using patterned catalyst islands such as by electron-beam lithography). When an uneven "forest" of straight-growing CNTs like this or even a patterned and uniform CNT arrays is re-grown, determining the initial location and length of the second growth stage along the linear length of nanotubes is practically impossible to identify and hence it is difficult to study and understand the re-growth phenomena. The very clearly defined sharp bends we introduce by changing the growth direction solve this problem.

Two samples showing very different extents of re-growth are presented in Figure 33. We first grew arrays of CNTs aligned perpendicular to the substrate surface under different conditions, one that resulted in a thick carbon coating forming over the CNTs' catalyst particles, and another that resulted in a much thinner carbon film being formed by adjusting multiple processing conditions as will be described below. The samples were then placed back in the chamber and both grown under identical conditions at an approximate 45 degree angle away from perpendicular. It can be seen from the scanning electron microscope (SEM) images in Figure 33 that some re-grown CNTs (Figure 33A) showed a small amount of continued growth, less than 100 nm in length, in contrast to other CNTs with the same second growth stage conditions (Figure 33B), which grew 500 nm on average. The CNTs have the same average heights and diameters during the first growth stage, it is the second growth stage that we are considering when discussing the CNT re-growth. The extent of re-growth is made clear by the sharp change in growth direction which allows us to identify the start of the second growth stage; otherwise, the two images would appear quite similar. The samples had identical growth times of 15 min for both their first and second growth stages. TEM images of the bends show that the CNTs continue growing by precipitating new graphene planes along the bottom surfaces of the catalyst particles. There are many graphene plane stacking defects at the bends, but they are arranged such that the second growth stage is a true extension of the first growth stages with hollow cores at the bends. The difference in the extent of re-growth is due to the different degrees of carbon capping present on the catalyst particles and will be discussed in more detail below.

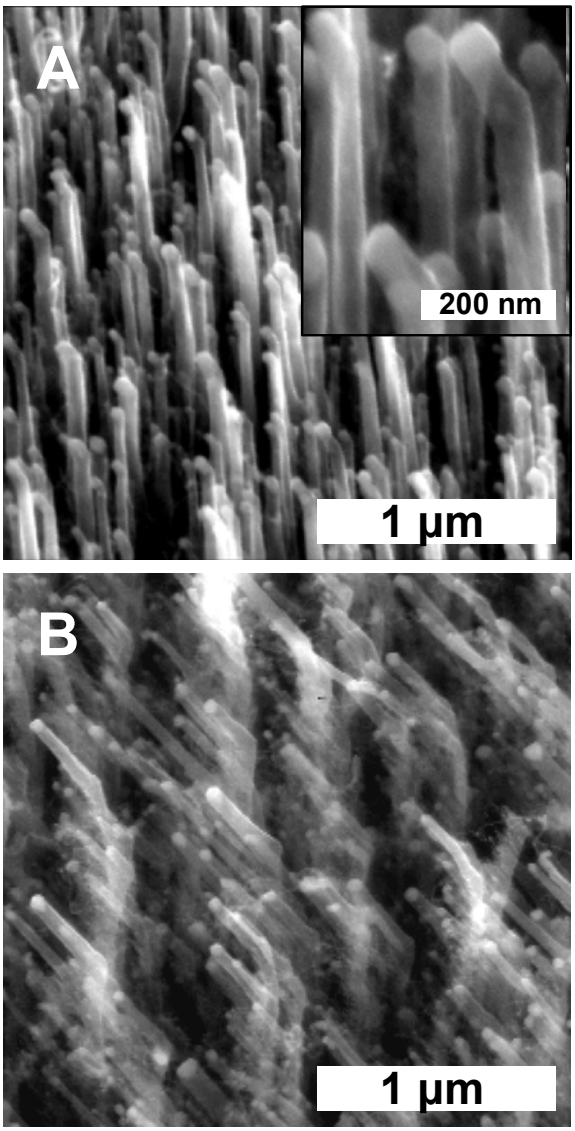

Figure 33: Two arrays of CNTs with growth continued at 45° displaced from perpendicular. Both samples have the same CNT diameters and heights during the first growth stage (before the bend). A) CNTs that had a thick carbon film over the surface of their catalyst particles after their first growth stage show very little re-growth in their second growth stage (after the bend). B) CNTs with a much thinner carbon film on their catalyst particles showing significantly longer re-growth in their second growth stage. The samples had identical growth times of 15 min. for each growth stage.

In this work, since the arrays of aligned CNT samples were grown through a dc PECVD process using Ni catalyst particles, the catalyst particles were always present at

the top ends of the CNTs making this a “tip-growth” mechanism. In general, CNTs grown by dc plasma CVD have their graphene layer walls inclined at some angle rather than parallel to the growth direction of each CNT. The inclined walls in our CNTs will give them different electrical transport properties than CNTs with walls parallel to their tube axes, so they are not as favorable for applications such as circuit interconnections; however, the subject of this section, re-growth of CNTs by control of catalyst carbon capping, is relevant for other nanostructures grown through by a catalyst particle tip-growth mechanism including CNTs with walls parallel to their tube axes.

These growth conditions appear to be similar to those reported by Merkulov et al. where the growth of the CNTs is limited by the supply of carbon at the exposed catalyst surface. However, for this to be true, there needs to be another process taking place at the end of the growth processing since it is reported that following growth, most catalyst particles are completely coated in a carbon film of some sort. We believe a possible explanation for this could be that a carbon shell forms around the catalyst particles during the period after the plasma is turned off at the end of the growth processing. When the catalyst particle cools, it should precipitate carbon at its surface as the solubility of carbon decreases with temperature for all potential catalyst metals. We have also seen indication that right after the plasma is extinguished in the growth chamber and the substrate heater is turned off, the sample is still under conditions to allow thermal CVD growth for a brief time. We see evidence of slight growth that we think occurs after the plasma processing in the form of some small random CNTs of 5 to 10 nm in diameter that form unaligned near the tops and on some of the side surfaces of our main array of aligned CNTs. We believe that these could be formed by small

catalyst particles that had broken off from the main particle during growth or were possibly sputtered off of one of the main catalyst particles and deposited on the sides of a nearby CNT.

Along with the small unaligned CNTs, there also appears to be additional amorphous carbon deposited during the brief time the sample is under thermal CVD conditions. While under plasma growth conditions, the NH_3 present has an etching effect and removes much of this disordered carbon deposition, however, it is not able to do so once the plasma has been stopped. We attempt to limit this terminal thermal CVD time by evacuating the CVD chamber and then purging with flowing hydrogen immediately after stopping the plasma processing. The amount of the carbon capping present on a catalyst particle following all growth processing and cooling can be controlled by several factors including carbonaceous gas content in the growth chamber, growth temperature, plasma power, and chamber purging during cooling. We generally observe a thicker carbon coating under conditions with a higher carbon containing gas content (higher acetylene to ammonia ratio in our case), higher temperature, higher plasma power, and slower chamber purging following the plasma processing. Although we can make samples with thicker or thinner carbon films on their catalyst particles by adjusting the above variables, it is still difficult to determine at what point and how the carbon deposition occurs without being able to look at the sample while growing it, i. e. in situ transmission electron microscopy (TEM). One might think another possible way to limit the formation of a carbon cap at the end of growth processing could be to gradually decrease the concentration of the carbon containing species in the reactor to zero before turning off the plasma. This would not solve the problem of carbon

precipitating from the catalyst particle as it is cooled, and is also quite difficult to achieve considering the relatively high pressure in the chamber during plasma processing. The time required to remove the carbon containing species would require the CNTs to be subjected to equal time of destructive NH_3 plasma etching since the etching effect increases as the concentration of carbon containing species is decreased.

Although we have an understanding of how many of the processing conditions affect the formation of a carbon capping layer and we can endeavor to avoid its formation, in order to ensure clean catalyst surface with no or minimal carbon capping, we devised a room temperature hydrogen sputter etching process to remove the carbon capping layer once it has been formed. This process has been found effective as shown in Figure 34. Briefly, the mechanism of the sputter etching process involves incident positive ions in the plasma, such as hydrogen, colliding with the nanotube material and preferentially eroding the disordered carbon on the tops of the catalyst particles faster than the carbon in the CNT walls; this is due to the difference in sputtering rates of disordered carbon and graphitic carbon.

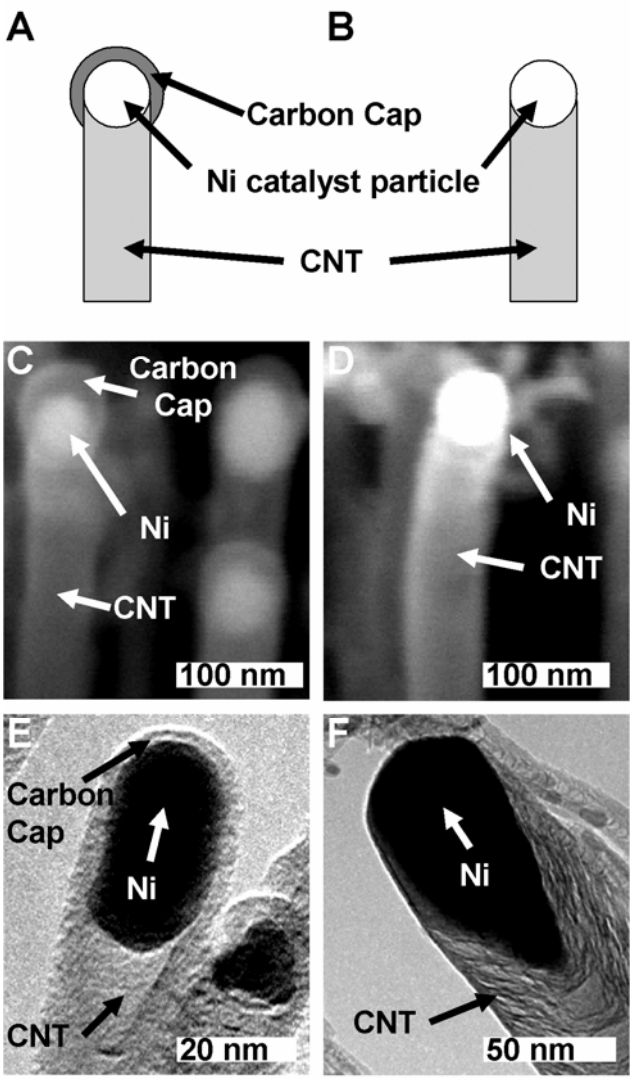

Figure 34: A) Schematic drawing illustrating the locations of the CNT, Ni catalyst particle, and the catalyst particle's carbon capping layer, B) a similar schematic with the carbon capping layer removed. C) SEM image of CNTs showing a thick carbon coating surrounding their catalyst particles and D) after sputter etching, the carbon coating on the CNTs was removed leaving a clean Ni catalyst particle. E) TEM image of Ni catalyst particle showing encapsulation by a carbon capping layer and another catalyst particle (F) with almost no carbon capping on its end.

If this is carried out in an extensive way, it is found that the process can eventually lead to the catalyst particles being completely etched and removed leaving an aligned array of open ended CNTs, which we will present in the following section.[111]

Using this same process under weaker and carefully controlled plasma conditions, we have been able to remove the carbon coating that had formed on the catalyst particles of an aligned CNT sample.

A schematic illustration of a CNT end is shown in Figure 34A with the locations of the carbon capping layer, Ni catalyst particle, and CNT labeled. A similar schematic is shown in Figure 34B for a CNT end with no carbon capping layer. Figure 34C shows an SEM image of the tops of CNTs. The thick carbon film can be seen covering each of the catalyst particles. After sputter etching with hydrogen plasma, the image in Figure 34D shows the carbon coating has been completely removed. Since the sample shown in Figure 34 had processing done after the initial SEM images were taken, it was not possible to show the exact same CNT, but the results presented are typical of what was seen from all of the CNTs we examined on the sample. Figure 34E shows a TEM image of a catalyst particle clearly exhibiting complete carbon encapsulation. This encapsulation contained both graphitic and amorphous carbon. In Figure 34F, another TEM image shows a different catalyst particle that has almost no carbon capping on its end. The variation in carbon capping between Figures 34E and 34F was due to processing conditions (higher plasma power for the sample in Figure 34E in this case.)

Using two samples of vertically aligned CNTs that had thick carbon coatings on their catalyst particles following growth, we attempted to see if our process for removal of the carbon coating improved the ability for continued CNT growth. One of the vertically aligned CNT arrays was sputter etched to remove the catalyst carbon capping as shown in Figure 34D, then the two samples were placed back into the CVD chamber and grown under conditions that should produce a second growth stage with a different

growth direction as described before. The results were similar to those presented in Figure 33, where the CNTs that had had their carbon films sputter etched grew significantly longer than the un-etched sample.

Revived growth of CNTs can lead to many new nanostructures; Figure 35 shows a few of the example structures we have been able to obtain. These nanoscale bent structures were obtained by controlled CVD using the electric field near the recessed intersection of conducting plates as discussed in a preceding section. Despite all of the great potential CNTs have shown as interconnections, simple straight nanotubes are not particularly useful for circuit connections as many of the conductors in modern, nano-electronic circuits need to bend for routing and other device design or packaging reasons. Bent nanotubes can serve a useful purpose in this regards. Sharply bent structures containing bend angles over 90° with a short second growth stage (Figure 35A) resemble nanohooks. Such CNTs could be potentially used as arms for a nanomanipulation device or for AFM or other probe tips where a bent tip could be useful for nanoscale metrology- or conductivity-probing of sidewalls inside vertical pores or channels. One can envision placing two such bent probes side by side for local conductivity measurements. Split electrodes, such as used by Lieber et al.,[112] may be employed for such configurations. For nanotweezer applications, a pair of bent CNTs could allow easier grasping of a nano sized object than a pair of straight CNTs. Bent structures with longer second growth stages that are grown horizontally (Figure 35B) could be potentially used as in-plane nanointerconnections.

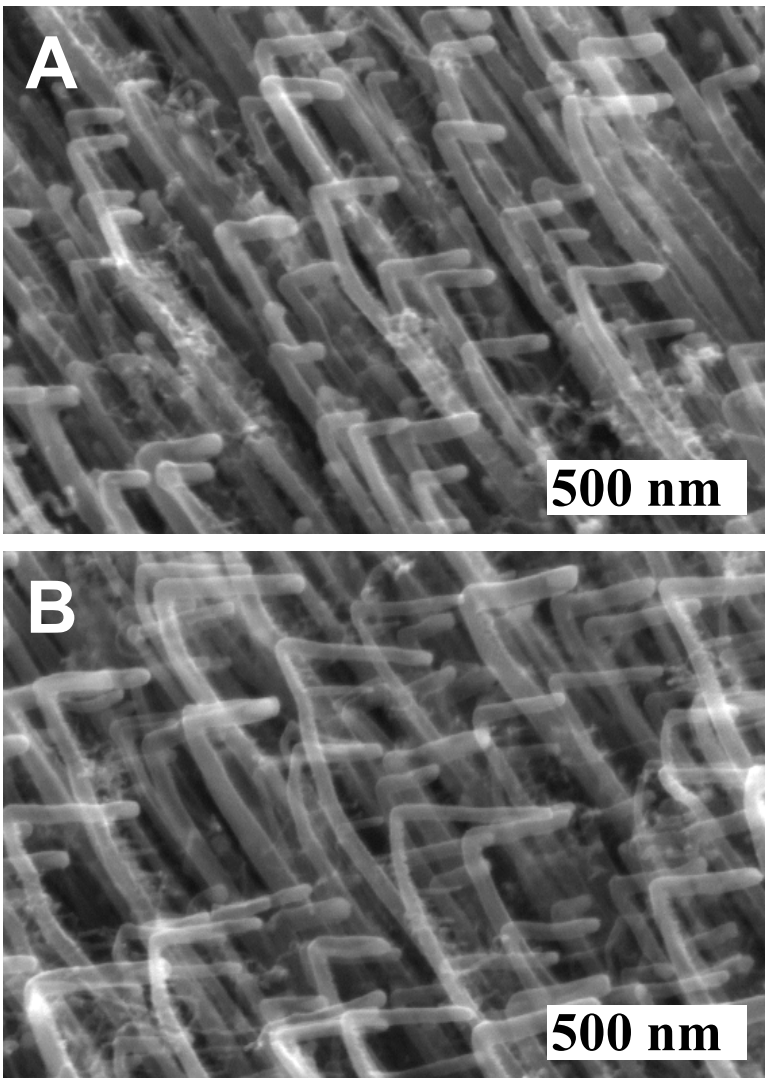

Figure 35: Structures obtained utilizing continued growth of CNTs. A) CNTs with over 90° bends and B) longer structures with 2nd growth stage parallel to substrate surface.

4.5.2 Opening the ends of aligned carbon nanotubes:

The ends of CNTs as synthesized are normally capped by a hemispherical carbon structure of various forms or by a catalyst particle,[113] but several methods of opening the ends of carbon nanotubes have been demonstrated. One way is to heat CNTs in the presence of air for short durations at temperatures around 700 °C results in the burning away of the tube caps and the thinning of tube walls; however, opening all of the tubes by this method often requires oxidizing the majority of the CNTs.[114] Acid solutions such as hydrochloric acid have been shown to chemically etch and remove catalyst particles leaving open CNT ends.[115] Cutting of CNTs leaving open ends on both cut ends has been demonstrated using acid solutions such as nitric acid, supercritical water, ball milling,[116] diamond particle abrasive, and dynamic nano-fragmententation.[117] Open ends of CNTs from the bottom of nanotubes detached from a substrate have been shown to exhibit improved field emission at much lower fields than capped CNTs.[118] Intentional opening of the top ends of aligned CNTs has been demonstrated by introducing CO_2 into the same CVD chamber that CNTs were grown to oxidize the caps.[119] Opened Aligned CNTs were also achieved by H_2O plasma etching followed by hydrochloric acid etching.[120]

These various methods are based primarily on three principles of i) wet chemical dissolution, ii) mechanical break-up, or iii) high temperature oxygen-assisted burning. However, CNTs opened through these methods are normally of greatly different lengths, the vertical alignment configuration is often significantly disrupted, e.g., by their bundling during wet processing, and the nanotube walls often become damaged and their surfaces functionalized by strong acids.[121] It is therefore desirable to

find a new method of nanotube end-opening which avoids these deleterious effects on aligned CNTs. In this section, we report end-opening of aligned CNTs by a sputter etching process which is conveniently carried out at room temperature, without any high temperature oxidation reactions, chemical acid etching, or mechanical break-up.

The multiple stages of the plasma processing were carried out to allow observation of the CNT opening process as it occurred so that the mechanism could be clearly understood. The images presented in Figure 36 show the evolution of microstructure at different stages of processing under H_2 plasma. Figure 36a is of the aligned CNTs in a forest-like array as CVD grown. The CNTs have typical diameters ranging from 30 to 40 nm and heights of 1 to 1.5 μm. The presence of additional small diameter CNTs that are not aligned is also visible. These small diameter CNTs sometimes occur during the CVD growth of aligned CNTs and are usually present near the tops of the aligned CNT array. We believe that small pieces of the main catalyst particle break off during growth and serve as catalyst particles for smaller CNTs. In Figure 36b, we see the sample after it has been subjected to sputter etching under low pressure plasma for a short duration. The Ni catalyst particles are clearly visible as white balls at the tips of each CNT and the small unaligned CNTs have been removed. After additional plasma processing (Figure 36c), the walls of the CNTs just below the catalyst particles appear to be preferentially removed. Many of the catalyst particles are left hanging on by only remnants the CNT walls (labeled by arrows in Figure 36c) and some of the catalyst particles have completely fallen off leaving open CNTs behind. By comparing the catalyst particle size distribution at the start of sputter etching to right before the particles begin to detach, we notice that the average catalyst particle size

appears to be reduced slightly after sputter etching. Once the catalyst particles begin to detach, we are unable to tell what the size distribution of the remaining catalyst particles was at the start of processing After sufficient processing time of ~30 minutes, most of the catalyst particles are completely detached. The detached particles, together with the remnant nanotube segments still attached to the particles, are completely removed from the sample, and none of them are observed on the "forest floor" between CNTs after processing (Figure 36d). We believe that the plasma gas flow somehow blows away the detached catalyst particles and small nanotube segments still attached to them.

Additional SEM images of a sample before processing and after CNT opening are shown in Figure 37. Theses images are taken perpendicular to the sample surface, looking at the aligned CNTs along their growth direction. In Figure 37a, the Ni catalyst particles are, as earlier, visible as bright white balls. Also visible are the additional small diameter CNTs that are not aligned and can be seen around and between the larger aligned CNTs. As a side benefit of our sputter etch process, these small diameter CNTs are also preferentially etched away due to their orientations allowing sputter etching to occur across most of their surfaces. An overall cleaner nanotube array structure is obtained as a result. After the sputter etching process has removed all of the catalyst particles, it is easy to see the circular cross sections of the open CNTs shown in Figure 37b. It is seen that the small diameter CNTs that were present initially are also completely sputtered away by the end of the hydrogen plasma processing.

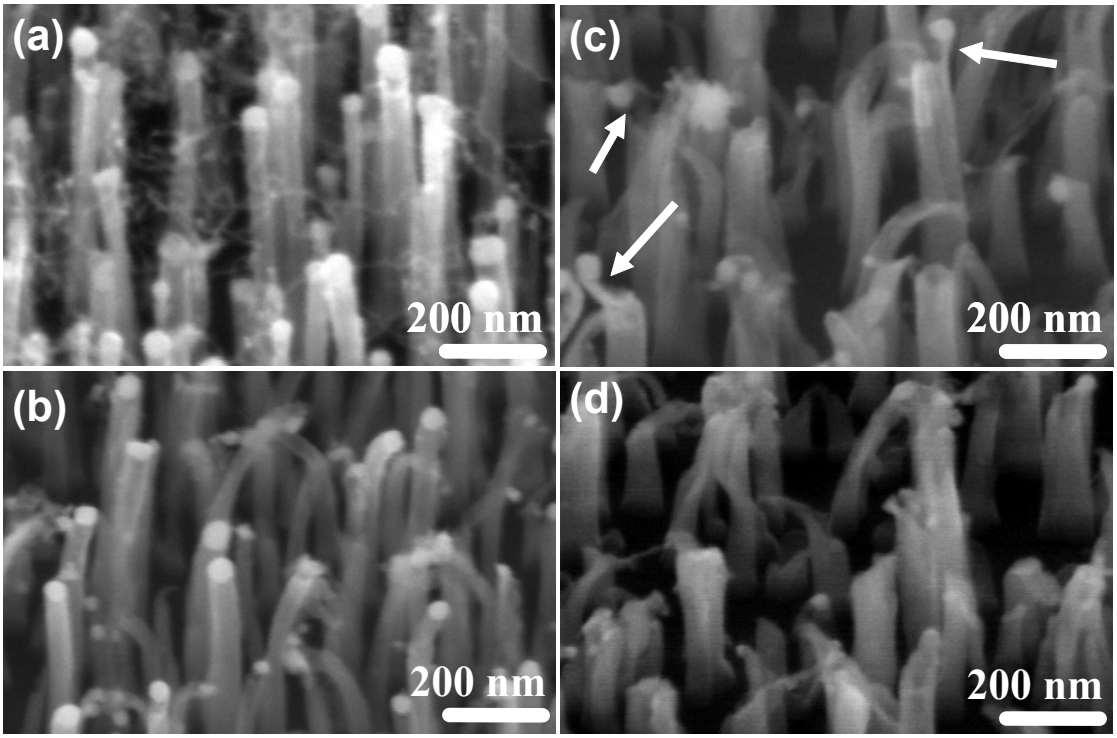

Figure 36: Scanning electron microscopy (SEM) images of CNTs taken with the sample tilted at 45° showing (a) the CNTs as grown with many small diameter CNTs unaligned near the tops of the main aligned CNT array, (b) the start of the H_2 sputter etching processing where the small unaligned CNTs have been removed, (c) during CNT opening process with some of the catalyst particles already detached and others attached to the CNTs by only remnants of their original supporting walls (identified by arrows), and (d) after catalyst particles have been removed leaving CNTs open at their top ends.

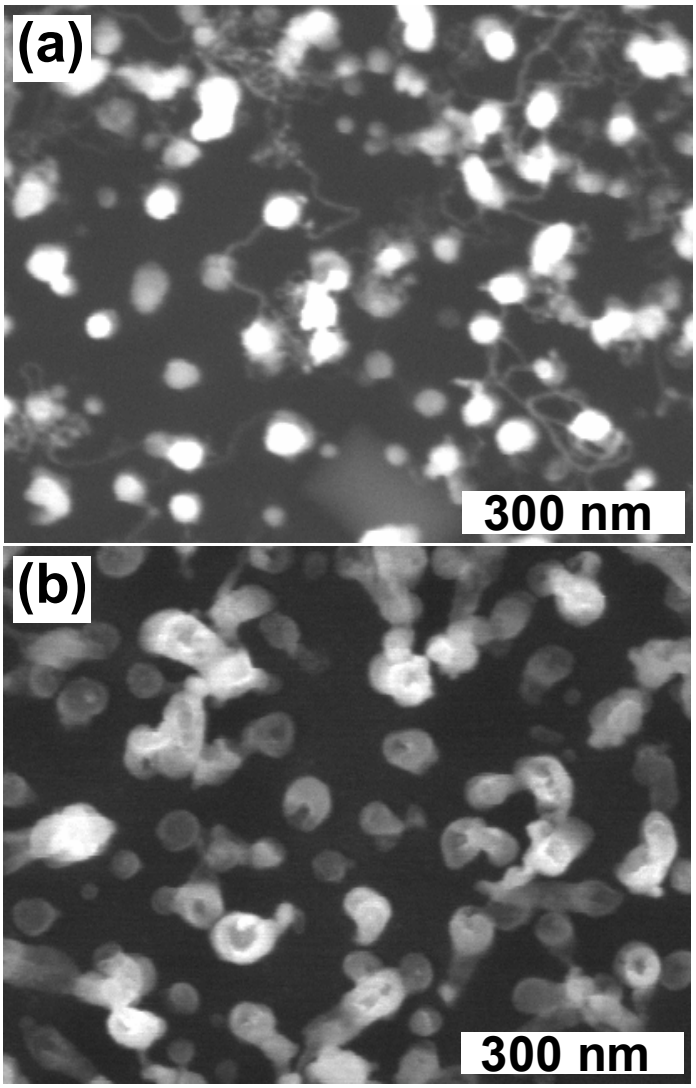

Figure 37: Typical top view SEM images for CNTs; (a) before H_2 plasma processing, and (b) after catalyst particles have been removed leaving open CNTs.

The mechanism for the removal of the catalyst particles and opening of the CNTs appears to be a, preferential sputter etching of selected locations in the nanotubes just below the catalyst particles, which is followed by the occurrence of neck severing. The positive hydrogen ions in the plasma are accelerated towards the substrate and collide with the CNTs. The electric fields within the dc plasma sheath cause an

acceleration of positive ions along the field lines until they terminate at the sample surface. The field lines above the sample are perpendicular to the surface of the sample and the relatively small lengths of the CNTs insure that the incident ions are always accelerated perpendicular to the substrate surface. Although the electric field is accelerating the ions generally perpendicular to the substrate surface, individual ions are actually moving in all directions due to the many collisions that occur in our relatively high pressure plasma. The distribution of ion directions results in sputter etching occurring on all surfaces of the CNTs, but the electric field results in a strong preference for the incident hydrogen ions to be moving perpendicular to the surface when they collide with the surface or with a CNT. This tendency results in preferential sputter etching from the top ends of the CNTs.

A schematic illustration of the proposed mechanism for nanotube end opening is shown in Figure 38 as a sequence of events. Initially the carbon nanotube is vertically aligned with its catalyst particle at its tip. The catalyst particle usually has a thin amorphous carbon coating on it after growth (Figure 38a), as is often seen on SEM analysis. Initial sputter etching causes the removal of this amorphous carbon layer (Figure 38b). Additional processing causes the CNT to bend to one side (Figure 38c). The direction of bending appears to be random initially, but after the CNT begins to bend in one direction, further plasma processing causes the CNT to continue to bend further in the same direction. This is presumably due to the defects and stresses caused by ion bombardment on one side of the nanotube.[122] A small degree of sputtering of the catalyst particle which reduces its size slightly is also observed. As the sputter etching process continues, the walls of the CNT that have been bent over are quickly sputtered

away preferentially. The parts of the CNT that have bent over provide a larger cross sectional area for the vertically descending ion bombardment of their surface which results in faster sputter etching. Eventually, the sputtering will lead to a hole forming in part of the bent over wall, and that opening will continue to grow (Figure 38d). After sufficient plasma processing, the portions of the CNT that had bent over are completely removed causing detachment of the catalyst particle and leaving behind an aligned and open CNT (Figure 38e). Under this model, the geometry of our CNTs might affect the sputter etching rates. We would expect it to take longer to remove the catalyst particle from larger diameter CNTs since there will be more supporting CNT wall to be sputter etched away. The density of our CNTs allows for etching from the sides of the CNTs due to the distribution of incident ion directions in our relatively high pressure plasma process; a very high density CNT forest might slow this process down.

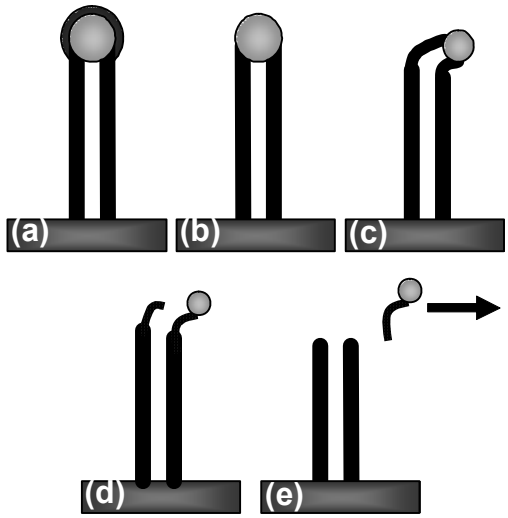

Figure 38: Schematic illustration of the proposed nanotube end opening mechanism. (a) The catalyst particle is initially covered with an amorphous carbon layer before (b) preliminary sputter etching removes this layer. (c) Further sputter etching causes the removal of the CNT walls on the sides of the catalyst particles and bending of the CNT to one side. (d) After a CNT begins to bend, the upper part of the bend over nanotubes is preferentially sputter etched leading to the formation of an opening. (e) The opening grows and eventually the catalyst particle completely detaches from the CNT leaving an open ended CNT.

The proposed sputter etching mechanism is strongly supported by the images presented in Figure 36. Similar results are also shown in Figure 39 for the case of Ar plasma. The removal of the amorphous carbon layer and destruction of the small diameter non-aligned CNTs is almost identical to the case for H_2 plasma discussed above. However, additional Ar plasma processing results in far more bending over of the CNTs and a greater degree of catalyst particle size reduction. Both of these results also support the sputter etching theory. Since the ions resulting from Ar plasma are much heavier than those resulting from a H_2 plasma due to difference in molecular masses, a much stronger sputtering effect is anticipated, which would explain the greater degree of catalyst particle size reduction observed experimentally. The faster

etching with Ar also implies that this is the result of a sputter etching process, and not the result of a chemical reaction that we might envision occurring with the hydrogen plasma. The heavier ions also will cause more defects on the CNT walls and lead to a greater amount of bending. A significantly shorter etching time is required to achieve with Ar plasma similar results as with H_2 plasma, also supporting the sputter etching mechanism. We can confirm the CNTs in Figure 39d are open by looking at the sample from various angles, such as perpendicular to the growth direction as we did for Figure 37. As a side effect of the greater degree of bending resulting from Ar plasma, we see in Figure 39d the final opened CNT array after Ar plasma sputter etching has a greater reduction in height since most of the portions of the CNTs that bent off to a side are sputter etched away. With H_2 plasma, normally less than the top 100 nm of a CNT was removed, but with Ar plasma, an average of 250 nm was removed from the top of each CNT. The estimations of CNT height reduction is done by measuring the CNTs heights at specific locations in the sample where we introduced scratch lines in the original Ni thin film which resulted in no CNT growth along those lines. Along the sides of these voids, we can clearly see CNTs from their tops to their bases and determine the height distributions used in the above estimates. In general, the hydrogen sputter etching process with the lighter atoms appears to provide a better control in nanotube end-opening.

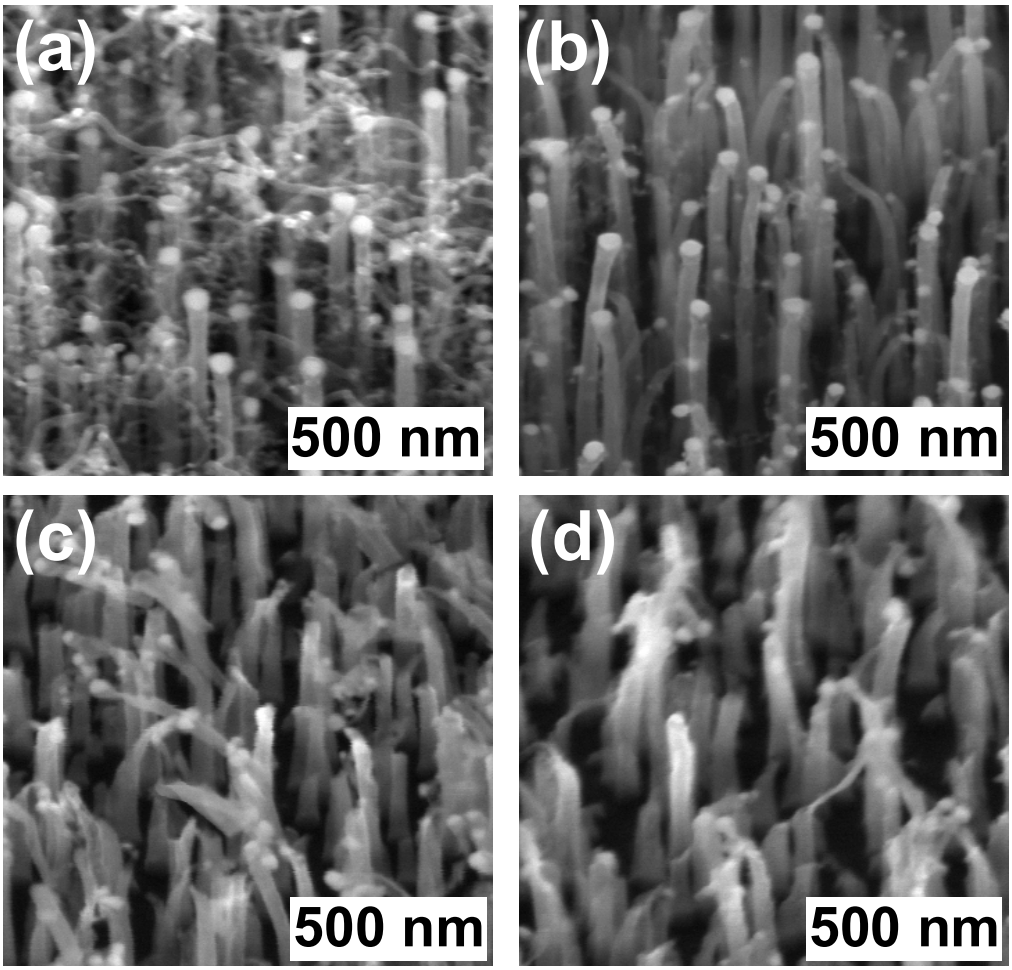

Figure 39: Series of SEM images of CNTs etched with Ar plasma. (a) As-CVD grown, vertically aligned CNTs. (b) After Ar sputter etching the amorphous carbon layer is cleaned off of the catalyst particles and the small diameter CNTs that grew unaligned are completely removed. (c) Further Ar plasma sputter processing causes much bending of the CNTs while reducing the catalyst particle size and removing the carbon walls on the sides of the CNTs. (D) After sufficient Ar plasma processing, the catalyst particles are removed leaving opened aligned CNTs.

Quantitative graphs comparing the rates of etching are shown in Figure 40. The earlier reported faster sputter etching by Ar compared to H_2 is shown in Figure 40a. The percentage of CNTs that have their catalyst particle completely removed leaving behind open CNTs is plotted against sputter etching time. The percentage of CNTs

open was determined by analyzing all of the CNT tips visible from three different areas on each sample. We see in Figure 40b that Ar etches faster at higher pressures. The applied voltage used to form the plasma is also found to be critical in the sputter etching process. In Figure 40c we see no CNT opening after sputter etching at 300V. There must be a critical amount of energy required for an ion in the plasma to be able to sputter etch the carbon, and from our experiment we see that for our system under these conditions, forming a plasma with only 300V is below this threshold. The rate of removal of the small diameter CNTs is presented in Figure 40d, where we see that for most conditions, they are removed very quickly by the plasma processing. Their small sizes and orientations at angles intersecting with the bulk of the plasma ion bombardment explain why this occurs so rapidly.

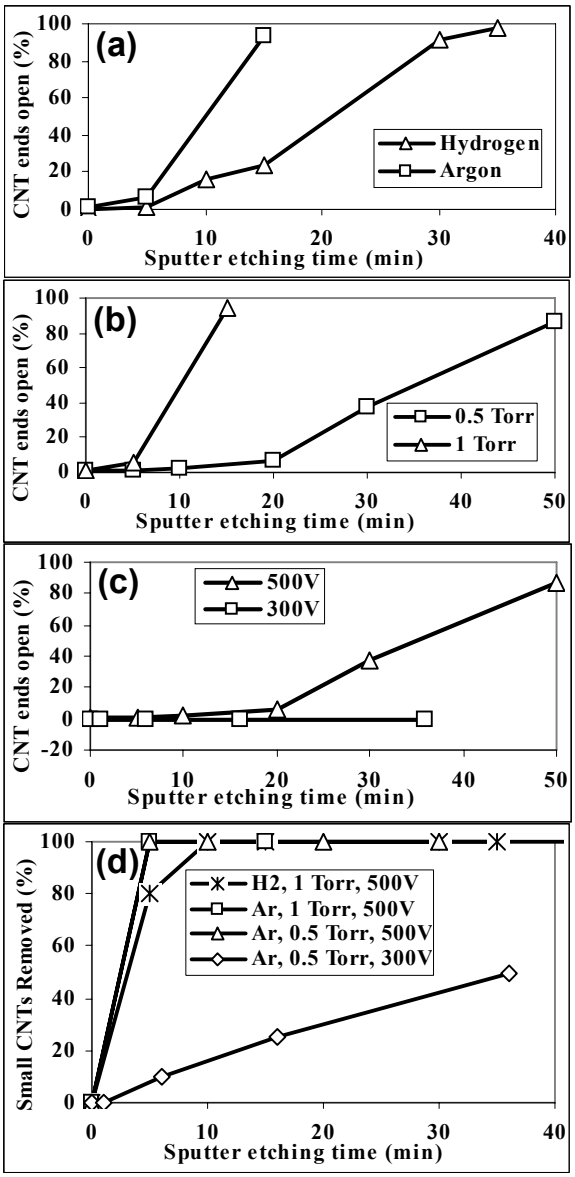

Figure 40: Percentage of CNT ends opened as a function of sputter etching time for (a) H_2 vs. Ar at 500V applied bias and 1 Torr pressure, (b) 0.5 Torr vs. 1 Torr for At at 500V, and (c) 300V vs. 500V for Ar at 0.5 Torr. (d) Comparison of the percentage of small CNTs removed as a function of time under various conditions. As expected from the proposed sputter etching process, there is a greater etching rate for larger ions, higher pressure, and higher applied bias forming the plasma.

4.6 Aligned multibranching of carbon nanotubes:

A subset of CNTs attracting great attention is CNT branchings such as Y-junctions. Recently, sharp electronic switching[123] and differential current gain[124] have been demonstrated using any of the 3 branches as an in-situ control gate. An array of such carbon nanotube Y-junctions formed by multiple branchings from a single CNT would be beneficial for more complex devices and it would be desirable if such an array could be constructed on existing carbon nanotubes which can be patterned and positioned on a substrate. In this section, I show how such an array of multibranching CNTs can be fabricated.

Stable CNT Y-junctions have been produced by various methods. Some of the early ones were synthesized by arc-discharge[125] while slightly later, individual Y-junction CNTs were grown in large and uniform quantities through a CVD process in Y-branched nanochannel alumina templates.[126] Another method is to grown CNTs in a CVD process and during the growth processing add precursors containing a catalyst metal suitable for CNT growth which can attach to the growing CNTs and nucleate a branch.[127] Y-junctions in single walled CNTs (SWNTs) have been reported by means of thermal decomposition of fullerene in the presence of various transition metals[128] and also by welding together separate SWNTs using an electron beam in a high acceleration voltage transmission electron microscope (TEM).[129] The electronic properties of CNT Y-junctions have been modeled theoretically[130] and measurements have been achieved,[131] showing great potential of CNT Y-junctions as elements in simple nanoelectronic devices.

The CNTs in this section were grown similar to as before where after the main CNTs have been grown, the experimental setup was then changed to cause the subsequent growth stage to occur aligned along a different direction. In the previously reported results, the goal was to grow CNTs with sharp bends where I had control of both bend angles and locations. In contrast, here I used modified conditions to cause the creation of multiple CNT branches along the side of the original CNT "backbone" all aligned with the direction that the CNT growth was continued in.

Images both after the initial CNT growth but before branching, and after the growth of the aligned branches (Figure 41) show a dramatic change in the structure. The many branches that form from each of the initial backbone CNTs are much smaller in diameter than the original CNTs. The branches have a range of diameters, with only the larger branches clearly visible in the scanning electron microscopy (SEM) images of Figure 41. High resolution TEM images of CNTs shown in Figure 41 are presented in Figure 42. In the CNTs shown before branching, we can see the herringbone structure associated with CNTs grown by dc PECVD processes. The only metal particle that can be seen is the Ni catalyst particle residing at the tip end of the CNT (Figure 42a). After the branching growth (Figure 42b), we see many new CNTs with the majority of the diameters 5-10 nm. Each of these new smaller CNT branches has its own equally small catalyst particle at its tip which lets us conclude that they grew under a tip growth mechanism just as the initial CNTs that support them were. The side of the backbone CNT that faces the direction of the branch growth has a much more complicated surface than the side facing the opposite direction. There are not only the beginnings of many more CNT branches, but also small Ni particles and damaged graphene plane ends. The

CNT branches shown in the TEM images of Figure 42b do not appear to be as aligned as those in the SEM image in Figure 41b. This is likely due to the fact that these very small diameter CNTs can be easily disturbed during sample preparation to obtain the TEM samples such as during the sonication process for CNT distribution on a TEM grid.

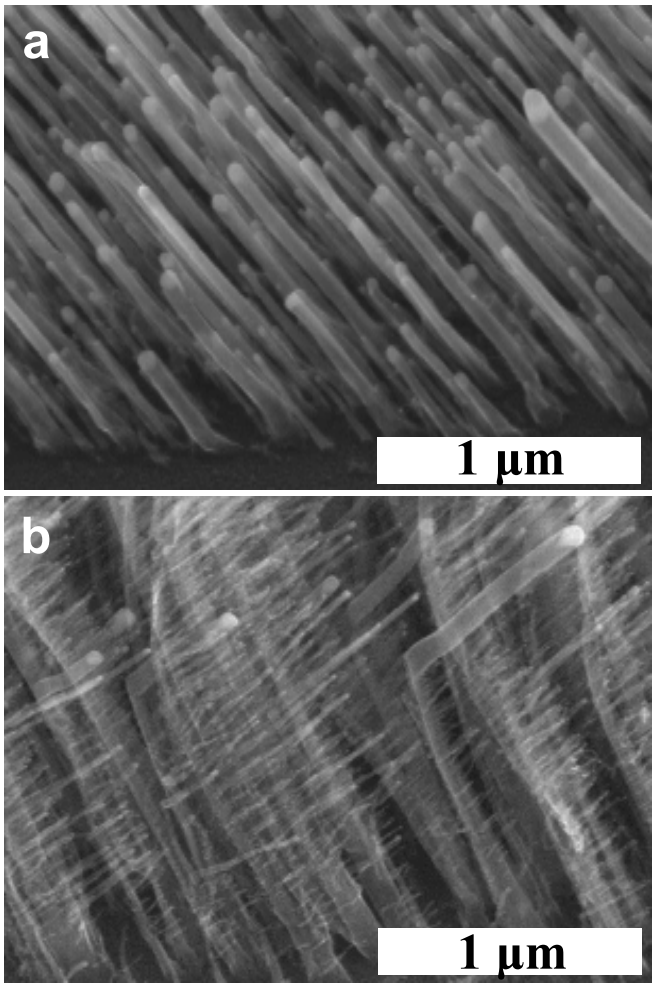

Figure 41: Scanning electron microscopy (SEM) images taken of CNTs (a) after their initial growth stage, and (b) after the second growth stages results in the aligned multibranched structure.

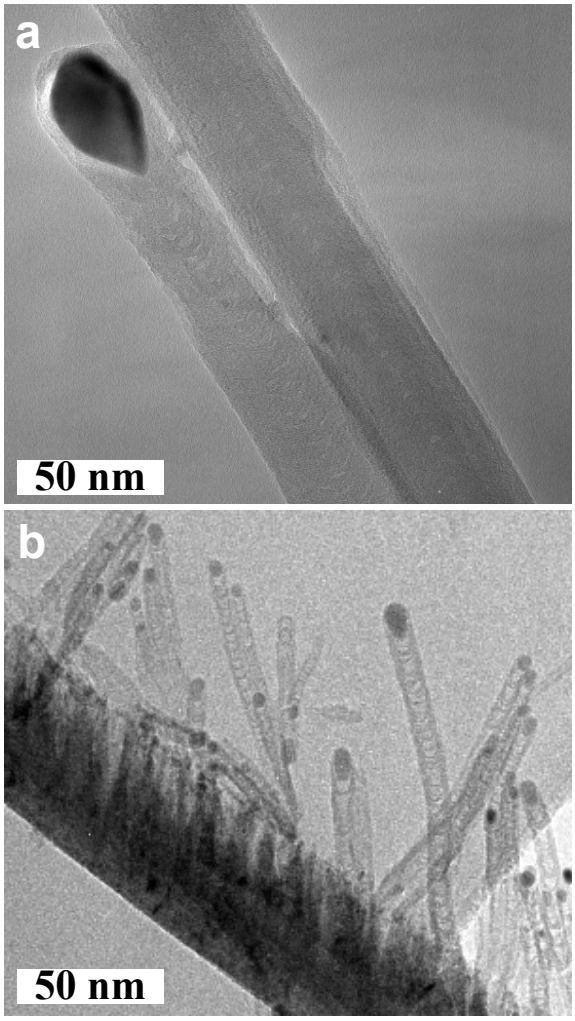

Figure 42: (a) TEM images of as-initially-grown CNTs showing Ni only present in the main catalyst particles, (b) Branched CNTs with much smaller Ni catalyst particles present at the tips of each branched CNT.

The basic CVD conditions that result in this novel structure are similar to those that enabled the continuing the growth of the CNTs in a new direction; however, some of the different processing conditions employed here resulted in clearly distinct growth morphologies. I believe that the critical factor was weather or not the plasma power was high enough to allow sputtering of the Ni catalyst particle. It is clear from the TEM

images in Figure 42b that every branch was grown from a Ni catalyst particle under a tip-growth mechanism. Since the Ni was confined to the main catalyst particles at the tips of each of the initially grown CNT backbones (Figure 42a), the Ni catalysts particles that form the CNT branches must somehow form during the plasma processing. Although our CVD chamber is not 100% contamination free, we do not believe that there is any source of Ni nanoparticles anywhere else in the chamber. Therefore, we conclude that these new smaller Ni catalyst particles originate from the only accessible source of Ni, the main catalyst particles of the original backbone CNTs.

We have observed that the Ni catalyst particles can break up during growth and that some of these particles can become trapped in the CNT.[132] We have also seen that under the right plasma conditions that the Ni catalyst particle can be reduced in size by sputtering. Both of these result in the redistribution of Ni from the initial catalyst particle. The breaking up of the Ni catalyst particle does not appear to be occurring in this work since in our previous observations it occurred during the growth of the CNT and here we do not see any Ni particles attached along the length of the initially grown CNTs. It is also unlikely that after growth, larger chunks of Ni would break off of the large catalyst particle and attach to the sides of the CNTs in relatively uniform size and distribution. The second option, sputtering of the Ni catalyst particle, does appear to be a strong possibility. We would expect that if sputtering were occurring, a small amount of Ni would be deposited in thin film form on the surfaces of the CNTs near each of the catalyst particles that was being sputtered. This processing is being carried out at an elevated temperature with the substrate above 700 °C and the actual temperature near the tips of the CNTs locally much higher due to ion bombardment from the plasma. At

these temperatures, a thin film of depositing Ni on the surface of the CNTs is expected to break up and agglomerate into nanoparticles to minimize surface energies.[133] Further, since we observe an onset of branching formation with an increase in the applied field used to form the DC glow discharge (the field strength roughly parallels to the energy of the ions in the plasma), we have additional support for the proposed mechanism of CNT-end Ni particle sputtering for formation of the new smaller Ni catalyst particles. Keeping the other experimental conditions fixed, if during the second growth stage we use an applied voltage of under 525 V to form the dc glow discharge, then no branching occurs. If we apply over 550 V, then branching is observed. From this we conclude that somewhere between 525 and 550 V, the plasma power becomes such that sputtering of the Ni catalyst particles are possible. If sputtering is occurring from the original Ni catalyst particle, we might also expect to see a reduction in size when this main particle continues to grow in the 2nd growth stage. We do not see very clear evidence of this, but due to the sizes differences between the original CNTs and the branches, it is estimated that only a 1 nm reduction in the diameter of the initial Ni catalyst particles would provide more than enough Ni to seed all of the observed branches. A schematic illustration summarizing the sequence of events in our proposed grown model is shown in Figure 43.

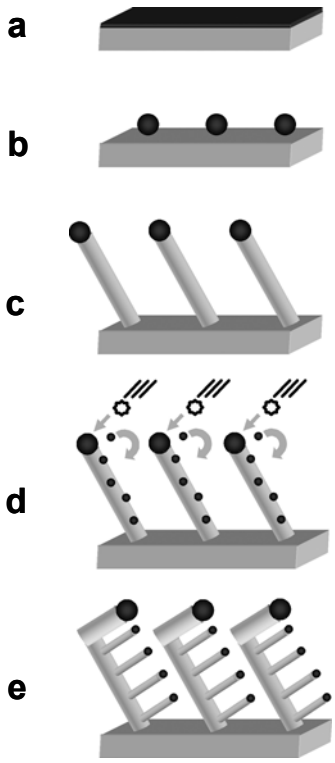

Figure 43: Schematic illustration of the sequence of events leading to the formation of a multibranched CNT structure. A thin film of Ni catalyst is initially deposited onto a Si substrate (a). After heating, the thin film breaks up and agglomerates into nanoparticles (b). Each of the Ni particles serves as a catalyst for the growth of a CNT (c). The CNTs are grown aligned to each other and at some acute angle with respect to the substrate. After the initial CNT growth stage, the processing conditions are altered to cause the initial Ni catalyst particle to be sputtered by the ion bombardment from the dc plasma (d). The sputtered Ni deposits on the surfaces of the initially grown CNTs and eventually agglomerates into new smaller catalyst particles and nucleate new CNTs which grow as branches on the original CNTs. Due to changes in the cathode geometry, the initial CNTs to continue to grow aligned with the newly formed CNT branches along a different direction than the original growth step (e).

The self-seeding processing that results in the CNT branchings has some inherent randomness. It is not possible for us to precisely control the size and location of each CNT branch using the method we demonstrate here, but we do have some control. We can increase the degree of sputtering that occurs from the initial Ni catalyst

particle by increasing the plasma power. This allows us to control the density of the branches. The positions of the branches might also be controlled if we added in an additional step of patterning a mask over parts of the initial CNT surfaces, or by directly patterning the catalyst particles for each branch using electron beam lithography.

In addition to the great potential for new forms of electronic devices, one of the possible applications of nanotubes which may have major industrial impact much sooner is as high-surface-area electrodes in fuel cells. Due largely to the rising costs of energy and to many environmental concerns for present energy sources, an interest in fuel cell research is rapidly growing. For hydrogen as well as direct methanol fuel cells, electrocatalysts based on Pt are often used.

The size, shape, and distribution of catalyst particles plays a key role in their catalytic activitites.[134] A number of ways are being investigated to manufacture an effective structure with Pt catalyst particles of the appropriate size and distribution, some of which include using CNTs as the support scaffold for the catalyst particles.[135, 136, 137, 138, 139] While in some of these works Pt particles of 2-4 nm have been synthesized, they all have other drawbacks. Most require deposition of the Pt nanoparticles onto the CNTs by means of an aqueous solution. After such an aqueous processing, the CNTs tend to form severely agglomerated bundles greatly reducing the available surface area. For an improved Pt catalyst particle supporting structure, it is desirable to have an as-grown CNT array with smaller diameter and higher density CNTs containing all of the Pt catalyst particles exposed on the surfaces of the CNTs.

To demonstrate a use for our new multibranching CNT structure, we used it as a scaffold for the support of Pt nanoparticles (Figure 44). This application enables us to

have a high concentration of Pt particles that are separated from each other within the three dimensional CNT branches while not requiring control over individual branch locations. Although the most common methods of attaching Pt nanoparticles to CNTs involve aqueous solutions, we sought to avoid the problems associated with that since we wanted to maintain the unique multibranching CNT structure. We simply sputtered a thin film of Pt on our multibranched CNT structure while rapidly rotating the sample and followed this deposition by annealing under an inert atmosphere. The Pt formed into isolated nanoparticles which covered the surfaces of the CNTs and, as predicted, the smaller diameter CNT branches lead to smaller diameter Pt particles forming on their surfaces. This composite structure could potentially serve as the catalyst support for future fuel cells and other electrochemical catalytic reactions.

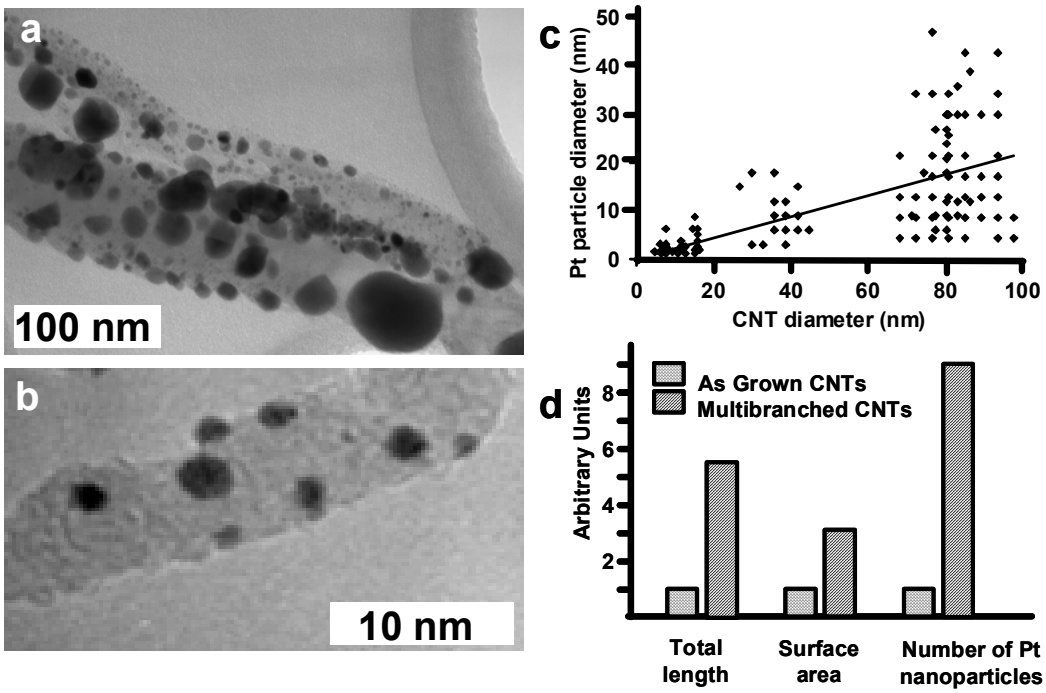

Figure 44: A TEM image of a few CNTs of various diameters is shown in (a). The largest dark contrast particles in the lower right are Ni catalyst particles that led to the growth of the CNTs. The majority of the other particles lining their surface are Pt Shown in (b) is a higher magnification TEM image showing a small diameter CNT with many ~2 nm Pt particles. A plot illustrating the trend of Pt particle size versus the diameter of the CNT they were formed on is presented in (c). It is clear that on the smaller diameter CNTs, only small Pt particles form. Three histograms comparing the total length, surface area, and number of Pt nanoparticles formed on each original CNT for both the as initially grown CNT array, and for the multibranched structure is shown in (d). As expected, all of these values are significantly higher for the multibranched CNT structure.

4.7 Coiled carbon nanotubes:

For several applications such as nanosprings or nanosolenoids, CNT coils would be desirable. Although others have produced coiled CNTs, there have been no demonstrations of being able to control that structure. Since I have demonstrated the ability to sharply change the directions of the electric fields and the resulting CNT

growth directions, we might envision being able to continuously rotate the electric field directions and guide the CNTs to grow into coils.

To make an initial demonstration of this, I grew CNTs in four growth stages where the intended angle that the CNT would make with the substrate was kept constant, but the substrate was rotated clockwise (from above) 90° between each of the growth stages. The resulting box spiral morphologies are shown in Figure 45. It is quite difficult to observe the coiling shape of the CNTs since in this forest configuration the majority of the CNTs have their views obstructed by others. Also, from the 2D SEM images, its difficult to see what direction the CNT is growing into and out of the page. An enlarged image of one coil that can be seen is shown in b) while a schematic illustration is in c). An example of a more tightly coiled CNT that was grown at a different time is shown in d)

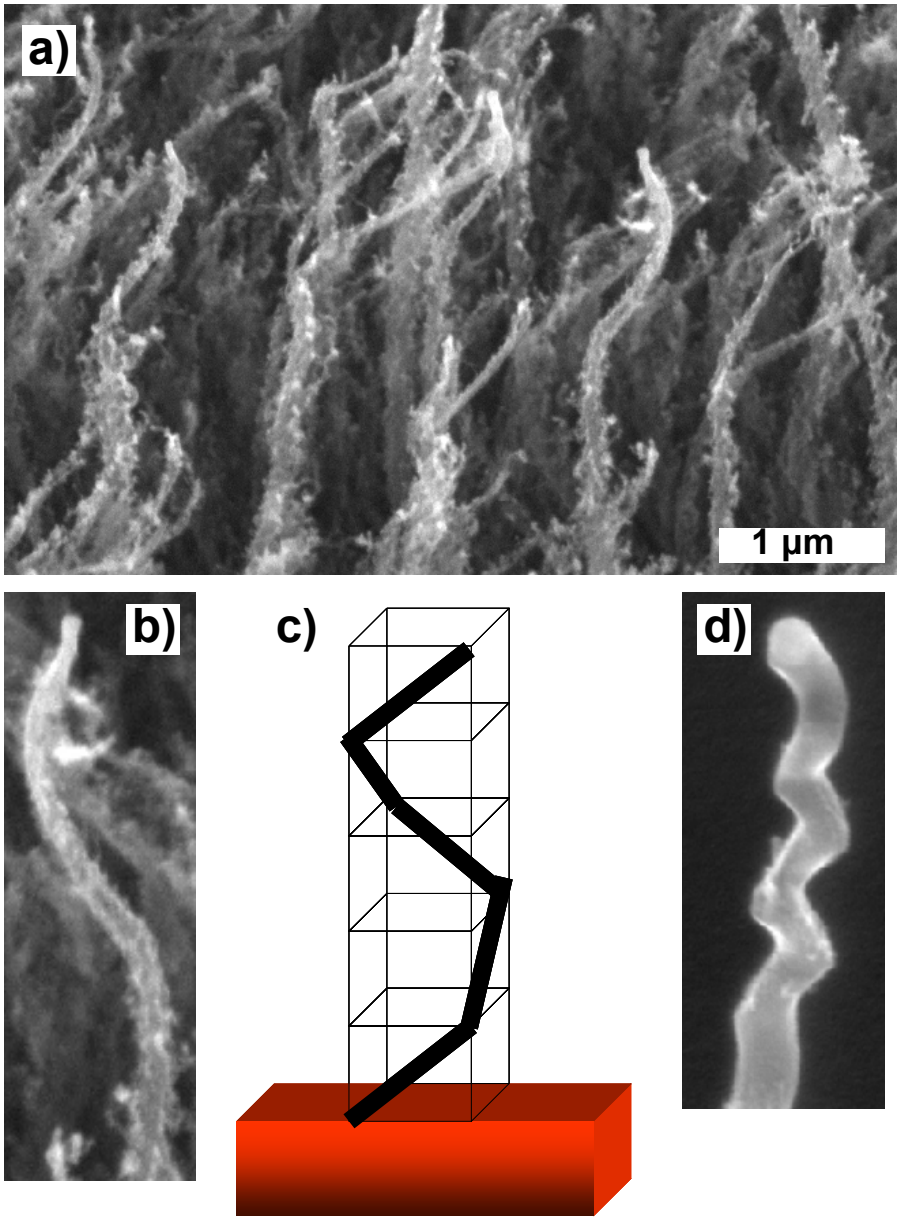

Figure 45: a) SEM images of forests of CNTs grown with a single counter clockwise coil as seen from above. b) An enlarged images of a single CNT coil which corresponds to the four step box spiral schematic illustration shown in c). In d) there is an example of a CNT from a different sample which is more tightly coiled.

4.8 Applications of controlled geometry carbon nanotubes:

Although there are a tremendous number of potential applications for CNTs that can be grown using what was presented in this work, I will only discuss a few here.

4.8.1 Electron field emission source:

The market for displays for televisions, computers, and other electronic devices is one of the biggest in the world. One application of CNTs that might significantly affect this market is the use of CNTs as electron field emitters in a Field Emission display (FED.) The basic concept of a FED is to use something very much like a traditional phosphor panel found in CRTs but to replace the scanning electron beam with many gated CNT field emitters. This would take advantage of the superior image quality associated with the very mature phosphor display technologies but also allow for smaller form factors (flat panel) and less power consumption.

The cone shaped CNTs that were shown in Figure 14 were grown in at attempt to optimize the morphology of CNTs for use in a field emission device. CNTs such as those would be grown in insulator holes so that a gate electrode could be above their tips but electrically isolated from the CNT substrate. By biasing the gate, the field emitted electrons could be extracted from the CNTs and then accelerated towards the anode at the phosphor display. A schematic illustration of this is shown in Figure 46.

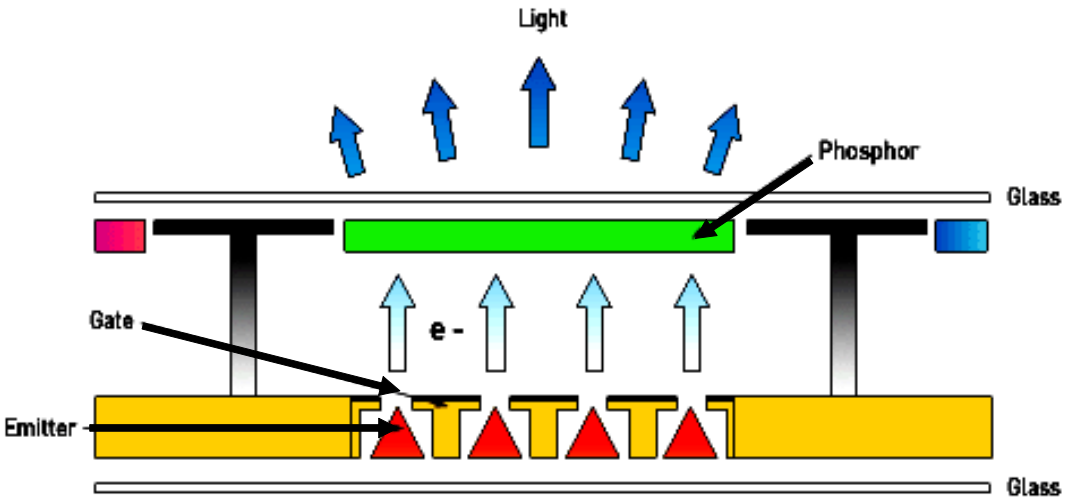

Figure 46: Schematic illustration of cone shaped CNTs being used as electron field emitters for use in a field emission display. The emitted electrons would be accelerated and excite a traditional phosphor display layer.

For a similar application, CNTs grown in an almost identical gated structure could be used to form a projection e-beam lithography source. Such a lithography system could draw from the advantages of the small feature sizes that are capable with e-beam lithography and the fast speeds that that are possible by photolithography.

4.8.2 Scanning probe microscopy:

In addition to the potential improvements in the resolution and durability of AFM probe tips that CNTs offer, there are a few applications where being able to use bent CNTs could be of particular interest. For probing the side walls of channels and pores, a probe that had a bend CNT at its tip would be far superior than trying to tilt a sample and use a conventional probe tip. Also, when inspecting the bottom of channels, such as after one has been etched, it is often necessary to inspect the bottom corners to see weather over or under etching has occurred resulting in either undercutting of the

channel side wall or partial blocking of the channel. The shape of a traditional pyramidal probe tip does not allow it to inspect features in areas like this since the sides of the probe tip contact the sample; using a bent CNT probe could solve this problem. A schematic illustration of such a tip is shown in Figure 47 and an example of CNTs that might be useful for this application were already presented in Figures 29 and 33.

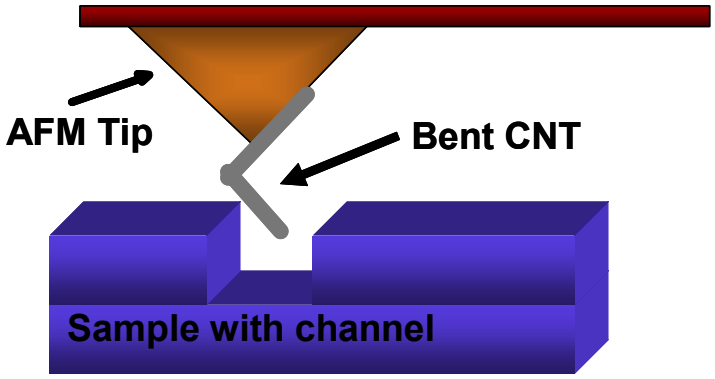

Figure 47: Schematic illustration of an improved AFM probe with a bent CNT at its tip that could be used for probing side walls of channels and pores or for inspecting the features at the bottom of channels where conventional pyramidal probes can not get.

4.8.3 Template for neuronal growth:

Many things in nature occur at the nanoscale. While nerve cells are actually up at the micro scale, the tiny filipodia arms that they send out to grab onto their surroundings are in fact nano-scale. Since it is known that cells grow differently on different surfaces and there are a number of surfaces available for cells that have various surface textures, I attempted to see whether I could use a CNT template to influence the growth of nerve cells. Being able to control or stimulate nerve cell growth could have great impact since there are almost no good treatments for nerve damage at this time.

CNT templates were fabricated with various line patterns. Photolithography was used to allow the deposition of Ni lines of various widths and spacing. After a Ni thin film was deposited on these patterns, vertically aligned arrays of CNTs were grown from them. Images of the patterned Ni lines before CNT growth and the final patterned CNTs are shown in Figure 48.

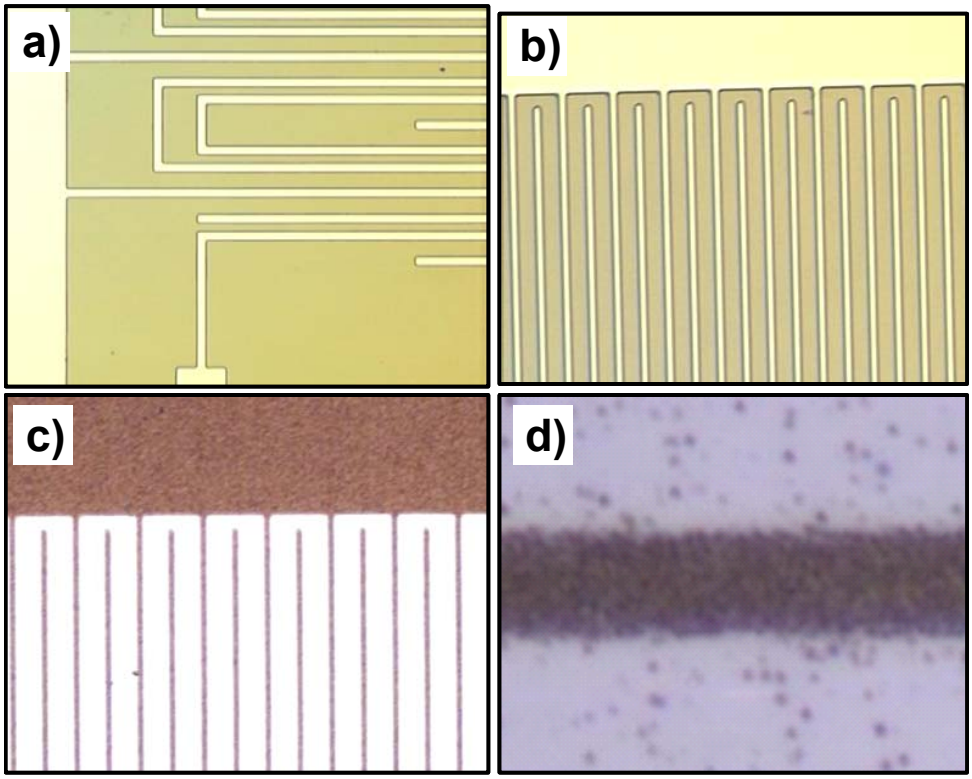

Figure 48: Photolithography patterned Ni lines with different patterns are in a) and b). CNTs were grown on these Ni patterns to form vertically aligned arrays in line patterns in c) and d).

PC-12 rat brain nerve cells are commonly used for initial nerve cell research and are easily available for purchase. We cultured these cells and experimented with various concentrations. The CNT on Si substrates were treated with bovine serum

albumin (BSA), a protein used commonly for rendering surfaces non-adhesive to cells, was used to prevent nerve cells from attaching directly to the Si substrate. After this treatment, the entire Si substrate that the CNTs were grown on was immersed in a well that contained the nerve cell culture. The well was placed back into its incubator and left for 8 hours.

After the 8 hours of incubation, the samples were observed by optical microscopy. There was a clear tendency for the nerve cells to grow along the directions of the CNT lines. Lines of 5 μm width and 20 μm spacing seemed to match he size of nerve cells well and worked best for us. The results are presented in Figure 49. The nerve cells can be seen both on top of the CNT lines and between them, but in all cases we see that the cells connect to the CNTs lines with filipodia in many locations. When we looked for cells on the Si substrate in areas that there was no CNT pattern (where we would not expect to find any cells attached), we could only find a couple of cells, and all of these did not seem to have grown like the one shown in Figure 49c.

Although some people have shown that CNTs be used to direct the growth of nerve cells before, they all attached a chemical growth factor that stimulated nerve cell growth. Due to the very defective nature of the surface of the CNTs growth by dc PECVD, even without any such growth factor, we were able to have nerve cells attach to our CNT patters and grown aligned with those lines.

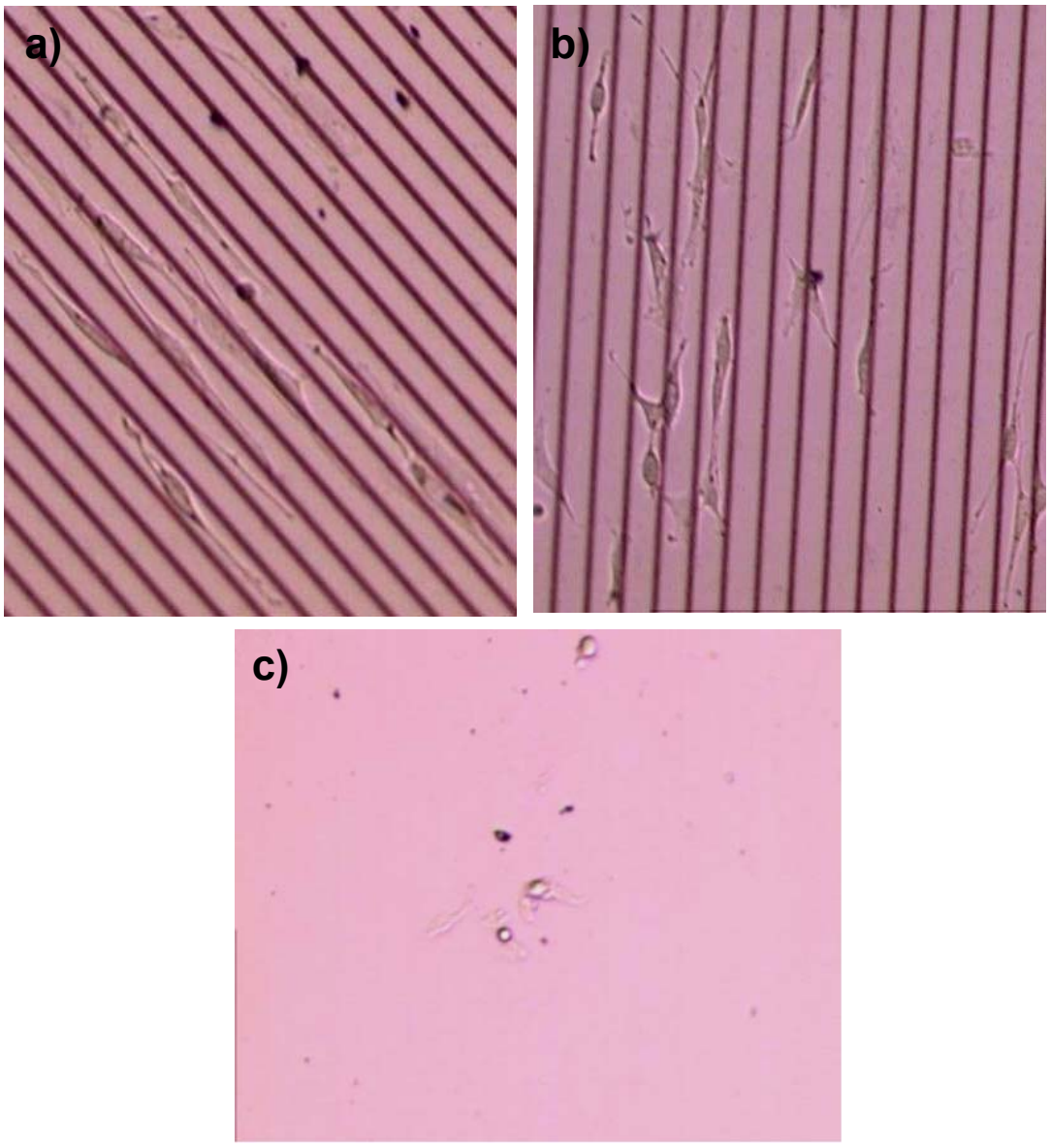

Figure 49: PC-12 nerve cells grow aligned with the patterned lines of CNTs in a) and b). The samples were coated with bovine serum albumin (BSA) to prevent cell attachment to the substrate directly and even when a cell was found away from the CNT pattern, it did not appear to have grown as shown in c).

CHAPTER 5: SUMMARY, CONCLUSIONS, AND FUTURE WORK

In summary, I have demonstrated that CNT growth directions can be controlled by a dc PECVD process. The CNTs are grown within the dc plasma cathode sheath and it is the electric field directions within this sheath that we can alter by careful control of cathode geometry. The forces and directions of these electric fields were calculated and used to grow CNTs along specific directions. It was also shown that the growth directions of CNTs could be sharply changed if the same was done to these electric fields and this was utilized to create sharp bends in CNTs and structures with multiple bends such as zigzagged.

Additional process control combined with the directional growth control also resulted in other morphology control over CNTs such as opening the ends of aligned CNTs, making multiple aligned branchings form a single CNT, or making coiled CNTs.

Some CNTs were fabricated for specific applications and CNTs suitable for use as electron field emitters, AFM probe tips, catalyst support structures for fuel cells, and templates for neuronal growth were all demonstrated.

Although some major steps in the ability to grow CNTs have been demonstrated, there is still much that needs to be done. Despite the added control demonstrated in this work, it is still very difficult to grow uniform CNTs in sufficiently large quantities. Assembly and integration of CNTs for most devices is still not economically feasible.

Some of the first things that need to be done in relation to this work specifically are detailed electrical transport measurements and microstructural analysis. For any

electronic device application, the electrical transport properties of the CNTs will be paramount. The potential to use CNTs as electrical interconnections is currently being investigated. Figure 50 shows 100nm gold electrodes that were deposited for taking four point probe measurements on individual CNTs. The tiny probes route to 100 µm square contact pads where we can make electrical connections by carefully touching these pads with a probe station needle. We will also want to measure the transport of sharply bent CNTs and branching CNTs to see what properties these new structures have. There are a number of very interesting and unexpected properties that have been observed on various CNT structures, and some of these new structures have high potential to add to that list.

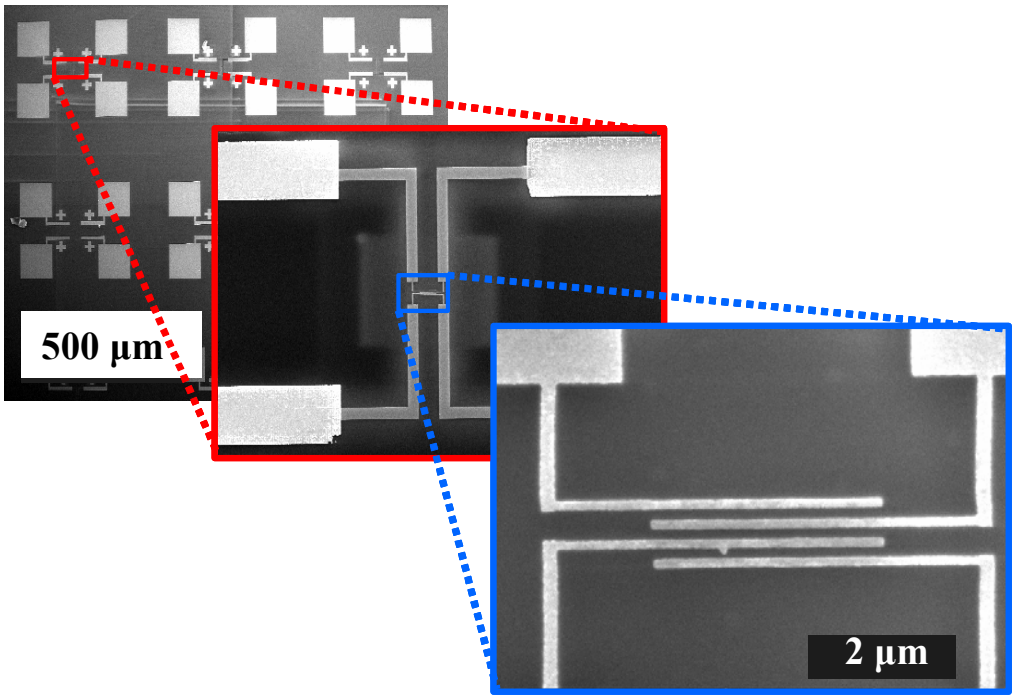

Figure 50: Au electrodes and contact pads which were fabricated for four point electrical measurements of various morphologies of CNTs.

Another thing of great importance will be the microstructure of the CNTs, especially around some of the new structures that were created. As defects in CNTs often give rise to fascinating properties, understading how to control the microstructure of the CNTs could lead to the growth of CNTs with tailored properties. A high resolution TEM image of a sharp bend is shown in Figure 51. Here we can see that at the bend there is an additional pile up of graphene planes on the outer side but that the relationship between any two of these graphene planes does not appear much different when comparing it to two graphene planes away from that bend. This would lead me to believe that this bend would have electrical properties very similar to that of a straight CNT of this length, which would be important if it were to be used as a simple interconnection.

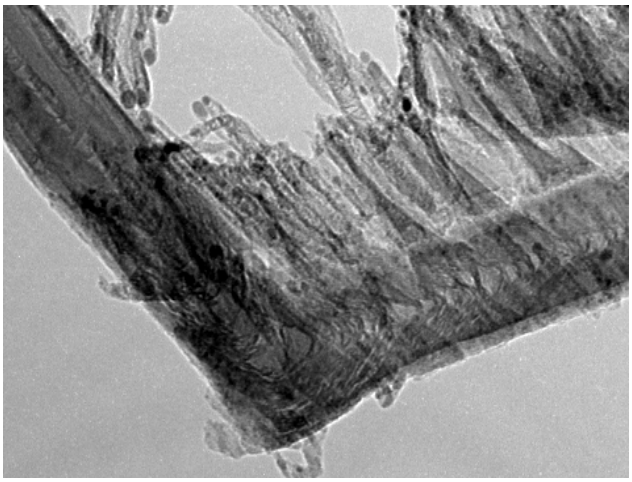

Figure 51: TEM image of a sharp bend in a branching CNT. The inclined graphene plane angle consistent with CNTs grown by dc PECVD can be seen before and after the bend.

Although CNTs that appear suitable for AFM probe tips have been grown, and tips are currently being grown one at a time on real AFM cantilevers, this process still

needs to be extended to one that can be used on a wafer scale to produce AFM probes tips, which need to be cheaply made, uniform, and in large quantities. Although field emission displays have been demonstrated by several display manufactures, there are still major lifetime issues related to how long a CNT can be used as a field emitter before burning out. Although many simple electronic devices have been demonstrated, integrating many of these devices together currently can't be done well enough to show benefits over current Si based semiconductor technology.

The potential applications for CNTs are still great and I believe that there will be real world devices that contain them at some point. Some applications, such as scanning probe tips, are very near commercialization, while others, such as in circuit interconnections, still do not appear probable to occur. Hopefully the control over CNT growth directions and morphology demonstrated in this work will help take another step towards CNTs making their way into everyday life.

REFERENCES

[1] H. W. Kroto, J. R. Heath, S. C. Obrien, R. F. Curl, and R. E. Smalley, *Nature (London)* **318**, 162 (1985).

[2] S. Iijima, *Nature (London)* **354**, 56 (1991).

[3] T. V. Hughes and C. R. Chambers, *Manufacture of Carbon Filaments*, US Patent No. 405,480 (1889).

[4] L. V. Radushkevich and V. M. Lukyanovich, Zh. Fiz. Khim. **26**, 88 (1952).

[5] R. T. K. Baker, Carbon **27**, 315 (1989).

[6] R. T. K. Baker and P. S. Harris, in *Chemistry and Physics of Carbon*, edited by P. L. Walker, Marcel Dekker, New York, (1978).

[7] S. Iijima and T. Ichihashi, Nature (London) **363**, 603 (1993).

[8] D. S. Bethune, C. H. Kiang, M. S. DeVries, G. Gorman, R. Savoy and R. Beyers, , Nature (London) **363**, 605 (1993).

[9] T. W. Ebbesen, P. M. Ajayan, Nature **358**, 200 (1996).

[10] L. C. Qin, S. Iijima, Chem. Phys. Lett. **269**, 65 (1997).

[11] L. C. Qin, J. Mater. Sci. Lett. **16**, 457 (1997).

[12] Y. Chen, D. T. Shaw, L. P. Guo, Appl. Phys. Lett. **76**, 2469 (2000).

[13] M. S. Dresselhaus, *Encyclopedia of Materials: Science and Technology*, Elsevier Science, New York, 2001.

[14] W. D. J. Callister, *Materials Science and Engineering an Introduction*, 6th ed., Wiley, New York, 2003.

[15] D. P. Kim, Y. R. Suhng, and M. M. Labes, *Carbon* **30**, 729 (1992).

[16] E. W. Wong, P. E. Sheehan, and C. M. Lieber, *Science* **277**, 1971 (1997).

[17] B. T. Kelly, *The Physics of Graphite*, Applied Science Publishers, London, (1981).

[18] *The Properties of Natural and Synthetic Diamond*, edited by J. E. Field, Academic, London (1992).

[19] A. Krishnan, E. Dujardin, T. W. Ebbesen, P. N. Yianilos, and M. M. J. Treacy, *Phys. Rev. B* **58**, 14013 (1998).

[20] M. F. Yu, O. Lourie, M. J. Dyer, K. Moloni, T. F. Kelly, and R. S. Ruoff, *Science* **287**, 637 (2000).

[21] M. M. J. Treacy, T. W. Ebbesen, and J. M. Gibson, *Nature (London)* **381**, 678 (1996).

[22] B. G. Demczyk, Y. M. Wang, J. Cumings, M. Hetman, W. Han, A. Zettl, and R. O. Ritchie, *Mater. Sci. Eng., A* **334**, 173 (2002).

[23] B. McEnaney, *Encyclopedia of Materials: Science and Technology*, Amsterdam, New York, (2001).

[24] R. Bacon, *J. Appl. Phys.* **31**, 323 (1960).

[25] J. D. H. Hughes, *J. Phys. D* **20**, 276 (1987).

[26] T. Hashishin, H. Kohara, H. Iwanaga, and S. Takeuchi, *J. Ceram. Soc. Jpn.* **110**, 772 (2002).

[27] R. L. Jacobsen, T. M. Tritt, J. R. Guth, A. C. Ehrlich, and D. J. Gillespie, *Carbon* **33**, 1217 (1995).

[28] R. S. Ruoff, D. Qian, and W. K. Liu, *C. R. Phys.* **4**, 993 (2003).

[29] S. B. Lee, K. B. K. Teo, M. Chhowalla, D. G. Hasko, G. A. J. Amaratunga, W. I. Milne, and H. Ahmed, *Microelectron. Eng.* **61**, 475 (2002)

[30] C. Schonenberger, A. BAchtold, C. Strunk, J. P. Salvetat, and L. Forro, *Appl. Phys. A: Mater. Sci. Process.* **A69**, 283 (1999).

[31] A. Thess et al., *Science* **273**, 483 (1996).

[32] L. Zhang, D. Austin, V. I. Merkulov, A. V. Melechko, K. L. Klein, M. A. Guillorn, D. H. Lowndes, and M. L. Simpson, *Appl. Phys. Lett.* **84**, 3972 (2004).

[33] T. Utsumi, *IEEE Trans. Electron Devices* **38**, 2276 (1991).

[34] F. S. Baker, J. Williams, and A. R. Osborn, *Nature (London)* **239**, 96 (1972).

[35] C. Lea, *J. Phys. D* **6**, 1105 (1973).

[36] R. L. McCreery, Electroanalytical Chemistry, edited by A. J. Bard, Marcel Dekker, New York, 1991.

[37] R. J. Chen, Y. G. Zhan, D. W. Wang, and H. J. Dai, *J. Am. Chem. Soc.* **123**, 3838 (2001).

[38] J. L. Bahr and J. M. Tour, *J. Mater. Chem.* **12**, 1952 (2002).

[39] E. T. Mickelson, C. B. Huffman, A. G. Rinzler, R. E. Smalley, R. H. Hauge, and J. L. Margrave, *Chem. Phys. Lett.* **296**, 188 (1998).

[40] G. T. Hermanson, *Boiconjugate Techniqures*, Academic, San Diego, (1996).

[41] Y. H. Lin, F. Lu, Y. Tu, and Z. F. Ren, *Nano Lett.* **4**, 191 (2004).

[42] R. L. McCreery, in *Electroanalytical Chemistry*, edited by A. J. Bard, Marcel Dekker, New York, (1991).

[43] J. Li, A. Cassell, L. Delzeit, J. Han, and M. Meyyappan, *J. Phys. Chem. B* **106**, 9299 (2002).

[44] M. A. Murphy, G. D. Wilcox, R. H. Dahm, and F. Marken *Electrochem. Commun.*, **5**, 51 (2003).

[45] Y. Tu, Y. H. Lin, and Z. F. Ren, *Nano Lett.* **3**, 107 (2003).

[46] T. E. McKnight et al., *J. Phys. Chem. B*, **107**, 10722 (2003).

[47] W. Kratschmer, L. D. Lamb, K. Fostiropoulos, and Dr. R. Huffman, *Nature (London)* **347**, 354 (1990).

[48] P. A. Tesner, R. Ey, I. S. Rafalkes, *Dokl. Akad. Nauk SSSR* **87**, 821 (1952).

[49] P. A. Tesner, R. Ey, I. S. Rafalkes, and E. F. Arefieva, *Carbon* **8**, 453 (1970).

[50] R. T. K. Baker, M. A. Barber, R. J. Waite, P. S. Harris, and F. S. Feates, *J. Catal*. **26**, 51 (1972).

[51] L. Delzeit, I. McAninch, B. A. Cruden, D. Hash, B. Chen, J. Han, and M. Meyyappan, *J. Appl, Phys.* **91**, 6027 (2002).

[52] A. V. Melechko, V. I. Merkulov, D. H. Lowndes, M. A. Guillorn, and M. L. Simpson, *Chem. Phys. Lett.* **356**, 527 (2002).

[53] A. M. Cassell, J. A. Raymakers, J. Kong, and H. J. Dai, *J. Phys. Chem. B* **103**, 6484 (1999).

[54] M. J. Bronikowski, P. A. Willis, D. T. Colbert, K. A. Smith, and R. E. Smalley, *J. Vac. Sci. Technol. A* **19**, 1800 (2001).

[55] W. Z. Li, S. S. Xie, L. X. Qian, B. H. Chang, B. S. Zou, W. Y. Zhou, R. A. Zhao, and G. Wang, *Science* **274**, 1701 (1996).

[56] A. Moisala, A. G. Nasibulin, and E. I. Kauppinen, *J. Phys.: Condens. Matter* **15** S3011 (2003).

[57] H. Kanzow and A. Ding, *Phys. Rev. B* **60**, 11180 (1999).

[58] G. Eres, A. A. Puretzky, D. B. Geohegan, and H. Cui, *Appl. Phys. Lett.* **84**, 1759 (2004).

[59] R. T. Yang and J. P. Chen, *J. Catal* **115**, 52 (1989).

[60] J. R. Nielsen and D. L. Trimm, J. Catal. 48, 155 (1977).

[61] A. Sacco, P. Thacker, T. N. Chang, and A. T. S. Chiang, J. Catal. 85, 224 (1984).

[62] I. Alstrup, J. Catal. 109, 241 (1988).

[63] J. W. Snoeck, G. F. Froment, and M. Fowles, J. Catal. 169, 240 (1997).

[64] S. Helveg, C. Lopez-Cartes, J. Sehested, P. L. Hansen, B. S. Clausen, J. R. Rostrup-Nielsen, F. Abild-Pedersen, and J. K. Norskov, *Nature (London)* **427**, 426 (2004).

[65] J. Li, C. Papadopoulos, J. M. Xu, and M. Moskovits, Appl. Phys. Lett. 75, 367 (1999).

[66] V. I. Merkulov, A. V. Melechko, M. A. Guillorn, D. H. Lowndes, and M. L. Simpson, Appl. Phys. Lett. 80, 476 (2002).

[67] Z. F. Ren, Z. P. Huang, J. W. Xu, J. H. Wang, P. Bush, M. P. Siegal, and P. N. Provencio, *Science* **282**, 1105 (1998).

[68] B. O. Boskovic, V. Stolojan, R. U. A. Khan, S. Haq, and S. R. P. Silva, *Nat. Mater*, **1**, 165 (2002).

[69] C. Bower, O. Zhou, W. Zhu, D. J. Werder, and S. H. Jin, *Appl. Phys. Lett.* **77**, 2767 (2000).

[70] J. B. O. Caughman, L. R. Baylor, M. A. Guillorn, V. I. Merkulov, D. H. Lowndes, and L. F. Allard, *Appl. Phys. Lett.* **83**, 1207 (2003).

[71] C. H. Lin, H. L. Chang, C. M. Hsu, A. Y. Lo, and C. T. Kuo, *Diamond Relat. Mater.* **12**, 1851 (2003).

[72] A. Huczko, H. Lange, M. Sioda, Y. Q. Zhu, W. K. Hsu, and D. R. M. Walton, *J. Phys. Chem. B* **106**, 1534 (2002).

[73] M. W. Li, Z. Hu, X. Z. Wang, Q. Wu, and Y. Chen, *J. Mater. Sci. Lett.* **22**, 1223 (2003).

[74] V. I. Merkulov, D. H. Lowndes, Y. Y. Wei, G. Eres, and E. Voelkl, *Appl. Phys. Lett*. **76**, 3555 (2000).

[75] W. Zhu, C. Bower, O. Zhou, G. Kochanski, S. Jin, *Appl. Phys. Lett.* **75**, 873 (1999).

[76] D. Chung, S. Park, H. Lee, J. Choi, S. Cha, J. Kim, J. Jang, K. Min, S. Cho, M. Toon, J. Lee, C. Lee, J. Too, J. Kim, J. Jung, Y. Jin, Y. Park, J. You, *Appl. Phys. Lett.* **80**, 4045 (2002).

[77] C. Bower, W. Zhu, D. Shalom, D. Lopez, L. –H. Chen, P. L. Gammel, S. Jin, *Appl. Phys. Lett.* **80**, 3820 (2002).

[78] P. Kim, C. M. Lieber, *Science* **286**, 2148 (1999).

[79] A. Fennimore, T. Yuzvinsky, W. Han, M. Fuhrer, J. Cumings, A. Zettl, *Nature (London)* **393**, 49 (1998)

[80] S. Tans, A. Verschueren, C. Dekker, *Nature (London)* **393**, 49 (1998).

[81] T. Rueckes, K. Kim, E. Joselevich, G. Tseng, C. Cheung, C. Lieber, *Science* **289**, 94 (2000).

[82] E. Snow, P. Campbell, J. Novak, *Appl. Phys. Lett.* **79**, 1172 (2001).

[83] J. Li, Q. Ye, A. Cassell, H. Ng, R. Stevens, J. Han, M. Meyyappan, *Appl. Phys. Lett.* **82**, 2491 (2003).

[84] B. Wei, R. Vajtai, P. Ajayan, *Appl. Phys. Lett*. **80**, 2002 (2002).

[85] M. Diehl, S. Yaliraki, R. Beckman, M. Barahona, J. Heath, *Angew Chem., Int. Ed.* **41**, 353 (2002).

[86] F. Banhart, *Nano Lett.* **1**, 329 (2001).

[87] M. A. Guillorn, A. V. Melechko, V. I. Merkulov, E. D. Ellis, M. L. Simpson, L. R. Baylor, and G. J. Bordonaro, *J. Vac. Sci. Technol. B* **19**, 2598 (2001).

[88] X. P. Xu and G. R. Brandes, *Appl. Phys. Lett.* **74**, 2549 (1999).

[89] G. Pirio, P. Legagneux, D. Pribat, K. B. K. Teo, M. Chhowalla, G. A. J. Amaratunga, and W. I. Milne, *Nanotechnology* **13**, 1 (2002).

[90] M. A. Guillorn, A. V. Melechko, V. I. Merkulov, D. K. Hensley, M. L. Simpson, and D. H. Lowndes, *J. Vac. Sci. Technol. B* **19**, 573 (2001).

[91] M. A. Guillorn, A. V. Melechko, V. I. Merkulov, D. K. Hensley, M. L. Simpson, and D. H. Lowndes, *Appl. Phys. Lett.* **81**, 3660 (2002).

[92] M. A. Guillorn et al., *J. Vac. Sci. Technol. B* **22**, 35 (2004).

[93] L. R. Baylor et al., *J. Vac. Sci. Technol. B* **22**, 3021 (2004).

[94] G. Binnig, C. F. Quate, G. Gerber, *Phys. Rev. Lett.* **56**, 930 (1986).

[95] L. Delzeit, C. Nguyen, R. Stevens, J. Han, M. Meyyappan, *Nanotechnology* **13**, 280 (2002).

[96] J. H. Fafner, C. L. Cheung, C. M. Lieber, *J. Am. Chem. Soc.* **121**, 9750 (1999).

[97] Q. Ye, A. Cassell, H. Liu, K. –J. Chao, J. Han, M. Meyyappan, *Nano Lett.* **4**, 1301 (2004).

[98] A. Ural, Y. Li, H. Dai, *Appl. Phys. Lett.* **81**, 3464 (2002).

[99] C. Hsu, C. Lin, H. Chang, C. Kuo, *Thin Solid Films* **420**, 225 (2002).

[100] V. Merkulov, A. Melechko, M. Guillorn, D. Lowndes, M. Simpson, *Appl. Phys. Lett.* **79**, 2970 (2001).

[101] B. Chapman, *Glow Discharge Processes*, Wiley, New York (1980).

[102] J. Blazek, P. Spatenka, F. Pacal, Ch. Taschner, A. Leonhardt, *Diamond Relat. Mater.* **13**, 504 (2004).

[103] S. Maniv. W. D. Westood, P. J. Scanlon, *J. Appl. Phys*., **53**, 856 (1982).

[104] D. B. Hash, M. S. Bell, K. B. K. Teo, B. A. Cruden, W. I. Milne, M. Meyyappan, *Nanotechnology* **16**, 925 (2005).

[105] C. Bower, W. Zhu, S. Jin, O. Zhou, *Appl. Phys. Lett.* **77**, 830 (2000).

[106] V. Merulov, A. Melenchko, M. Gullorn, M. Simpson, D. Lowndes, J. Whealton, R. Raridon, *Appl. Phys. Lett.* **80**, 4816 (2002).

[107] M. Chhowalla, K. Teo, C. Ducati, N. Rupesinghe, G. Amaratunga, A. Ferrari, D. Roy, J. Robertson, W. Milne, *J. Appl. Phys*. **90**, 5308 (2001).

[108] V. I. Merkulov, D. K. Hensley, A. V. Melechko, M. Guillorn, D. H. Lowndes, M. L. Simpson, *J. Phys. Chem. B* **106**, 10570 (2002).

[109] K. Y. Lim, C. H. Sow, J. Lin, F. C. Cheong, Z. X. Shen, T. L. Thong, K. C. Chin, T. S. Wee, *Adv. Mater.* **15**, 300 (2003).

[110] J. F. AuBuchon. L. –H. Chen, A. I. Gapin, D. –W. Kim, C. Daraio, S. Jin, *Nano Lett*. **4**, 1781 (2004).

[111] J. F. AuBuchon, L. –H. Chen, A. I. Gapin, S. Jin, *J. Appl. Phys*. **97**, 124310 (2005).

[112] P. Kim, C. M. Lieber, *Science* **286**, 2148 (1999).

[113] M. S. Dresselhaus, G. Dresselhaus, P. C. Eklund, *Science of Fulleerenes and Carbon Nanotubes*, Academic, San Diego (1996).

[114] P. M. Ajayan, T. W. Ebbesen, T. Ichihashi, S. Iijima, K. Tanigaki, H. Hiura, *Nature (London)* **362**, 522 (1993).

[115] I. W. Chiang, B. E. Brinson, R. E. Smally, J. L. Margrave, R. H. Hauge, *J. Phys. Chem. B* **105**, 1157 (2001).

[116] N. Pierard, A. Fonseca, Z. Konya, I. Willems, G. Van Tendeloo, J. B. Nagy, *Chem. Phys. Lett.* **335**, 1 (2001).

[117] C. Daraio, V. F. Nesterenko, J. F. AuBuchon, S. Jin, *Nano Lett.* **4**, 1915 (2004).

[118] Z. W. Pan et al., *J. Phys. Chem. B* **105**, 1519 (2001).

[119] Z. Xiafeng, C. Anyuan, S. Qunhui, X. Cailu, W. Dehai, *Mater. Trans., JIM* **43**, 1707 (2002).

[120] S. Huang, L. Dai, *J. Phys. Chem. B* **106**, 3543 (2002).

[121] K. Neesz, A. Siska, I. Vesselenyi, K. Hernadi, D. Mehn, G. Galbaes, Z. Konya, I. Kiricsi, *Catal. Today* **76**, 3 (2002).

[122] H. Lim, H. Jung, S. –K. Joo, *Microelectron. Eng*. **69**, 81 (2003).

[123] P. R. Bandaru, C. Daraio, S. Jin, A. M. Rao, *Nat. Mater.* **4**, 663 (2005).

[124] B. R. Perkins, D. P. Wang, D. Soltman, A. J. Yin, J. M. Xu, Z. Zaslavsky, *Appl. Phys. Lett*. **87**, 123504 (2005).

[125] D. Zhou, S. Seraphin, *Chem. Phys. Lett*. **238**, 286 (1995).

[126] J. Li, C. Papadopoulos, J. Xu, *Nature* **402**, 6759 (1999).

[127] N. Gothard, C. Daraio, J. Gaillard, R. Zidan, S. Jin, A. M. Rao, *Nano Lettt.* **4**, 213 (2004).

[128] P. Nagy, R. Ehlich, L. P. Gyulai*, J. Appl. Phys. A* **70**, 481 (2000).

[129] M. Terrones, F. Banhart, N. Grobert, J. –C. Charlier, H. Terrones, P. M. Ajayan, *Phys. Rev. Lett.* **89**, 075505 (2002).

[130] G. Treboux, *J. Phys. Chem B* **103**, 10378 (1999).

[131] C. Papadopoulos, A. Rakitin, J. Li, A. S. Vedeneev, J. M. Xu, *Phys. Rev. Lett.* **85**, 3476 (2000).

[132] D. –W. Kim, L. –H. Chen, J. F. AuBuchon, I. C. Chen, S. –H. Jeong, I. K. Yoo, S. Jin, *Carbon* **43**, 835 (2005).

[133] J. Zhong, G. M. Stocks, *Appl. Phys. Lett.* **87**, 133105 (2005).

[134] I. S. Armadi, Z. L. Wang, T. C. Green, A. Henglein, M. A. El-Sayed, *Science* **272**, 1924 (1996).

[135] B. Xue, P. Chen, Q. Hong, J. Lin, K. L. Tan, *J. Mater. Chem* **11**, 2378 (2001).

[136] J. –Han, S. H. Choi, T. Y. Lee, J. –B. Yoo, C. –Y. Park, T. Jung, S. Yu, W. Yi, I. H. Han, J. M. Kim, *Diamond Relat. Mater*. **12**, 878 (2003).

[137] Z. He, J. Chen, D. Liu, H. Tang, W. Deng, Y. Kuang, *Mater. Chem. Phys.* **85**, 396 (2004).

[138] S. Hrapovic, Y. Liu, K. B. Male, J. H. T. Luong, *Anal. Chem.* **76**, 1083 (2004).

[139] Z. Liu, L. M. Gan, L. Hong, W. Chen, J. Y. Lee, *J. Power Sources* **139**, 73 (2005).